ADAPTIVE TARGET DETECTION IN RADAR IMAGING

by

Hyung Soo Kim

A dissertation submitted in partial fulfillment
of the requirements for the degree of
Doctor of Philosophy
(Electrical Engineering: Systems)
in The University of Michigan
2001

Doctoral Committee:
        Professor Alfred O. Hero III, Chair
        Associate Professor Jeffrey A. Fessler
        Professor John L. Volakis
        Professor William J. Williams

ABSTRACT

ADAPTIVE TARGET DETECTION IN RADAR IMAGING

by
Hyung Soo Kim

Chair: Alfred O. Hero III

This thesis addresses a target detection problem in radar imaging for which the covariance matrix of an unknown Gaussian clutter background has block diagonal structure. This block diagonal structure is the consequence of a target lying along a boundary between two statistically independent clutter regions. We consider three different assumptions on knowledge of the clutter covariance structure: both clutter types totally unknown, one of the clutter types known except for its variance, and one of the clutter types completely known. Here we design adaptive detection algorithms using both the generalized likelihood ratio (GLR) and the invariance principles. There has been considerable recent interest in applying invariant hypothesis testing as an alternative to the GLR test. This interest has been motivated by several attractive theoretical properties of invariant tests including: exact robustness to variation of nuisance parameters, possible finite-sample min-max optimality, and distributional robustness, i.e. insensitivity to changes in the underlying probability distribution over a particular class. Furthermore, in some important cases the invariant test gives a reasonable test while the GLR test has worse performance than the trivial coin flip decision rule. By exploiting the known covariance structure, a set of maximal invariants is obtained and compared to the GLR procedure. These maximal invariants are a compression of image data which retain target information while being invariant to clutter parameters. In our deep-hide target detection problem, however, there are regimes for which either of the GLR and the invariant tests can outperform the other. We explore the relative advantages of GLR and invariance procedures and their robustness to segmentation errors in the context of this radar imaging and target detection application.

To Sejung and my parents

ACKNOWLEDGEMENTS

First and foremost, I would like to thank my thesis advisor Prof. Alfred Hero. I appreciate his patience and inspiration throughout this study. Without his support and guidance, this work would not have been possible. It owes much of its quality to his suggestions on how to approach problems, his in-depth analysis of results, and his vast knowledge of the literature. Those will also be a tremendous and invaluable asset to me. I also thank him for providing me financial support through a research assistantship. I would like to thank the other members of my dissertation committee, Prof. Jeffrey Fessler, Prof. John Volakis, and Prof. William Williams. I deeply appreciate their help in making this thesis as complete as possible. I also thank Beth Olsen and Susan Yale in the Systems office for their kind help which has been always accompanied by big smiles.

I am grateful to many members of Image Computing Laboratory and Communications and Signal Processing Laboratory including Bing, Jia, Robby, and Robinson for the fellowship over the years. They have been caring friends as well as great colleagues. I owe special thanks to my former office mate Hyun-Mog Park for his devoted friendship which has been and will always be invaluable to me. I would also like to thank a lot of Korean students in Ann Arbor and East Lansing for the happy memories in Michigan over the years, and helping appease my homesickness. On this opportunity, I would like to say good-byes to my old friend Yongjae Kim and my youngest cousin Hyunsoo whom I lost during this study.

My special gratitude extends to my brother Taesoo for his consistent encouragement and unusual confidence in me. Also, many thanks to my parents-in-law and my three sisters-in-law for their support and love.

Above all, I cannot thank my parents enough for their love and sacrifices. They have been a source of my wisdom and consolation. Without their patient support, I would not have been able to complete this study; without them, I would not even have planned to start it. I am definitely indebted to my parents for what I am today. Finally, I would like to thank my wife Sejung for everything. For more than a decade we have been together, she

has been always there for me loving me, understanding me, following me, and completing me. While I know how small it is, I dedicate this thesis to Sejung and my parents.

TABLE OF CONTENTS

LIST OF TABLES

LIST OF FIGURES

LIST OF APPENDICES

APPENDIX

CHAPTER 1

Introduction

In this chapter, we introduce the detection problem addressed in this thesis, and describe the organization of the thesis.

1.1 Motivation and Contribution

The objective of this thesis is to develop and analyze adaptive detection algorithms for imaging radar (IR) targets in *structured* clutter. In this context, both the generalized likelihood ratio (GLR) principle and the invariance principle are exploited.

In automatic target recognition (ATR), it is important to be able to reliably detect or classify a target in a manner which is robust to target and clutter variability yet maintains the highest possible discrimination capability. When the clutter statistics are unknown or highly variable, the false alarm rate of classical detection algorithms, e.g. the matched filter, cannot be controlled and target detection decisions become unreliable. The reason for this is lack of robustness of the test statistics to clutter variations, and recent statistical signal processing development is constant false alarm rate (CFAR) detection. The objective of robust CFAR detection is to produce a test statistic whose probability distribution does not depend on the unknown noise parameters, e.g. noise power or clutter spectrum, while ensuring a high probability of signal detection. Such a detector is also sometimes referred to as a noise adaptive detector. For a CFAR test statistic, the detection threshold can be set to guarantee a prespecified false alarm rate.

The GLR and invariance principles are worthwhile approaches since they often yield good CFAR tests. The GLR principle implements the intuitive estimate-and-plug procedure: replacing all unknowns in the likelihood ratio (LR) test by their maximum likelihood

1

estimates (MLEs). The GLR is known to be asymptotically optimal, i.e. GLR becomes uniformly most powerful (UMP) in that it attains the highest probability of correct detection for given probability of false alarm (P_{FA}), as the number of observations become much larger than the number of unknown clutter parameters [65]. In contrast, the application of the principle of invariance, also called exact robustness [30], seeks to project away the clutter parameters by compressing the observations down to a lower dimensional statistic while retaining the maximal amount of information for discrimination of the target [16, 18, 44, 56]. This statistic is called the maximal invariant and, if one is lucky, the form of the most powerful (MP) LR test based on the maximal invariant does not depend on the nuisance parameters, resulting in a uniformly most powerful invariant (UMPI) test [57, 58]. When properly applied, the invariance principle can yield adaptive target detection algorithms which outperform the GLR test, sometimes by a significant margin. As we will show in this thesis, for the problem of target detection in unknown but structured clutter background, this margin of improvement can be quite significant at low signal-to-noise ratio (SNR) for small fixed P_{FA}.

A common assumption in homogeneous but uncertain clutter scenarios is that the target is of known form but unknown amplitude in Gaussian noise whose covariance matrix is totally unknown or *unstructured*. This assumption induces parameter uncertainty for which the general multivariate analysis of variance (GMANOVA) model applies and optimal and suboptimal detection algorithms can be easily derived using the GLR principle [11, 34, 35, 50, 53]. In [34], the GLR principle produced an adaptive detector for detecting spatio-temporal signals in Gaussian noise with unknown spatial covariance. A different adaptive detector was derived using the GLR in [11] for the case of optical images. The GLR for a general multi-channel measurement was derived in [35] which specializes to the cases derived in [34] and [11] via a coordinate transformation. A related result was presented in [52] where exact confidence regions for the GLR maximizing the signal vector were derived for unknown spatial covariance. Additional applications of the GLR to multi-spectral infrared images can be found in [51] and [67].

When some structure on the covariance matrix is known a priori, improvements over this GLR test are possible. For example, in the context of antenna arrays for detection of an impinging wavefront in clutter whose covariance matrix has Toeplitz structure, Fuhrmann [19] showed through simulation that a significant improvement over the GLR test [34] is achieved by incorporating a Toeplitz constraint into the covariance estimation step in the

GLR detector. As previously mentioned, an alternative approach to estimation of the partially known noise covariance is to project the data down to a test statistic whose noise-alone distribution does not depend on this covariance. Bose and Steinhardt [6] proposed such an invariant detector and showed that it outperforms the GLR for unstructured covariance when the noise covariance matrix is assumed to have a priori known block diagonal structure. In [24], the difficult deep-hide scenario was considered where the target parks along a known boundary separating two adjacent clutter regions, e.g. an agricultural field and a forest canopy. It was shown there that under the reasonable assumption that the two clutter types are statistically independent, the induced block diagonal covariance structure can be used to derive an invariant test with performance advantage similar to Bose and Steinhardt's test.

In this thesis, we derive the form of the GLR for block structured covariance. Then the invariant approach considered in [6] and [24] is developed in the context of imaging radar for deep-hide targets, and compared to the GLR. In this context, the spatial component has clutter covariance matrix $\mathbf{R}$, which decomposes into a block diagonal matrix under an independence assumption between the two clutter regions, and the target is assumed to come from a known set of signatures of unknown amplitudes and orientations. Several cases, denoted in decreasing order of uncertainty as Cases 1, 2 and 3, of block diagonal covariance matrices are examined:

$$\mathbf{R} = \left[\begin{array}{cc} \mathbf{R}_A & \mathbf{O} \\ \mathbf{O} & \mathbf{R}_B \end{array} \right] \tag{1.1}$$

- Case 1: $\mathbf{R}_A > 0$, $\mathbf{R}_B > 0$

- Case 2: $\mathbf{R}_A > 0$, $\mathbf{R}_B = \sigma^2 \mathbf{I}$ where $\sigma^2 > 0$

- Case 3: $\mathbf{R}_A > 0$, $\mathbf{R}_B = \mathbf{I}$

where the subscripts denote the two different regions A and B. Case 1 corresponds to two completely unknown clutter covariance matrices $\mathbf{R}_A$ and $\mathbf{R}_B$, and Case 2 corresponds to one clutter covariance $\mathbf{R}_A$ completely unknown and the other $\mathbf{R}_B$ known up to a scale parameter. As shown in [6] the known clutter covariance matrix in $\mathbf{R}_B$, represented by the matrix $\mathbf{I}$, can be taken as the identity matrix without loss of generality. Case 3 corresponds to $\mathbf{R}_B$ known exactly. Cases 2 and 3 arise, for example, in application where one of the clutter regions is well characterized.

For real valued observations, the GLR method is shown to have explicit form for each of Cases 1, 2 and 3, involving the roots of a 4th order algebraic equation. For complex valued observations, 4th order algebraic equations for real and imaginary parts of the unknown target amplitude must be solved numerically. The maximal invariant statistics for Cases 1 and 2 were previously derived by Bose and Steinhardt and invariant tests were proposed based on these statistics in [6]. We treat Cases 1-3 in a unified framework and propose alternative maximal invariant (MI) tests which are better adapted to the deep-hide target application.

We show via simulation that there are regimes of operation which separate the performance of the GLR and MI tests. When there are a large number of independent snapshots of the clutter, the MLEs of the target amplitude and the block diagonal clutter covariance are reliable and accurate, and the GLR test performs as well as the MI test. Conversely, when a limited number of snapshots are available and SNR is low, the MLEs are unreliable and the MI test outperforms the GLR test. This property is also confirmed by the real data example, i.e. the MI test can detect weaker targets than the other tests when the number of snapshots is few. We show that the relative advantages between the GLR and MI tests are robust to errors in segmenting an unknown but structured clutter image. The main results of this thesis are presented in [37, 38, 39].

1.2 Organization

In Chapter 2, the image model for the detection problem is introduced in the context of radar imaging. We first establish the general unstructured model from the GMANOVA assumption, which is extended to the structured one. For each model, a canonical form is obtained by coordinate transformation, and the detection problem is stated accordingly as hypothesis testing. We then review the detection theory including the principles of GLR and invariance in Chapter 3. Kelly's GLR test [34] for an unstructured covariance matrix is derived as an illustration of these two principles. There we show that the GLR test is also an invariant test under the totally unknown clutter covariance, which does not hold for structured clutter.

Chapter 4 reviews the application of these two principles to detect a target across a clutter boundary. Three GLR tests are derived matched to one of the three cases listed in the previous section. Then, based on the sets of maximal invariants defined in propositions,

we propose three MI tests. All the results for the test statistics are summarized in tables in Section 4.4 for a quick review. We also extend the detection problem from a single target to one of multiple targets. This problem, discussed in Chapter 5, arises from the fact that a single target can seem differently in different positions or different pose angles. There we consider both unstructured and structured cases.

Chapter 6 explores the relations between the GLR and MI tests by simulation and by analysis. The relative advantages of those two principles are investigated according to several factors including SNR, dimensional parameters, and the prior uncertainty in the spatial covariance. The properties developed there are also confirmed by experiments with a real synthetic-aperture radar (SAR) image which consists of a forest canopy and a grass field. Then we investigate the sensitivity of our structured detectors to segmentation errors. Finally, possible extensions of this research are proposed in Chapter 7.

CHAPTER 2

Image Model

In this chapter, we briefly review radar imaging for target detection application and define the image model under which our detection algorithms will be developed. Problems of interest are stated for both the unstructured and the structured models.

2.1 Radar Imaging

Detection of targets in radar images is a multi-stage process involving pre-processing, image formation from raw data, and formation of a test statistic. In this section, we review some issues regarding imaging radars and their image outputs to which we can apply detection algorithms. Further information on the image formation problem for radar can be found in remote sensing books such as [28, 45, 59, 60, 64].

Radiometric sensors are usually divided into two groups according to their modes of operation: passive sensors or radiometers, and active sensors such as imaging or non-imaging radar. Most imaging radars used for remote sensing are divided into two groups: the real-aperture systems that depend on the beamwidth determined by the baseline of a fixed antenna, and the synthetic-aperture systems that form a virtual baseline with a moving antenna. Synthetic-aperture radar (SAR) systems can acquire fine resolution using a small antenna with spatial resolution independent of the radial distance to target, which has made spaceborne imaging radar with fine resolution feasible [64]. Although we restrict our attention to detection problems for radar images, the same techniques can be applied to passive sensors such as long-wave infrared or thermal radiometers.

In active imaging radars, the returned signals are processed to extract complex images of target reflectivity which consist of magnitude and phase information. Figure 2.1 displays
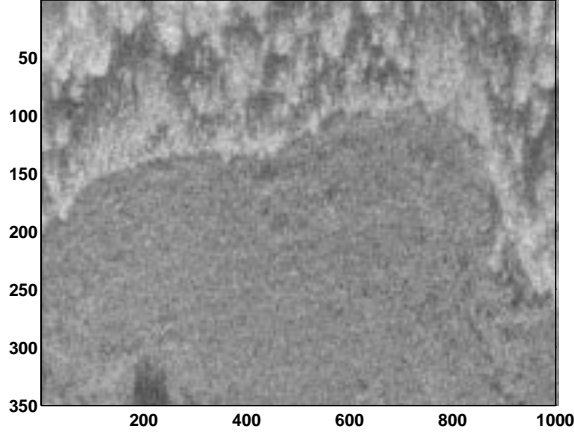
Figure 2.1: SAR image example.

the magnitude of such a complex valued SAR image which has been converted into decibels (dB). It is common to model a complex valued radar image as linear in the target with additive Gaussian distributed clutter. Examples where a Gaussian model is justified for terrain clutter can be found in [13]. Even in cases when such a model is not applicable to the raw data, a whitening and local averaging technique can be implemented to obtain a Gaussian approximation, e.g. by subtracting the local mean from the original image while minimizing the third moment of the residual image [11, 51].

Assume that the complex image has been scanned or reshaped into an $m \times 1$ column vector $\underline{x}$. If multiple snapshots $\underline{x}_1, \ldots, \underline{x}_n$ of the terrain are available, they can be concatenated into a spatio-temporal matrix $\mathbf{X}$ with columns $\{\underline{x}_i\}_{i=1}^{n}$. We will call each of these columns subimages or chips. Let $\underline{s}$ be the reshaped target vector to be detected in a clutter background $\mathbf{N}$ having independent, identically distributed (i.i.d.) Gaussian columns with zero mean. Then we have the simple image model

$$\mathbf{X} = a\, \underline{s}\, \underline{b}^H + \mathbf{N}$$

where a is an unknown target amplitude and $\underline{b}^H$ accounts for the articulation of the target vector into the snapshot sequence, e.g. possible chip locations of the target. Concrete examples are: multi-spectral images where subimages correspond to a scene at n different optical or radar wavelengths (Figure 2.2); multiple pulse SAR images where repeated probing of a scene produces a sequence of n subimages (Figure 2.3); polarized L or C band SAR where subimages correspond to $m = 3$ polarization components (HH, HV, VV) at n different spatial locations; or n non-contiguous spatial cells of a single IR/SAR image (Figure 2.4).

7
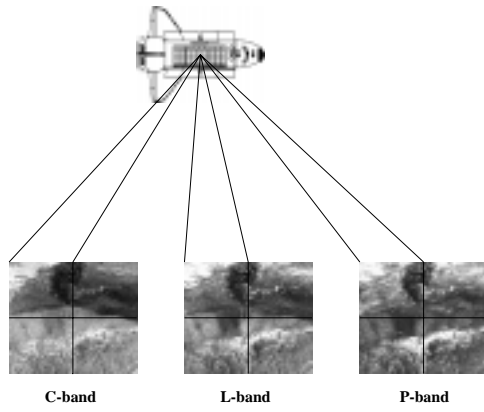
Figure 2.2: Multi-spectral radar example.

Figure 2.3: Multiple-dwell radar example.
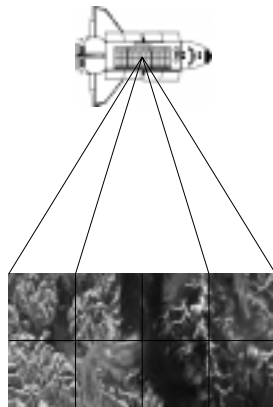
Figure 2.4: Spatially-scanned radar example.

In spatially scanned radar images, the vector $\underline{b}^H$ would be equal to $[1, 0, \ldots, 0]$ if the target presence is to be detected in the first image chip (1st column of $\mathbf{X}$). In this case, this column will be called primary data while the rest of $\mathbf{X}$ will be called secondary data. In multi-spectral images, described in [60] and studied by Reed [51], $a\underline{s}$ can be thought of as a vector of unknown spectral intensities and $\underline{b}^H$ represents the known spatial signature. We will consider a more general p target model in Section 2.3 and later in Chapter 5.

2.2   Deep-Hide Scenario under Structured Covariance

The most common assumption for clutter is that its spatial covariance matrix is completely unknown. This assumption makes derivation of the GLR decision rule easy and leads to a CFAR test for which the false alarm rate is independent of the actual covariance of the clutter [34, 35]. However, when available, inclusion of side information about the noise clutter covariance will give improved performance, even though the derivation of the GLR is often rendered more difficult. Such examples of side information are positivity or Toeplitz constraints [19].

In [6], Bose and Steinhardt applied the structured covariance matrix to the array detection problem, which is equivalent to the one defined as Case 2 in the previous chapter. Then the corresponding image model can be partitioned as

$$
\left[\begin{array}{c} \mathbf{X}_A \\ \mathbf{X}_B \end{array} \right] = a\,\underline{s}\,\underline{b}^H + \left[\begin{array}{c} \mathbf{N}_A \\ \mathbf{N}_B \end{array} \right]
$$

with $\mathbf{N}_A$ having the unknown covariance matrix $\mathbf{R}_A$, and $\mathbf{N}_B$ having the diagonal covariance matrix with unknown variance σ^2. This structure corresponds to the multi-path environment in which there is a low-rank interference component superimposed on the white noise. We also applied a block diagonal structure to the clutter covariance matrix by assuming that a target to be detected may lie along the boundary of two statistically independent clutter regions. This assumption may lead to a deep-hide scenario compared to that of totally unknown clutter. Also the structure of the covariance matrix may complicate the design of optimal detectors. Nonetheless, as will be shown later, the payoff can be quite significant.

2.3 Problem Formulation

2.3.1 Unstructured Covariance Model

As explained in Section 2.1, let $\{\underline{x}_i\}_{i=1}^n$ be n statistically independent $m \times 1$ complex Gaussian vectors constructed by raster scanning a set of n 2-D images. These vectors are assumed to each have identical $m \times m$ covariance matrices $\mathbf{R}$ but with possibly different mean vectors (targets). Then by concatenating these n vectors we obtain the measurement image matrix ($m \times n$) $\mathbf{X} = [\underline{x}_1, \ldots, \underline{x}_n]$. This matrix can be modeled as follows

$$\mathbf{X} = \mathbf{S}\,\underline{a}\,\underline{b}^H + \mathbf{N} \tag{2.1}$$

where $\mathbf{S} = \begin{bmatrix} \underline{s}_1, \ldots, \underline{s}_p \end{bmatrix}$ is an $m \times p$ matrix consisting of signature vectors of p possible targets, $\underline{a} = [a_1, \ldots, a_p]^T$ is a $p \times 1$ unknown target amplitude vector for p targets, and $\underline{b}^H = [b_1, \ldots, b_n]$ is a $1 \times n$ target location vector which accounts for the presence of target(s) in each subimage. Also we assume that $\mathbf{N}$ is a complex multivariate Gaussian matrix with i.i.d. columns: $vec\{\mathbf{N}\} \sim \mathcal{CN}(\underline{0}, \mathbf{R} \bigotimes \mathbf{I}_n)$ where $\underline{0}$ is an $mn \times 1$ zero vector, $\mathbf{I}_n$ is an $n \times n$ identity matrix, and $\bigotimes$ is the Kronecker product. This model is a simplified form of the GMANOVA model

$$\mathbf{X} = \mathbf{S}\,\mathbf{A}\,\mathbf{B} + \mathbf{N}$$

where $\mathbf{S}$ ($m \times p$) of rank p and $\mathbf{B}$ ($p \times n$) of rank p are known matrices, and $\mathbf{A}$ ($p \times p$) is a matrix of unknown amplitudes [30]. In this paper, the simpler form (2.1) will be used throughout and correspond to the assumption that the target location vectors (rows of $\mathbf{B}$) for p targets are all identical, i.e. the target components in different subimages differ only by a scale factor.

The detection problem is to seek the presence of target(s) for $\mathbf{S}$ and $\underline{b}$ known, $\underline{a}$ unknown, and the independent columns of $\mathbf{N}$ having the unknown covariance matrix $\mathbf{R}$. By applying coordinate rotations to both of the column space and the row space of $\mathbf{X}$ we can put the image model into a convenient canonical form as in [35]. Let $\mathbf{S}$ and $\underline{b}$ have the QR decompositions

$$\mathbf{S} = \mathbf{Q}_S \begin{bmatrix} \mathbf{T}_S \\ \mathbf{O} \end{bmatrix} \text{ and } \underline{b} = \mathbf{Q}_b \begin{bmatrix} t_b \\ \underline{0} \end{bmatrix},$$

respectively, where $\mathbf{Q}_S(m \times m)$ and $\mathbf{Q}_b(n \times n)$ are unitary matrices, $\mathbf{T}_S$ is a $p \times p$ upper-triangular matrix, and t_b is a scalar. Multiplying $\mathbf{X}$ on the left and right by $\mathbf{Q}_S^H$ and $\mathbf{Q}_b$,

respectively, we have the canonical representation

$$\tilde{\mathbf{X}} = \mathbf{Q}_S^H \, \mathbf{X} \, \mathbf{Q}_b = \begin{bmatrix} \mathbf{T}_S \\ \mathbf{O} \end{bmatrix} \underline{a} \begin{bmatrix} t_b^H & \underline{0}^H \end{bmatrix} + \tilde{\mathbf{N}}$$

where $\tilde{\mathbf{N}}$ is still n-variate normal with $vec\{\tilde{\mathbf{N}}\} \sim \mathcal{CN}(\underline{0}, (\mathbf{Q}_S^H \, \mathbf{R} \, \mathbf{Q}_S) \bigotimes \mathbf{I}_n)$ and the target detection problem is not altered since $\mathbf{R}$ is unknown. Now the transformed data has the partition

$$\tilde{\mathbf{X}} = \begin{bmatrix} \underline{x}_{11} & \mathbf{X}_{12} \\ \underline{x}_{21} & \mathbf{X}_{22} \end{bmatrix}$$

where $\underline{x}_{11}$ is a $p \times 1$ vector, $\underline{x}_{21}$ is a $(m - p) \times 1$ vector, $\mathbf{X}_{12}$ is $p \times (n - 1)$, and $\mathbf{X}_{22}$ is $(m - p) \times (n - 1)$. Note that $\mathbf{Q}_S^H$ and $\mathbf{Q}_b$ have put all the target energy into the first p pixels of the first subimage, $\underline{x}_{11}$. This canonical form is identical to the one found in [8]. In the sequel, unless stated otherwise, we will assume that the model has been put into this canonical form.

For the special case of $p = 1$ (single target), this model reduces to the one studied by Kelly [34]

$$\mathbf{X} = a \, \underline{\varepsilon}_1 \, \underline{e}_1^T + \mathbf{N} \tag{2.2}$$

where a is an unknown complex amplitude, $\underline{e}_1 = [1, 0, \dots, 0]^T$ is the $n \times 1$ unit vector, and the known target signature is transformed into an $m \times 1$ unit vector $\underline{\varepsilon}_1$. With the model (2.2) we can denote the unknowns by the unknown parameter vector $\theta = \{a, \mathbf{R}\} \in \Theta$ where Θ is the prior parameter range of uncertainty. Let Θ_0 and Θ_1 partition the parameter space into target absent (H_0) and target present (H_1) scenarios: $\Theta_0 = \{a, \mathbf{R} : a = 0, \mathbf{R} \in \text{Hermitian}(m \times m)\}$, $\Theta_1 = \{a, \mathbf{R} : a \neq 0, \mathbf{R} \in \text{Hermitian}(m \times m)\}$. Then the general form for the detection problem is expressed via the two mutually exclusive hypotheses:

$$H_0 \quad : \quad \mathbf{X} \sim f(\mathbf{X}; \theta_0), \; \theta_0 = \{0, \mathbf{R}\} \in \Theta_0$$
$$H_1 \quad : \quad \mathbf{X} \sim f(\mathbf{X}; \theta_1), \; \theta_1 = \{a, \mathbf{R}\} \in \Theta_1.$$

2.3.2   Structured Covariance Model

Now, following [6], we extend (2.2) to the structured covariance case. Consider Case 1 in Section 1. This is the scenario where a target parks along a known boundary of the two unknown but independent clutter regions A and B. Then for $p = 1$ the target signature $\underline{s}$

11

is partitioned as

$$\underline{s} = \left[\begin{array}{c} \underline{s}_A \ (m_A \times 1) \\ \underline{s}_B \ (m_B \times 1) \end{array} \right]$$

where $m_A + m_B = m$, and the unitary matrices $\mathbf{Q}_{S_A}$ and $\mathbf{Q}_{S_B}$ can be obtained from the QR decompositions of $\underline{s}_A$ and $\underline{s}_B$, respectively. Using

$$\mathbf{Q}_S = \left[\begin{array}{cc} \mathbf{Q}_{S_A} & \mathbf{O} \\ \mathbf{O} & \mathbf{Q}_{S_B} \end{array} \right]$$

in the canonical transformation,the model is then composed of two parts from regions A and B

$$\mathbf{X} = \left[\begin{array}{c} \mathbf{X}_A \\ \mathbf{X}_B \end{array} \right] = a \left[\begin{array}{c} \tilde{\underline{s}}_A \\ \tilde{\underline{s}}_B \end{array} \right] \underline{e}_1^T + \left[\begin{array}{c} \mathbf{N}_A \\ \mathbf{N}_B \end{array} \right] \tag{2.3}$$

where $\tilde{\underline{s}}_A = \left[s_A^H, 0, \ldots, 0 \right]^H$ and $\tilde{\underline{s}}_B = \left[s_B^H, 0, \ldots, 0 \right]^H$. Note that s_A and s_B are the only nonzero element in the transformed signatures $\tilde{\underline{s}}_A$ and $\tilde{\underline{s}}_B$, respectively. Also $\mathbf{N}_A \ (m_A \times n)$ and $\mathbf{N}_B \ (m_B \times n)$ are independent Gaussian matrices with unknown covariance matrices $\mathbf{R}_A \ (m_A \times m_A)$ and $\mathbf{R}_B \ (m_B \times m_B)$, respectively. The target detection problem is now simply stated as testing $a = 0$ vs. $a \neq 0$ in (2.3).

CHAPTER 3

Detection Theory as Hypothesis Testing

3.1 Introduction

Detection and classification arise in signal processing problems whenever a decision is to be made among a finite number of hypotheses concerning an observed waveform [12, 43]. The fundamental theory behind detection and classification was developed in mathematical statistics and decision theory, and signal detection is a special case of hypothesis testing theory in statistical inference [18, 40].

As explained in the previous chapter, given an observation $\mathbf{X}$ a decision has to be made between two hypotheses corresponding to presence of a target (H_1) or no target (H_0), respectively. This is a simple binary hypothesis testing where the noise alone hypothesis H_0 is referred to as the null hypothesis, and the signal present hypothesis H_1 as the alternative hypothesis. Then, in the parametric problem, the measurement $\mathbf{X}$ has the probability density function (pdf) $f(\mathbf{X}; \theta)$ and under each hypothesis

$$
\begin{aligned}
H_0 &: \quad \theta \in \Theta_0 \\
H_1 &: \quad \theta \in \Theta_1
\end{aligned}
$$

where $\{\Theta_0, \Theta_1\}$ can be considered as a partition of the prior parameter space Θ in the sense that they are

$$
\begin{aligned}
\Theta_0 \cup \Theta_1 &= \Theta \quad \text{(exhaustive)}, \\
\Theta_0 \cap \Theta_1 &= \emptyset \quad \text{(disjoint)}.
\end{aligned}
$$

Now the objective is to make a decision between H_0 and H_1 with small error, based on a measurement $\mathbf{X}$. This decision is equivalent to partitioning the observation space $\mathbf{X}$ into

$\mathbf{X}_0$ and $\mathbf{X}_1$ where all values of $x \in \mathbf{X}_0$ or $x \in \mathbf{X}_1$ are such that H_0 or H_1 is decided, respectively.

There are two general strategies for deciding between H_0 and H_1: the Bayesian strategy and the frequentist strategy. In Bayes approach to detection, priors are assigned to the probabilities of H_0 and H_1, and it is assumed that θ is a random variable or vector with a known pdf $f(\theta)$. After assigning a set of costs to incorrect decisions, the Bayes objective is to find and implement a decision rule which has minimum average cost or risk. In many situations, however, it is difficult to assign not only the priors but also the cost under each hypothesis. Moreover, the Bayes approach assures good performance only for the average parameter values over Θ_0 and Θ_1. The Bayes approach does not control the performance of a test for any specific parameter value which can arise. Also it provides no guaranteed protection against false alarm (deciding H_1 when H_0 is true) and miss (deciding H_0 when H_1 is true). The other approach is to work with the probability of false alarm (P_{FA}) and the probability of detection (P_D). Note that P_D is the probability of deciding H_1 when H_1 is true and $P_D = 1 - P_M$ where P_M is the probability of miss. The basic idea behind this frequentist approach to detection is to constrain P_{FA} and maximize P_D or minimize P_M.

In the next section, we discuss different kinds of hypotheses and consider other optimal criteria for detection. More details of the detection theory can be found in [1, 18, 40, 44, 48, 62, 65].

3.2   Constrained Optimal Strategies

Hypotheses are divided into two classes according to the parameter θ underlying pdfs of each of the hypotheses. When θ can take on only one value, fixed and known, under each hypothesis, the hypotheses are said to be simple. In this case, the pdf $f(\mathbf{X}; \theta)$ is known given H_0 or H_1. Otherwise, hypotheses are said to be composite. In singly composite hypotheses, only one of Θ_0 or Θ_1 contains a set of values of θ, and in doubly composite hypotheses, both Θ_0 and Θ_1 contain a set of values of θ. Thus composite hypotheses only specify a family of pdfs for $\mathbf{X}$.

For simple hypotheses, $\Theta_0 = \{\theta_0\}$ and $\Theta_1 = \{\theta_1\}$, the frequentist approach attempts to maximize the conditional P_D for fixed conditional P_{FA}, or vice versa, resulting in the Neyman-Pearson test. Specifically, a maximum tolerable level α of false alarm is specified

14

as

$$P_{FA}(\theta_0) \leq \alpha$$

where $P_{FA}(\theta) = P(\text{decide} H_1 | H_0; \theta)$ and a decision rule is selected which attains the largest P_D among all tests of level α. This test is also called the most powerful (MP) test [40].

In testing simple hypotheses, both Bayes and Neyman-Pearson criteria lead to the same decision rule involving the likelihood ratio (LR) test. The only difference lies in the selection of the thresholds applied to the test statistic. However, in a general problem of testing composite hypotheses the two approaches differ substantially. For non-random θ, if such a test existed, a frequentist would select a test of level α satisfying

$$\max_{\theta \in \Theta_0} P_{FA}(\theta) \leq \alpha$$

which has the highest $P_D(\theta)$ among all tests of level α and for all $\theta \in \Theta_1$. Such a test is called a uniformly most powerful (UMP) test. Whenever a UMP test exists, it works as well as if we knew θ. Usually, however, such a test does not exist since the optimal decision region of an LR test depends on the unknown parameters $\{\theta_0, \theta_1\}$, and consequently we need to adopt other alternative strategies. For instance, in testing doubly composite hypotheses, most detectors will have their P_{FA} and P_D varying as functions of unknown $\theta \in \Theta_0$ and $\theta \in \Theta_1$, respectively. In such cases, two classes of strategies can be used: one is to optimize an alternative decision criterion and the other is to constrain the form of detectors to a class for which a UMP test may exist. Several methods utilizing one of these strategies are listed below.

Some examples of alternative criterion are the minimax test and the locally most powerful (LMP) test. A minimax test is a test of level α which maximizes the worst case power

$$\min_{\theta \in \Theta_1} P_D(\theta)$$

and it is sometimes possible to arrive at minimax optimal detectors [61] through the method of similar tests [40]. In order to implement this test, we need to find the least favorable density which maximizes P_D while constraining the specific level of P_{FA}. Thus the minimax detector can be viewed from the point of view of Bayesian detection implemented with a lease favorable prior on the unknown noise density. However, the performance of a minimax test can be overly conservative especially if least favorable priors concentrate on atypical

values of θ. Furthermore, the least favorable priors may be difficult to find in practice. The main idea behind a LMP test is to find the MP test for detecting a small perturbation of parameters from H_0. The LMP test is particularly useful for weak signals.

Some examples of constrained classes of tests are unbiased tests, CFAR tests, and invariant tests. Unbiased tests are all tests of level α whose $P_D(\theta)$ is greater than α for all $\theta \in \Theta_1$. CFAR refers to the property that the tests have constant false alarm probability over Θ_0. Sometimes UMP CFAR tests exist when UMP tests do not exist. Finally, invariant tests seek to find a transformation or compression of the data, which results in reducing the effect of nuisance parameters. In many cases, the invariant and unbiased classes of tests contain the minimax optimal test [18, 40].

3.3 GLR Principle

Generally, optimality is not guaranteed in a composite hypothesis test which involves highly variable nuisance parameters, and a UMP test rarely exists. When such a test does not exist, a popular sub-optimal strategy is to use the GLR principle. With unknown parameters θ in the likelihood ratio, a logical procedure is to find good estimates of θ under H_0 and H_1, and substitute these estimates into the likelihood ratio statistic as if they were true. This is akin to reformulating H_0 and H_1 as simple hypotheses depending on the estimated θ values for which an MP test always exists. In GLR procedures, the pdfs of the measurement under both hypotheses are maximized separately over all unknown parameters by replacing them with their maximum likelihood estimates (MLEs), $\hat{\theta}_0$ and $\hat{\theta}_1$:

$$\frac{\max_{\theta \in \Theta_1} f(\mathbf{X}; \theta)}{\max_{\theta \in \Theta_0} f(\mathbf{X}; \theta)} = \frac{f(\mathbf{X}; \hat{\theta}_1)}{f(\mathbf{X}; \hat{\theta}_0)}.$$

One of the main justifications of the GLR principle is its asymptotic optimality [31, 32]. As a function of MLEs, the GLR test is asymptotically UMP since, under broad conditions [26], MLEs are consistent estimators as the number of observations goes to infinity. And in many physical problems of interest, either a UMP test will exist or a GLR test will give satisfactory results [65]. However, there are two factors which can make the GLR test unworkable in applications. First, the optimization or maximization involved in deriving a GLR test may be intractable to obtain in closed form in some instances, e.g. when the clutter covariance has block diagonal structure. Moreover, similarly to small sample MLEs, the performance of a GLR test can be poor (not even unbiased) in a finite sample regime [40]. In other words, use of the GLR principle entails a loss in efficiency [36, 50] which can

severely impact finite sample performance. In the next section, we review the principle of invariance as an alternative strategy.

3.4 Invariance Principle

The method of invariance involves expressing uncertainty in the unknown clutter parameters as resulting from the set of algebraic actions on the observation by an appropriate group of transformations. Once the uncertainty has been mapped to group actions, one can often identify statistics whose statistical distributions are functionally invariant to unknown noise parameters yet entail minimum loss of target discrimination capability. On the basis of these statistics likelihood ratio tests which have constant false alarm rate can often be specified. These statistics are called the maximal invariants. Despite the difficulty in finding maximal invariants and their statistical distributions, the payoff for the extra effort in signal processing applications can be high [6, 7, 55, 57, 58].

3.4.1 Sufficiency vs. Invariance

The main idea behind the invariance principle is to find a statistic which maximally condenses the data while retaining the discrimination capacity of the original data set. It is instructive to first consider the mechanism of data reduction associated with the minimal sufficient statistic [18, 40]. Recall that a function $\mathbf{T} = T(\mathbf{X})$ of the data is a sufficient statistic for testing between H_0 and H_1 if, for all $\theta_0 \in \Theta_0$ and $\theta_1 \in \Theta_1$, the likelihood ratio Λ depends on $\mathbf{X}$ only through $T(\mathbf{X})$:

$$\Lambda(\mathbf{X}; \theta_0, \theta_1) \triangleq \frac{f(\mathbf{X}; \theta_1)}{f(\mathbf{X}; \theta_0)} = g(T(\mathbf{X}); \theta_0, \theta_1).$$

The sets $\{\mathbf{X} : T(\mathbf{X}) = t\}_t$ can be thought of as sufficiency orbits of $\mathbf{X}$ which specify constant contours of $\Lambda(\mathbf{X})$. Thus a sufficient statistic $T(\mathbf{X})$ indexes the orbits and preserves all information needed to discriminate between H_0 and H_1. Sufficient statistics are not unique and $T(\mathbf{X})$ is a minimal sufficient statistic if it is a function, i.e. a compression, of any other sufficient statistic.

On the other hand, data reduction via invariance is achieved by finding a statistic $\mathbf{Z} = Z(\mathbf{X})$, called the maximal invariant statistic, which indexes the set values (which we can think of as constant contours) of the set function

$$\tilde{\Lambda}(\mathbf{X}) \triangleq \{\Lambda(\mathbf{X}; \theta_0, \theta_1) : \theta_0 \in \Theta_0, \theta_1 \in \Theta_1\}. \tag{3.1}$$

17

To make this practical, a tractable mathematical characterization of this set function must be adopted.

To illustrate the statistical reduction or data compression associated with sufficiency and invariance, consider the signal model defined in (2.2) for real valued measurements. For the special case of $m = 1$, this model reduces to

$$\underline{x} = a\,\underline{e}_1^T + \underline{N}^T$$

where, as before, $\underline{e}_1$ is an $n \times 1$ unit vector and $\underline{N}^T$ is a normal row vector with zero mean and covariance matrix $\sigma^2 \mathbf{I}$. The above model corresponds to testing for target presence at a single pixel in a sequence of n snapshots. This is a simple i.i.d. real Gaussian example with unknown parameters $\theta = \{a, \sigma^2\}$, and the pdf of $\underline{x}$ [63] is

$$f(\underline{x}) = \frac{1}{(2\pi)^{n/2}\sigma^n} \exp\left[-\frac{1}{2}\left\{\frac{(x_1 - a)^2}{\sigma^2} + \sum_{i=2}^{n}\frac{x_i^2}{\sigma^2}\right\}\right] \tag{3.2}$$

where $\underline{x} = [x_1, x_2, \ldots, x_n]$. Since the objective is to decide whether $a = 0$ or $a \neq 0$ when σ^2 is unknown, we define $\theta_0 = \{0, \sigma_0^2\}$ and $\theta_1 = \{a, \sigma_1^2\}$ which are points in $\Theta_0 = \{a, \sigma^2 : a = 0, \sigma^2 > 0\}$ and $\Theta_1 = \{a, \sigma^2 : a \neq 0, \sigma^2 > 0\}$, respectively. The likelihood ratio is

$$\Lambda(\underline{x}; \theta_0, \theta_1) = \frac{f(\underline{x}; a, \sigma_1^2)}{f(\underline{x}; 0, \sigma_0^2)}.$$

With the pdf (3.2), we can express the log likelihood ratio as a function of $\underline{x}$:

$$\ln \Lambda(\underline{x}; \theta_0, \theta_1) = \frac{a}{\sigma_1^2} \cdot \underline{e}_1^T \underline{x} + \frac{\sigma_1^2 - \sigma_0^2}{2\sigma_0^2 \sigma_1^2} \cdot \underline{x}^T \underline{x} - \frac{a^2}{2\sigma_1^2} + n \ln \frac{\sigma_0}{\sigma_1}$$

where $a \in \mathbb{R}$ and $\sigma_0^2, \sigma_1^2 > 0$. Thus Λ depends on $\underline{x}$ only through $T(\underline{x}) = \{t_1, t_2\}$ where $t_1 = \underline{e}_1^T \underline{x}$ and $t_2 = \underline{x}^T \underline{x}$. $T(\mathbf{X})$ is a minimal sufficient statistic indexing the sufficiency orbit illustrated in Figure 3.1 as a circle in $\mathbb{R}^3$ when $n = 3$. Given t_1 and t_2 we can recover all of the information in the entire n-sample required to discriminate between different values of the parameter pair $\{a, \sigma^2\}$ [44]. Generally for $n > 2$, the sufficiency orbit of $\underline{x}$ is the surface of an $n - 1$ dimensional hypersphere defined by the intersection of the surfaces of the hypersphere $\{\underline{x} : \sum_{i=1}^{n} x_i^2 = t_2\}$ and the hyperplane $\{\underline{x} : x_1 = t_1\}$.

This sufficient statistic is the minimum amount of information required of $\underline{x}$ to estimate the parameters $\{a, \sigma^2\}$. The maximal invariant is the minimum amount of information required to discriminate between the sets of parameter values Θ_0 and Θ_1, i.e. detection of the target. To determine the maximal invariant, the set function (3.1) of the likelihood
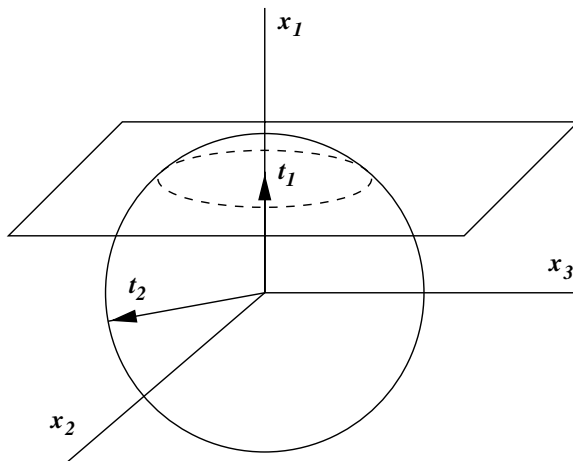
Figure 3.1: Sufficiency orbit is a circle in $\mathbb{R}^3$

ratio needs to be defined first. Since, under H_1, $a \in \mathbb{R}$ and $\sigma_0^2, \sigma_1^2 > 0$ are unknown, the contours of the log likelihood ratio can be equivalently indexed by the parameters

$$
\begin{aligned}
\tilde{a} &= a/\underline{e}_1^T \underline{x} \\
\tilde{\sigma}_0^2 &= \sigma_0^2/\underline{x}^T \underline{x} \\
\tilde{\sigma}_1^2 &= \sigma_1^2/\underline{x}^T \underline{x}.
\end{aligned}
$$

That is, we can express the set function (3.1) as

$$
\ln \tilde{\Lambda}(\underline{x}) = \left\{ \frac{\tilde{a}}{\tilde{\sigma}_1^2} \cdot \frac{\left|\underline{e}_1^T \underline{x}\right|^2}{\underline{x}^T \underline{x}} + \frac{\tilde{\sigma}_1^2 - \tilde{\sigma}_0^2}{2\tilde{\sigma}_0^2 \tilde{\sigma}_1^2} - \frac{\tilde{a}^2}{2\tilde{\sigma}_1^2} \cdot \frac{\left|\underline{e}_1^T \underline{x}\right|^2}{\underline{x}^T \underline{x}} + n \ln \frac{\tilde{\sigma}_0}{\tilde{\sigma}_1} : \tilde{a} \in \mathbb{R}; \tilde{\sigma}_0^2, \tilde{\sigma}_1^2 > 0 \right\}.
$$

We conclude that the set function (3.1) is indexed by the scalar:

$$
z(\underline{x}) = \frac{\left|\underline{e}_1^T \underline{x}\right|^2}{\underline{x}^T \underline{x}} \tag{3.3}
$$

which is the maximal invariant in this example. In Figure 3.2, the invariance orbit is illustrated as a cone in $\mathbb{R}^3$. Each invariance orbit $\{\underline{x} : \left|\underline{e}_1^T \underline{x}\right|^2 / \underline{x}^T \underline{x} = z\}$ is indexed by the equivalent maximal invariant, $x_1^2 / \sum_{i=2}^n x_i^2$, which determines the tangent of this cone. Thus, the compression to a scalar function of $\underline{x}$ provided by the maximal invariant is a more vigorous compression than that provided by the minimal sufficient statistic above.

3.4.2 Issues in Finding Maximal Invariant

The invariance principle is essentially a systematic method for data reduction which accounts for parameter uncertainty. This can be accomplished when the probability model
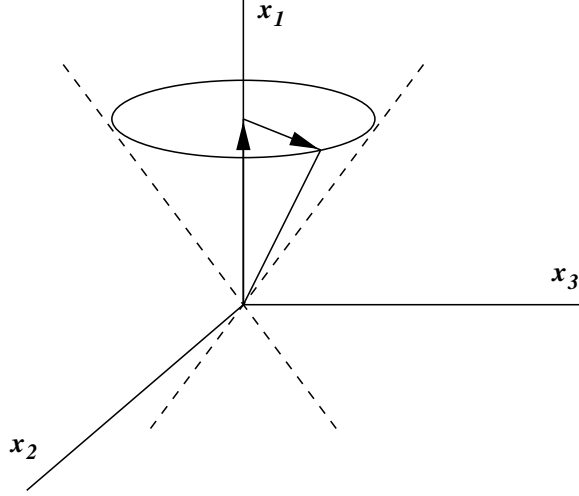
19

Figure 3.2: Invariance orbit is a cone in $\mathbb{R}^3$

has functional invariance which can be characterized by group actions on the measurement space $\mathbf{X}$ and induced group actions on the parameter space Θ. Let $\mathcal{G}$ be a group of transformations $g : \chi \to \chi$ acting on $\mathbf{X}$. Assume that for each $\theta \in \Theta$ there exists a unique $\bar{\theta} = \bar{g}(\theta)$ such that

$$f_\theta(g(\mathbf{X})) = f_{\bar{\theta}}(\mathbf{X}).$$

$\bar{g} \in \bar{\mathcal{G}}$ is called the induced group action on Θ. The above relation implies that the natural invariance which exists in the parameter space of θ implies a natural invariance in the space of measurement $\mathbf{X}$. If we further assume that $\bar{g}(\Theta_0) = \Theta_0$, $\bar{g}(\Theta_1) = \Theta_1$, then the model and the decision problem are said to be invariant to the group $\mathcal{G}$. The orbits of $\mathbf{X}$ under actions of $\mathcal{G}$ are defined by

$$\mathbf{X} \equiv \mathbf{Y} \text{ if } \exists\, g \in \mathcal{G} \text{ such that } \mathbf{Y} = g(\mathbf{X}).$$

The orbits of θ under actions of $\bar{\mathcal{G}}$ are similarly defined. Note that to capture natural invariance of the model, the groups $\mathcal{G}$ and $\bar{\mathcal{G}}$ must have group actions with the largest possible degrees of freedom among all groups leaving the decision problem invariant.

The principle of invariance stipulates that any optimal decision rule should only depend on $\mathbf{X}$ through the maximal invariant $\mathbf{Z} = Z(\mathbf{X})$ which indexes the invariance orbits in the sense that

1. (invariant property) $Z(g(\mathbf{X})) = Z(\mathbf{X})$, $\forall\, g \in \mathcal{G}$

2. (maximal property) $Z(\mathbf{X}) = Z(\mathbf{Y}) \Rightarrow \mathbf{Y} = g(\mathbf{X})$, $g \in \mathcal{G}$.

Clearly, the maximal invariant is not unique. Any other functions of $\mathbf{X}$ related to $Z(\mathbf{X})$ in a one-to-one manner can be maximal invariant. It can also be shown that the probability density $f(\mathbf{Z}; \delta)$ of $\mathbf{Z}$ only depends on θ through a reduced set of parameters $\delta = \delta(\theta)$, which is the induced maximal invariant under $\bar{\mathcal{G}}$. Use of $\mathbf{Z}$ for detection gives the equivalent set of hypotheses

$$
\begin{aligned}
H_0 &: \quad \mathbf{Z} \sim f(\mathbf{Z}; \delta(\theta_0)),\ \theta_0 \in \Theta_0 \\
H_1 &: \quad \mathbf{Z} \sim f(\mathbf{Z}; \delta(\theta_1)),\ \theta_1 \in \Theta_1.
\end{aligned}
$$

Since the new parameterization $\delta(\theta)$ is generally a dimension reducing function of θ, use of the reduced data $\mathbf{Z}$ gives us better chances of finding a CFAR test whose false alarm rate is independent of θ. In particular, when $\delta(\theta_0)$ is constant over $\theta_0 \in \Theta_0$, the distribution of $\mathbf{Z}$ under H_0 is fixed and therefore any test based on $\mathbf{Z}$ will automatically be CFAR.

When there exists a group $\mathcal{G}$ that leaves a testing problem invariant, we can restrict our attention to the class of invariant tests where a test function ϕ on $\mathbf{X}$ satisfies

$$
\phi(g(\mathbf{X})) = \phi(\mathbf{X}), \forall g \in \mathcal{G}.
$$

Any one-to-one function of the maximal invariants produces an equivalent invariant test [30].

3.5 Example: Unstructured Covariance Case

We will first consider the case where the clutter is totally unknown. Suppose that the measurement matrix is Gaussian with i.i.d. columns each having the unknown covariance matrix and the problem is to decide the presence of a known target in a known subimage with an unknown amplitude. Then we can use the image model in (2.2), $\mathbf{X} = a\,\underline{\varepsilon}_1\,\underline{e}_1^T + \mathbf{N}$, and its partitioned form

$$
\mathbf{X} = [\underline{x}_1\ \mathbf{X}_2] = \begin{bmatrix} x_{11} & \underline{x}_{12} \\ \underline{x}_{21} & \mathbf{X}_{22} \end{bmatrix} \tag{3.4}
$$

where $\underline{x}_1$ is the first subimage which may contain the target and all the target energy has been put into the first pixel x_{11} of this subimage.

This is the case studied by Kelly [34], and the results are briefly reviewed here to help illustrate the application of the GLR principle and invariance principle discussed previously. This will help the reader understand more complicated structured models of interest, covered later in this thesis.

3.5.1 GLR Approach

Since the $m \times n$ measurement matrix $\mathbf{X}$ is complex multivariate normal with $m \times n$ mean $E[\mathbf{X}] = a\,\underline{\varepsilon}_1\,\underline{e}_1^T$ and $mn \times mn$ covariance $cov[vec(\mathbf{X})] = \mathbf{R} \bigotimes \mathbf{I}$ as described in Section 2.3, the problem is to decide whether a is 0 or not when $\mathbf{R}$ is unknown. If we write the i.i.d. columns of $\mathbf{X}$ as $\{\underline{x}_1, \underline{x}_2, \ldots, \underline{x}_n\}$, the pdf of $\mathbf{X}$ [46] is

$$
\begin{aligned}
f(\mathbf{X}) &= \frac{1}{\pi^{mn}|\mathbf{R}|^n} \exp\left[-(\underline{x}_1 - a\underline{\varepsilon}_1)^H \mathbf{R}^{-1}(\underline{x}_1 - a\underline{\varepsilon}_1) - \sum_{i=2}^{n} \underline{x}_i^H \mathbf{R}^{-1} \underline{x}_i \right] \qquad (3.5)\\
&= \frac{1}{\pi^{mn}|\mathbf{R}|^n} \exp\left[-tr\left\{ \mathbf{R}^{-1}\left((\underline{x}_1 - a\underline{\varepsilon}_1)(\underline{x}_1 - a\underline{\varepsilon}_1)^H + \sum_{i=2}^{n} \underline{x}_i \underline{x}_i^H \right) \right\} \right].
\end{aligned}
$$

Obviously, the likelihood ratio involves unknown parameters, a and $\mathbf{R}$, and we derive the GLR by maximizing the likelihood ratio over those parameters, i.e. by replacing them with their MLEs:

$$
l_1 = \frac{\max_{\theta \in \Theta_1} f(\mathbf{X}; \theta)}{\max_{\theta \in \Theta_0} f(\mathbf{X}; \theta)} = \frac{\max_a f(\mathbf{X}; a, \hat{\mathbf{R}}_1)}{f(\mathbf{X}; 0, \hat{\mathbf{R}}_0)}
$$

where $\hat{\mathbf{R}}_0$ and $\hat{\mathbf{R}}_1$ are the sample covariance matrices under H_0 and H_1, respectively. It is easily shown:

$$
\begin{aligned}
\hat{\mathbf{R}}_0 &= \frac{1}{n} \sum_{i=1}^{n} \underline{x}_i \underline{x}_i^H, \\
\hat{\mathbf{R}}_1 &= \frac{1}{n} \left[(\underline{x}_1 - a\underline{\varepsilon}_1)(\underline{x}_1 - a\underline{\varepsilon}_1)^H + \sum_{i=2}^{n} \underline{x}_i \underline{x}_i^H \right].
\end{aligned}
$$

To ensure these matrices be nonsingular with probability one, we must impose the condition that $n > m$. After canceling the exponential terms in the numerator and the denominator, the GLR l_1 can be reduced to

$$
l_1 = \max_a \frac{|\hat{\mathbf{R}}_0|^n}{|\hat{\mathbf{R}}_1(a)|^n}.
$$

To evaluate its determinant, write $\hat{\mathbf{R}}_0$ as

$$
\begin{aligned}
\hat{\mathbf{R}}_0 &= \frac{1}{n} \sum_{i=2}^{n} \underline{x}_i \underline{x}_i^H + \frac{1}{n} \underline{x}_1 \underline{x}_1^H \\
&= \bar{\mathbf{R}}^{\frac{1}{2}} \left[\mathbf{I} + \frac{1}{n} \bar{\mathbf{R}}^{-\frac{1}{2}} \underline{x}_1 \underline{x}_1^H \bar{\mathbf{R}}^{-\frac{1}{2}} \right] \bar{\mathbf{R}}^{\frac{1}{2}}
\end{aligned}
$$

where $\bar{\mathbf{R}} = \frac{1}{n} \sum_{i=2}^{n} \underline{x}_i \underline{x}_i^H$. Then from Section 8.4 in [20]

$$
\begin{aligned}
|\hat{\mathbf{R}}_0| &= |\bar{\mathbf{R}}| \cdot \left| \mathbf{I} + \frac{1}{n} \bar{\mathbf{R}}^{-\frac{1}{2}} \underline{x}_1 \underline{x}_1^H \bar{\mathbf{R}}^{-\frac{1}{2}} \right| \\
&= |\bar{\mathbf{R}}| \cdot \{ 1 + \underline{x}_1^H (n\bar{\mathbf{R}})^{-1} \underline{x}_1 \}
\end{aligned}
$$

22

and similarly,

$$|\hat{\mathbf{R}}_1| = |\bar{\mathbf{R}}| \cdot \{1 + (\underline{x}_1 - a\underline{\varepsilon}_1)^H (n\bar{\mathbf{R}})^{-1}(\underline{x}_1 - a\underline{\varepsilon}_1)\}.$$

With these results and the fact that $n\bar{\mathbf{R}} = \mathbf{X}_2\mathbf{X}_2^H$, we obtain the following simple form of the GLR for this example by taking the n-th root of l_1:

$$\sqrt[n]{l_1} = \max_a \left\{ \frac{1 + \underline{x}_1^H (\mathbf{X}_2\mathbf{X}_2^H)^{-1}\underline{x}_1}{1 + (\underline{x}_1 - a\underline{\varepsilon}_1)^H (\mathbf{X}_2\mathbf{X}_2^H)^{-1}(\underline{x}_1 - a\underline{\varepsilon}_1)} \right\}. \tag{3.6}$$

It remains to maximize this ratio over the unknown complex amplitude a. This can be done by completing the square in the denominator of (3.6):

$$1 + (\underline{x}_1 - a\underline{\varepsilon}_1)^H (\mathbf{X}_2\mathbf{X}_2^H)^{-1}(\underline{x}_1 - a\underline{\varepsilon}_1)$$
$$= \underline{\varepsilon}_1^T (\mathbf{X}_2\mathbf{X}_2^H)^{-1}\underline{\varepsilon}_1 \cdot \left| a - \frac{\underline{\varepsilon}_1^T (\mathbf{X}_2\mathbf{X}_2^H)^{-1}\underline{x}_1}{\underline{\varepsilon}_1^T (\mathbf{X}_2\mathbf{X}_2^H)^{-1}\underline{\varepsilon}_1} \right|^2 + 1 + \underline{x}_1^H (\mathbf{X}_2\mathbf{X}_2^H)^{-1}\underline{x}_1 - \frac{|\underline{\varepsilon}_1^T (\mathbf{X}_2\mathbf{X}_2^H)^{-1}\underline{x}_1|^2}{\underline{\varepsilon}_1^T (\mathbf{X}_2\mathbf{X}_2^H)^{-1}\underline{\varepsilon}_1}$$

giving the MLE of the amplitude as

$$\hat{a} = \frac{\underline{\varepsilon}_1^T (\mathbf{X}_2\mathbf{X}_2^H)^{-1}\underline{x}_1}{\underline{\varepsilon}_1^T (\mathbf{X}_2\mathbf{X}_2^H)^{-1}\underline{\varepsilon}_1}. \tag{3.7}$$

Thus the GLR test is equivalent to $1 - 1/\sqrt[n]{l_1}$, denoted T_{Ku}:

$$T_{Ku} = \frac{|\underline{\varepsilon}_1^T (\mathbf{X}_2\mathbf{X}_2^H)^{-1}\underline{x}_1|^2}{\underline{\varepsilon}_1^T (\mathbf{X}_2\mathbf{X}_2^H)^{-1}\underline{\varepsilon}_1 \cdot \{1 + \underline{x}_1^H (\mathbf{X}_2\mathbf{X}_2^H)^{-1}\underline{x}_1\}}. \tag{3.8}$$

This test was obtained by Kelly [34] and will be called the unstructured Kelly's test. Kelly also proved in [34] that this test has the CFAR property.

3.5.2 Invariance Approach

As defined above, an invariant test is a test statistic which is a function of the maximal invariants. Here, we review the derivation of the maximal invariants under the unstructured model described above, and prove that the Kelly's GLR test can be represented with the maximal invariant statistics.

With the previous model, we can define the following group of transformations acting on $\mathbf{X}$ as

$$g(\mathbf{X}) = \begin{bmatrix} \beta_1 & \underline{\beta}_2^H \\ \underline{0} & \mathbf{M} \end{bmatrix} \mathbf{X} \begin{bmatrix} 1 & \underline{0}^T \\ \underline{0} & \mathbf{U} \end{bmatrix} \tag{3.9}$$

where $\beta_1 \neq 0$, $\underline{\beta}_2(1 \times (m-1))$ and $\mathbf{M}((m-1) \times (m-1))$ are arbitrary, and $\mathbf{U}((n-1) \times (n-1))$ is a unitary matrix. In order to prove that the decision problem is invariant to this group,

23

it is worthwhile to recall the important property of the Kronecker product that if an $m \times n$ Gaussian matrix $\mathbf{X}$ has mean $E[\mathbf{X}] = \mu$ and covariance $cov[vec(\mathbf{X})] = \mathbf{R} \bigotimes \mathbf{C}$, then $\mathbf{FXH}$ has mean $\mathbf{F}\mu\mathbf{H}$ and covariance $\mathbf{FRF}^H \bigotimes \mathbf{HCH}^H$. With this property and the model $\mathbf{X}$ in (3.4), we have

$$g(\mathbf{X}) = \tilde{a}\underline{\varepsilon}_1\underline{e}_1^T + \tilde{\mathbf{N}}$$

where $\tilde{a} = \beta_1 a$ and $\tilde{\mathbf{N}}$ is still zero-mean Gaussian with $cov[vec(\tilde{\mathbf{N}})] = \tilde{\mathbf{R}} \bigotimes \mathbf{I}$ where

$$\tilde{\mathbf{R}} = \begin{bmatrix} \beta_1 & \underline{\beta}_2^H \\ \underline{0} & \mathbf{M} \end{bmatrix} \mathbf{R} \begin{bmatrix} \beta_1 & \underline{\beta}_2^H \\ \underline{0} & \mathbf{M} \end{bmatrix}^H .$$

Thus the problem remains unchanged under this group since the unknown amplitude a and covariance matrix $\mathbf{R}$ are just replaced by $\tilde{a}$ and $\tilde{\mathbf{R}}$, respectively. This group is also the group whose actions have the largest possible number of free parameters which guarantee that the decision problem remains unchanged. Indeed if the full linear group of row actions were used, i.e. the first column of the left multiplying matrix in (3.9) were to be arbitrary, the signal spatial structure $\underline{\varepsilon}_1$ would not be preserved. Likewise, if a larger group of right multiplying matrices than the one in (3.9) were applied to the columns of $\mathbf{X}$, the independence of the columns of $\mathbf{X}$ or the temporal (chip) structure $\underline{e}_1$ of the signal would not be preserved.

Once the invariant group of transformations is obtained, we can now define a set of statistics, i.e. maximal invariants, which indexes the orbits of $\mathbf{X}$ under this group.

Proposition 1 *With the model (3.4) and the group of transformations (3.9), the maximal invariant is 2-dimensional:*

$$
\begin{aligned}
z_{1'} &= \underline{x}_1^H (\mathbf{X}_2\mathbf{X}_2^H)^{-1}\underline{x}_1, \\
z_2 &= \underline{x}_{21}^H (\mathbf{X}_{22}\mathbf{X}_{22}^H)^{-1}\underline{x}_{21}.
\end{aligned}
$$

And $z_{1'}$ can be replaced by

$$z_1 = \frac{\left| x_{11} - \underline{x}_{12}\mathbf{X}_{22}^H (\mathbf{X}_{22}\mathbf{X}_{22}^H)^{-1}\underline{x}_{21} \right|^2}{\underline{x}_{12} \left[\mathbf{I} - \mathbf{X}_{22}^H(\mathbf{X}_{22}\mathbf{X}_{22}^H)^{-1}\mathbf{X}_{22} \right] \underline{x}_{12}^H}$$

since $z_{1'} = z_1 + z_2$.

    Proof: Bose and Steinhardt [6]. See the appendix for an independent derivation.   ■

To interpret this set of maximal invariants, consider the group of transformations (3.9) as

$$g(\mathbf{X}) = \begin{bmatrix} g_1(\underline{x}_1, \mathbf{X}_2) \\ g_2(\underline{x}_{21}, \mathbf{X}_{22}) \end{bmatrix} = \begin{bmatrix} \underline{\beta}^H \underline{x}_1 & \underline{\beta}^H \mathbf{X}_2 \mathbf{U} \\ \mathbf{M}\underline{x}_{21} & \mathbf{M}\mathbf{X}_{22}\mathbf{U} \end{bmatrix}$$

24
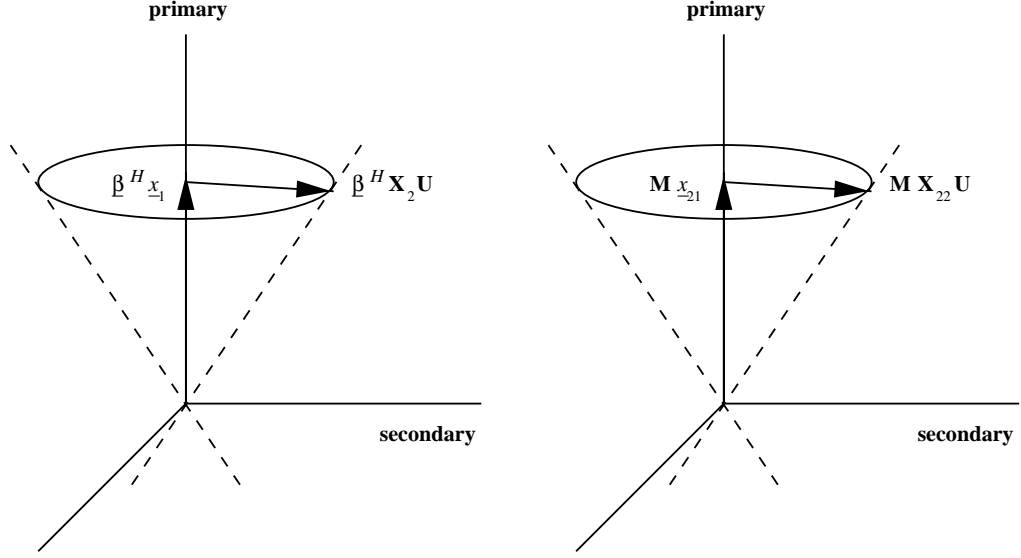
(a) Invariance orbit of g_1 indexed by $z_{1'}$ (b) Invariance orbit of g_2 indexed by z_2

Figure 3.3: Invariance orbits indexed by the maximal invariant

where $\underline{\beta}^H = [\beta_1 \ \underline{\beta}_2^H]$. From each group action on the measurement scaled by $\underline{\beta}$ or $\mathbf{M}$, and rotated by $\mathbf{U}$, we can construct a orbit (cone) as illustrated in Figure 3.3. Then each cone of g_1 and g_2 is indexed respectively by $z_{1'}$ and z_2 which are the ratios of the norm squared along the axis of the cone to that perpendicular to it. z_2 is the sample correlation between primary and secondary data whose distribution is same under H_0 and H_1. Thus it is an ancillary statistic [30]. Also the representation of z_1 gives it an interpretation as the estimated $\underline{s}$-prediction SNR, i.e. the ratio of the magnitude squared of the estimated target error to that of the estimated clutter prediction error, where $\underline{x}_{12}\mathbf{X}_{22}^H(\mathbf{X}_{22}\mathbf{X}_{22}^H)^{-1}\underline{x}_{21}$ is the least-squares estimate of x_{11} given $\underline{x}_{21}$ and $\mathbf{X}_2$.

Any invariant test will be functions of z_1 and z_2, and we can show that the Kelly's test (3.8) is one of them. As described in Proposition 1, $\underline{x}_1^H(\mathbf{X}_2\mathbf{X}_2^H)^{-1}\underline{x}_1 = z_1 + z_2$ and we have

$$T_{Ku} = \frac{|\underline{\varepsilon}_1^T(\mathbf{X}_2\mathbf{X}_2^H)^{-1}\underline{x}_1|^2}{\underline{\varepsilon}_1^T(\mathbf{X}_2\mathbf{X}_2^H)^{-1}\underline{\varepsilon}_1 \cdot \{1 + z_1 + z_2\}}.$$

Since the measurement $\mathbf{X}$ has the partition in (3.4), we write

$$\mathbf{X}_2\mathbf{X}_2^H = \begin{bmatrix} \underline{x}_{12}\underline{x}_{12}^H & \underline{x}_{12}\mathbf{X}_{22}^H \\ \mathbf{X}_{22}\underline{x}_{12}^H & \mathbf{X}_{22}\mathbf{X}_{22}^H \end{bmatrix} = \begin{bmatrix} R_{11} & R_{12} \\ R_{21} & R_{22} \end{bmatrix}.$$

Then using the relations for the inverse of partitioned matrices [20], define

$$(\mathbf{X}_2 \mathbf{X}_2^H)^{-1} = \begin{bmatrix} V_{11} & V_{12} \\ V_{21} & V_{22} \end{bmatrix}$$

where

$$
\begin{aligned}
V_{11} &= \{R_{11} - R_{12}R_{22}^{-1}R_{21}\}^{-1} \\
V_{21} &= -R_{22}^{-1}R_{21}V_{11}
\end{aligned}
$$

and since the $m \times m$ sample covariance matrix $\mathbf{X}_2 \mathbf{X}_2^H$ and its inverse are Hermitian [25], $V_{12} = V_{21}^H$. With these notations, we can show

$$
\begin{aligned}
\underline{\varepsilon}_1^T (\mathbf{X}_2 \mathbf{X}_2^H)^{-1}\underline{\varepsilon}_1 &= \{\underline{x}_{12}\left[\mathbf{I} - \mathbf{X}_{22}^H(\mathbf{X}_{22}\mathbf{X}_{22}^H)^{-1}\mathbf{X}_{22}\right]\underline{x}_{12}^H\}^{-1} \\
\underline{\varepsilon}_1^T (\mathbf{X}_2 \mathbf{X}_2^H)^{-1}\underline{x}_1 &= \frac{x_{11} - \underline{x}_{12}\mathbf{X}_{22}^H(\mathbf{X}_{22}\mathbf{X}_{22}^H)^{-1}\underline{x}_{21}}{\underline{x}_{12}\left[\mathbf{I} - \mathbf{X}_{22}^H(\mathbf{X}_{22}\mathbf{X}_{22}^H)^{-1}\mathbf{X}_{22}\right]\underline{x}_{12}^H}
\end{aligned}
$$

since $V_{11} = \{\underline{x}_{12}\left[\mathbf{I} - \mathbf{X}_{22}^H(\mathbf{X}_{22}\mathbf{X}_{22}^H)^{-1}\mathbf{X}_{22}\right]\underline{x}_{12}^H\}^{-1}$. Thus

$$T_{Ku} = \frac{z_1}{1 + z_1 + z_2} \tag{3.10}$$

which establishes that the GLR test is also an invariant test.

No optimal properties are claimed for this test, and as noted earlier the number of chips, n, must exceed the number m of spatial pixels per chip which can be quite large in many radar applications. Kelly derived the pdf of the test statistic and showed that it depends on the unknown covariance matrix $\mathbf{R}$ only through a SNR involving the unknown signal amplitude a. Thus, under the clutter-alone hypothesis H_0, the pdf of T_{Ku} is not affected by the unknown parameters, and hence the test is CFAR.

CHAPTER 4

Application to a Target Straddling a Clutter Boundary

4.1 Introduction

In this chapter, we consider the problem of detecting a known target straddling the boundary of two independent clutter regions. From the model (2.3), the measurement matrix $\mathbf{X}$ is composed of two different regions A and B and can be partitioned as

$$\mathbf{X} = \begin{bmatrix} \mathbf{X}_A \\ \mathbf{X}_B \end{bmatrix} = \begin{bmatrix} \underline{x}_{A1} & \mathbf{X}_{A2} \\ \underline{x}_{B1} & \mathbf{X}_{B2} \end{bmatrix} \tag{4.1}$$

where $\underline{x}_{A1}$ and $\underline{x}_{B1}$ are the primary vectors which may contain the separated canonical parts of a known target, $\underline{s}_A$ and $\underline{s}_B$, respectively, with the unknown common amplitude a. Here we remove the tildes from $\underline{\tilde{s}}_A$ and $\underline{\tilde{s}}_B$ for notational convenience. Under the clutter-alone hypothesis H_0, any of the i.i.d. columns of $\mathbf{X}$ will be multivariate Gaussian with zero mean and a covariance matrix $\mathbf{R}$ having a block diagonal structure as defined in (1.1):

$$\mathbf{R} = \begin{bmatrix} \mathbf{R}_A & \mathbf{O} \\ \mathbf{O} & \mathbf{R}_B \end{bmatrix}.$$

To construct test statistics, both of the GLR and invariance principles are applied under different assumptions on $\mathbf{R}_B$:

- Case 1: $\mathbf{R}_A > 0, \mathbf{R}_B > 0$

  (totally unknown clutter in regions A and B)

- Case 2: $\mathbf{R}_A > 0, \mathbf{R}_B = \sigma^2 \mathbf{I}$ where $\sigma^2 > 0$

  (clutter known in region B up to variance σ^2)

- Case 3: $\mathbf{R}_A > 0, \mathbf{R}_B = \mathbf{I}$

  (clutter known exactly in region B).

4.2 GLR Tests

Let $\{\underline{x}_{A1}, \underline{x}_{A2}, \dots, \underline{x}_{An}\}$ and $\{\underline{x}_{B1}, \underline{x}_{B2}, \dots, \underline{x}_{Bn}\}$ represent the i.i.d. columns of the two uncorrelated matrices $\mathbf{X}_A$ and $\mathbf{X}_B$, respectively, then the pdf of $\mathbf{X}$ factors as

$$f(\mathbf{X}) = f(\mathbf{X}_A)f(\mathbf{X}_B)$$

where $f(\mathbf{X}_A)$ and $f(\mathbf{X}_B)$ are defined similarly as (3.5) for each region:

$$f(\mathbf{X}_A) = \frac{1}{\pi^{m_A n}|\mathbf{R}_A|^n} \exp\left[-(\underline{x}_{A1} - a\underline{s}_A)^H \mathbf{R}_A^{-1}(\underline{x}_{A1} - a\underline{s}_A) - \sum_{i=2}^{n} \underline{x}_{Ai}^H \mathbf{R}_A^{-1} \underline{x}_{Ai} \right],$$

$$f(\mathbf{X}_B) = \frac{1}{\pi^{m_B n}|\mathbf{R}_B|^n} \exp\left[-(\underline{x}_{B1} - a\underline{s}_B)^H \mathbf{R}_B^{-1}(\underline{x}_{B1} - a\underline{s}_B) - \sum_{i=2}^{n} \underline{x}_{Bi}^H \mathbf{R}_B^{-1} \underline{x}_{Bi} \right].$$

Note that $\mathbf{R}_A$ and $\mathbf{R}_B$ are the regional covariances as given in (1.1), m_A and m_B are the dimensions of the data vectors in $\mathbf{X}_A$ and $\mathbf{X}_B$, respectively, and $m_A + m_B = m$. Now the decision problem is to decide whether the primary data contains clutter alone ($a = 0$) or clutter plus target ($a \neq 0$):

$$H_0 \quad : \quad \mathbf{X} \sim f(\mathbf{X}; 0, \mathbf{R}_A, \mathbf{R}_B)$$

$$H_1 \quad : \quad \mathbf{X} \sim f(\mathbf{X}; a, \mathbf{R}_A, \mathbf{R}_B).$$

As in the unstructured case, the GLR maximization can be performed for the unknown covariance matrices $\mathbf{R}_A$ and $\mathbf{R}_B$ by replacing them with their MLEs ($\hat{\mathbf{R}}_{A0}, \hat{\mathbf{R}}_{B0}$ under H_0, and $\hat{\mathbf{R}}_{A1}, \hat{\mathbf{R}}_{B1}$ under H_1):

$$\Lambda = \max_a \frac{f(\mathbf{X}; a, \hat{\mathbf{R}}_{A1}, \hat{\mathbf{R}}_{B1})}{f(\mathbf{X}; 0, \hat{\mathbf{R}}_{A0}, \hat{\mathbf{R}}_{B0})}.$$

Here, the required condition for non-singularity of the estimated covariance matrices ($n > m$) is relaxed since we need only $n > \max\{m_A, m_B\}$. This GLR, however, still involves a maximization over the unknown amplitude a in a complex quartic equation and cannot be represented in closed form. However, for real valued data the roots of the quartic equation are explicit. For complex data we implement the GLR tests, derived under the structured cases, using numerical root finding and compare their performance in Chapter 6.

4.2.1 Case 1: $\mathbf{R}_A > 0, \mathbf{R}_B > 0$

The GLR for this case is just the product of the likelihood ratios from regions A and B:

$$\Lambda_1 = \max_a \frac{f(\mathbf{X}_A; a, \hat{\mathbf{R}}_{A1})f(\mathbf{X}_B; a, \hat{\mathbf{R}}_{B1})}{f(\mathbf{X}_A; 0, \hat{\mathbf{R}}_{A0})f(\mathbf{X}_B; 0, \hat{\mathbf{R}}_{B0})}.$$

Next we can apply the results of the unstructured example in Section 3.5 to both of the two regions A and B separately:

$$\Lambda_1 = \max_a \left\{ \left[\frac{1 + p(0, \underline{s}_A, \mathbf{X}_A)}{1 + p(a, \underline{s}_A, \mathbf{X}_A)} \right]^n \cdot \left[\frac{1 + p(0, \underline{s}_B, \mathbf{X}_B)}{1 + p(a, \underline{s}_B, \mathbf{X}_B)} \right]^n \right\}$$

or

$$\frac{1}{n} \ln \Lambda_1 = \max_a \left\{ \ln \left[\frac{1 + p(0, \underline{s}_A, \mathbf{X}_A)}{1 + p(a, \underline{s}_A, \mathbf{X}_A)} \right] + \ln \left[\frac{1 + p(0, \underline{s}_B, \mathbf{X}_B)}{1 + p(a, \underline{s}_B, \mathbf{X}_B)} \right] \right\} \tag{4.2}$$

where

$$p(a, \underline{s}_A, \mathbf{X}_A) = (\underline{x}_{A1} - a\underline{s}_A)^H (\mathbf{X}_{A2}\mathbf{X}_{A2}^H)^{-1} (\underline{x}_{A1} - a\underline{s}_A). \tag{4.3}$$

Now we call (4.2) GLR 1 which reduces to the GLR in (3.6) when $\mathbf{R}$ is unstructured and for which the maximization over the quadratic equation in the denominator can be easily achieved.

With this structured model, however, the maximization over a cannot be completed explicitly. But since the maximizing value of the complex amplitude

$$\hat{a} = \arg\min_a \{ [1 + p(a, \underline{s}_A, \mathbf{X}_A)] \cdot [1 + p(a, \underline{s}_B, \mathbf{X}_B)] \}$$

involves a product of two positive quadratic equations, we can derive upper and lower bounds to aid in numerical search. Define the local solutions from each region A, B as in (3.7):

$$\begin{aligned}
\hat{a}_A &= \arg\min_a p(a, \underline{s}_A, \mathbf{X}_A) = \frac{\underline{s}_A^H (\mathbf{X}_{A2}\mathbf{X}_{A2}^H)^{-1} \underline{x}_{A1}}{\underline{s}_A^H (\mathbf{X}_{A2}\mathbf{X}_{A2}^H)^{-1} \underline{s}_A}, \\
\hat{a}_B &= \arg\min_a p(a, \underline{s}_B, \mathbf{X}_B) = \frac{\underline{s}_B^H (\mathbf{X}_{B2}\mathbf{X}_{B2}^H)^{-1} \underline{x}_{B1}}{\underline{s}_B^H (\mathbf{X}_{B2}\mathbf{X}_{B2}^H)^{-1} \underline{s}_B}.
\end{aligned} \tag{4.4}$$

Then we know that $\hat{a}$ lies between those local solutions which serve as bounds, and GLR 1 can be implemented or maximized while varying a in such a way so as to guarantee

$$\begin{aligned}
\min\{\mathrm{Re}\{\hat{a}_A\}, \mathrm{Re}\{\hat{a}_B\}\} \leq & \quad \mathrm{Re}\{\hat{a}\} \quad \leq \max\{\mathrm{Re}\{\hat{a}_A\}, \mathrm{Re}\{\hat{a}_B\}\}, \\
\min\{\mathrm{Im}\{\hat{a}_A\}, \mathrm{Im}\{\hat{a}_B\}\} \leq & \quad \mathrm{Im}\{\hat{a}\} \quad \leq \max\{\mathrm{Im}\{\hat{a}_A\}, \mathrm{Im}\{\hat{a}_B\}\}.
\end{aligned}$$

4.2.2 Case 2: $\mathbf{R}_A > 0, \mathbf{R}_B = \sigma^2 \mathbf{I}$

This case is just as above except that $\mathbf{R}_B$ is assumed to be diagonal with common unknown variance σ^2 along the diagonal. With this assumption, the pdf of $\mathbf{X}_B$ is

$$f(\mathbf{X}_B; a, \sigma^2) = \frac{1}{\pi^{m_B n} \sigma^{2 m_B n}} \exp\left[-\frac{1}{\sigma^2} \left\{ |\underline{x}_{B1} - a\underline{s}_B|^2 + \sum_{i=2}^n |\underline{x}_{Bi}|^2 \right\} \right]$$

29

and the GLR is expressed as

$$\Lambda_2 = \max_a \frac{f(\mathbf{X}_A; a, \hat{\mathbf{R}}_{A1}) f(\mathbf{X}_B; a, \hat{\sigma}_1)}{f(\mathbf{X}_A; 0, \hat{\mathbf{R}}_{A0}) f(\mathbf{X}_B; 0, \hat{\sigma}_0)}.$$

Again MLEs of the variance under both hypotheses can be easily found as

$$\hat{\sigma}_1^2 = \frac{1}{m_B n} q(a, \underline{s}_B, \mathbf{X}_B),$$

$$\hat{\sigma}_0^2 = \frac{1}{m_B n} q(0, \underline{s}_B, \mathbf{X}_B)$$

where

$$q(a, \underline{s}_B, \mathbf{X}_B) = \mathrm{tr}\left\{ (\mathbf{X}_B - a\underline{s}_B \underline{e}_1^T)^H (\mathbf{X}_B - a\underline{s}_B \underline{e}_1^T) \right\}. \tag{4.5}$$

As before, the maximization over a in Λ_2 cannot be completed in closed form. To bound $\hat{a}$, we first consider the GLR over the region B alone which can be simplified to

$$l_2 = \max_a \left\{ \frac{q(0, \underline{s}_B, \mathbf{X}_B)}{q(a, \underline{s}_B, \mathbf{X}_B)} \right\}^{m_B n}.$$

We named it l_2 after the previous unstructured GLR test statistic l_1 in (3.6). Then by rewriting $q(a, \underline{s}_B, \mathbf{X}_B)$ as

$$q(a, \underline{s}_B, \mathbf{X}_B) = |\underline{s}_B|^2 \cdot \left| a - \frac{\underline{s}_B^H \underline{x}_{B1}}{|\underline{s}_B|^2} \right|^2 + \sum_{i=1}^n |\underline{x}_{Bi}|^2 - \frac{|\underline{s}_B^H \underline{x}_{B1}|^2}{|\underline{s}_B|^2},$$

we see that the maximizing value of a is

$$\hat{a}_B = \frac{\underline{s}_B^H \underline{x}_{B1}}{|\underline{s}_B|^2} \tag{4.6}$$

where $\underline{s}_B$ is the canonical target of form $\underline{s}_B = [s_B, 0, \dots, 0]^T$. Thus we have the equivalent form of this GLR

$$1 - \frac{1}{m_B n \sqrt{l_2}} = \frac{|x_{B11}|^2}{\sum_{i=1}^n |\underline{x}_{Bi}|^2}. \tag{4.7}$$

Now back to Λ_2, GLR 2 can be expressed as

$$\frac{1}{n} \ln \Lambda_2 = \max_a \left\{ \ln \left[\frac{1 + p(0, \underline{s}_A, \mathbf{X}_A)}{1 + p(a, \underline{s}_A, \mathbf{X}_A)} \right] + m_B \cdot \ln \left[\frac{q(0, \underline{s}_B, \mathbf{X}_B)}{q(a, \underline{s}_B, \mathbf{X}_B)} \right] \right\}, \tag{4.8}$$

and the maximizing value of a can be found between $\hat{a}_A$ given as (4.4) for Case 1 and $\hat{a}_B$ given in (4.6).

4.2.3 Case 3: $\mathbf{R}_A > 0, \mathbf{R}_B = \mathbf{I}$

Suppose $\mathbf{R}_B$ is exactly known to be an identity matrix. Then from the results of Case 2 we can derive a bound on the maximizing value of a required to implement the GLR. Define the GLR l_3 over $\mathbf{X}_B$ alone:

$$l_3 = \max_a \{\exp[q(0, \underline{s}_B, \mathbf{X}_B) - q(a, \underline{s}_B, \mathbf{X}_B)]\}$$

where q is the same as defined previously in (4.5). Hence, the MLE of the amplitude a is equal to $\hat{a}_B$ given in (4.6), and the GLR over $\mathbf{X}_B$ is equivalent to

$$\ln l_3 = |x_{B11}|^2. \tag{4.9}$$

Thus, finally, we can define GLR 3 using the entire measurement $\mathbf{X}$ as

$$\frac{1}{n} \ln \Lambda_3 = \max_a \left\{ \ln \left[\frac{1 + p(0, \underline{s}_A, \mathbf{X}_A)}{1 + p(a, \underline{s}_A, \mathbf{X}_A)} \right] + \frac{1}{n} \left[q(0, \underline{s}_B, \mathbf{X}_B) - q(a, \underline{s}_B, \mathbf{X}_B) \right] \right\} \tag{4.10}$$

where the maximization over a can be implemented similarly to Case 2.

4.3 MI Tests

In this section, we apply the invariance principle to the structured covariance cases studied above and construct a test statistic as a function of the maximal invariants derived. These results parallel those of Bose and Steinhardt [6]. It will be convenient to first define the partition of $\mathbf{X}$ which is refined from (4.1):

$$\mathbf{X} = \left[\begin{array}{c} \mathbf{X}_A \\ \mathbf{X}_B \end{array} \right] = \left[\begin{array}{cc} x_{A11} & \underline{x}_{A12} \\ \underline{x}_{A21} & \mathbf{X}_{A22} \\ x_{B11} & \underline{x}_{B12} \\ \underline{x}_{B21} & \mathbf{X}_{B22} \end{array} \right]. \tag{4.11}$$

With this partition, the structured group of transformations induced by each model will be defined as

$$g(\mathbf{X}) = \left[\begin{array}{c} g_A(\mathbf{X}_A) \\ g_B(\mathbf{X}_B) \end{array} \right]$$

and the maximal invariants under each group can easily be obtained. For each case, MI test is proposed based on the maximal invariants and compared to the previous results of Kelly [34] and Bose and Steinhardt [6].

4.3.1 Case 1: $\mathbf{R}_A > 0, \mathbf{R}_B > 0$

In this case, the independent regions A and B both have unknown covariance matrices, and we can construct a structured group of transformations on $\mathbf{X}$ which is extended from (3.9):

$$
g(\mathbf{X}) = \left[\begin{array}{c} \left[\begin{array}{cc} \beta & \underline{\beta}_A^H \\ \underline{0} & \mathbf{M}_A \end{array} \right] \mathbf{X}_A \left[\begin{array}{cc} 1 & \underline{0}^T \\ \underline{0} & \mathbf{U}_A \end{array} \right] \\ \left[\begin{array}{cc} \beta & \underline{\beta}_B^H \\ \underline{0} & \mathbf{M}_B \end{array} \right] \mathbf{X}_B \left[\begin{array}{cc} 1 & \underline{0}^T \\ \underline{0} & \mathbf{U}_B \end{array} \right] \end{array} \right] \tag{4.12}
$$

where $\beta \neq 0$, $\underline{\beta}_A (1 \times (m_A - 1))$, $\underline{\beta}_B (1 \times (m_B - 1))$, $\mathbf{M}_A ((m_A - 1) \times (m_A - 1))$ and $\mathbf{M}_B ((m_B - 1) \times (m_B - 1))$ are arbitrary, and $\mathbf{U}_A$ and $\mathbf{U}_B$ are $((n-1) \times (n-1))$ unitary matrices. Showing the invariant property of this group is analogous to the unstructured example. With this group, the set of maximal invariants is defined in the following, which is also briefly covered in [6].

Proposition 2 *With the model in (2.3) and the partition in (4.11), the maximal invariant under the group of transformations in (4.12) is 5-dimensional:*

$$
\begin{aligned}
z_{A1} &= \frac{|u_A|^2}{D_A}, \\
z_{A2} &= \underline{x}_{A21}^H (\mathbf{X}_{A22} \mathbf{X}_{A22}^H)^{-1} \underline{x}_{A21}, \\
z_{B1} &= \frac{|u_B|^2}{D_B}, \\
z_{B2} &= \underline{x}_{B21}^H (\mathbf{X}_{B22} \mathbf{X}_{B22}^H)^{-1} \underline{x}_{B21}, \\
z_{AB} &= \frac{u_A}{u_B}
\end{aligned}
$$

where the subscripts denote whether the quantities are computed over the region A, B or both A and B, and

$$
\begin{aligned}
u_A &= x_{A11} - \underline{x}_{A12} \mathbf{X}_{A22}^H (\mathbf{X}_{A22} \mathbf{X}_{A22}^H)^{-1} \underline{x}_{A21}, \\
u_B &= x_{B11} - \underline{x}_{B12} \mathbf{X}_{B22}^H (\mathbf{X}_{B22} \mathbf{X}_{B22}^H)^{-1} \underline{x}_{B21}, \\
D_A &= \underline{x}_{A12} \left[\mathbf{I} - \mathbf{X}_{A22}^H (\mathbf{X}_{A22} \mathbf{X}_{A22}^H)^{-1} \mathbf{X}_{A22} \right] \underline{x}_{A12}^H, \\
D_B &= \underline{x}_{B12} \left[\mathbf{I} - \mathbf{X}_{B22}^H (\mathbf{X}_{B22} \mathbf{X}_{B22}^H)^{-1} \mathbf{X}_{B22} \right] \underline{x}_{B12}^H.
\end{aligned}
$$

And z_{AB} can be replaced by

$$
z_{AB'} = \frac{|u_A/s_A - u_B/s_B|^2}{D_A/|s_A|^2 + D_B/|s_B|^2}
$$

32

or

$$z_{AB''} = \frac{|u_A/s_A - u_B/s_B|^2}{q_A D_A/|s_A|^2 + q_B D_B/|s_B|^2}$$

where $q_A = 1 + z_{A1} + z_{A2}$ and $q_B = 1 + z_{B1} + z_{B2}$.

Proof: Bose and Steinhardt [6]. See the appendix for an independent derivation. ∎

We can see that z_{A1} and z_{A2} correspond to z_1 and z_2 in the unstructured case (Proposition 1) applied to region A, and z_{B1} and z_{B2} correspond to those applied to region B. The coupling term, z_{AB}, $z_{AB'}$, or $z_{AB''}$, not present in the unstructured test, captures the common amplitude a for both regions.

Bose and Steinhardt proposed a natural modification of Kelly's test (3.8) which reflects the block covariance structure:

$$T_{Ks} = \frac{\left|\underline{s}^H \mathbf{K}^{-1} \underline{x}_1\right|^2}{\underline{s}^H \mathbf{K}^{-1} \underline{s} \cdot \left\{1 + \underline{x}_1^H \mathbf{K}^{-1} \underline{x}_1\right\}} \tag{4.13}$$

where $\underline{x}_1 = [\underline{x}_{A1}^H \ \underline{x}_{B1}^H]^H$, $\underline{s} = [\underline{s}_A^H \ \underline{s}_B^H]^H$ and

$$\mathbf{K} = \begin{bmatrix} \mathbf{X}_{A2}\mathbf{X}_{A2}^H & \mathbf{O} \\ \mathbf{O} & \mathbf{X}_{B2}\mathbf{X}_{B2}^H \end{bmatrix}.$$

To see that this is a function of maximal invariants derived in Proposition 2, first look at the term in the bracket in the denominator of (4.13):

$$\begin{aligned} 1 + \underline{x}_1^H \mathbf{K}^{-1} \underline{x}_1 &= 1 + \underline{x}_{A1}^H (\mathbf{X}_{A2}\mathbf{X}_{A2}^H)^{-1} \underline{x}_{A1} + \underline{x}_{B1}^H (\mathbf{X}_{B2}\mathbf{X}_{B2}^H)^{-1} \underline{x}_{B1} \\ &= 1 + z_{A1} + z_{A2} + z_{B1} + z_{B2} \end{aligned}$$

using the relation, $z_{1'} = z_1 + z_2$, in Proposition 1. We can simplify the remaining factor in the test using the results of the unstructured example:

$$\begin{aligned} \frac{\left|\underline{s}^H \mathbf{K}^{-1} \underline{x}_1\right|^2}{\underline{s}^H \mathbf{K}^{-1} \underline{s}} &= \frac{\left|\underline{s}_A^H (\mathbf{X}_{A2}\mathbf{X}_{A2}^H)^{-1} \underline{x}_{A1} + \underline{s}_B^H (\mathbf{X}_{B2}\mathbf{X}_{B2}^H)^{-1} \underline{x}_{B1}\right|^2}{\underline{s}_A^H (\mathbf{X}_{A2}\mathbf{X}_{A2}^H)^{-1} \underline{s}_A + \underline{s}_B^H (\mathbf{X}_{B2}\mathbf{X}_{B2}^H)^{-1} \underline{x}_B} \\ &= \frac{\left|(D_A/|s_A|^2)^{-1} u_A/s_A + (D_B/|s_B|^2)^{-1} u_B/s_B\right|^2}{(D_A/|s_A|^2)^{-1} + (D_B/|s_B|^2)^{-1}} \end{aligned} \tag{4.14}$$

where s_A and s_B are the first elements which are only non-zero in $\underline{s}_A$ and $\underline{s}_B$, respectively.

Lemma 1 *Suppose that $p \times p$ matrices $\mathbf{D}_A$, $\mathbf{D}_B$ are hermitian and invertible, and $\underline{u}_A$, $\underline{u}_B$ are column vectors of size p, then*

$$\begin{aligned} & (\mathbf{D}_A^{-1}\underline{u}_A + \mathbf{D}_B^{-1}\underline{u}_B)^H (\mathbf{D}_A^{-1} + \mathbf{D}_B^{-1})^{-1} (\mathbf{D}_A^{-1}\underline{u}_A + \mathbf{D}_B^{-1}\underline{u}_B) \\ =\ & \underline{u}_A^H \mathbf{D}_A^{-1} \underline{u}_A + \underline{u}_B^H \mathbf{D}_B^{-1} \underline{u}_B - (\underline{u}_A - \underline{u}_B)^H (\mathbf{D}_A + \mathbf{D}_B)^{-1} (\underline{u}_A - \underline{u}_B). \end{aligned}$$

Proof: See the appendix. ∎

Using Lemma 1, the equation in (4.14) is a special case for $p = 1$. Hence the structured Kelly's test (4.13) can be expressed as

$$T_{Ks} = \frac{z_{A1} + z_{B1} - z_{AB'}}{1 + z_{A1} + z_{A2} + z_{B1} + z_{B2}}. \tag{4.15}$$

Alternatively, by looking at the maximal invariant representation of T_{Ks}, we can obtain another invariant test which reduces to the unstructured test (3.10):

$$T_1 = \frac{\left| \begin{bmatrix} \underline{s}_A^H & \underline{s}_B^H \end{bmatrix} \begin{bmatrix} q_A \mathbf{X}_{A2} \mathbf{X}_{A2}^H & \mathbf{O} \\ \mathbf{O} & q_B \mathbf{X}_{B2} \mathbf{X}_{B2}^H \end{bmatrix}^{-1} \begin{bmatrix} \underline{x}_{A1} \\ \underline{x}_{B1} \end{bmatrix} \right|^2}{\begin{bmatrix} \underline{s}_A^H & \underline{s}_B^H \end{bmatrix} \begin{bmatrix} q_A \mathbf{X}_{A2} \mathbf{X}_{A2}^H & \mathbf{O} \\ \mathbf{O} & q_B \mathbf{X}_{B2} \mathbf{X}_{B2}^H \end{bmatrix}^{-1} \begin{bmatrix} \underline{s}_A \\ \underline{s}_B \end{bmatrix}}. \tag{4.16}$$

Note that q_A and q_B are placed in the estimated covariance matrix attempting to separate the coupled denominator in (4.15). Thus T_1 is same as (4.14) except for $q_A D_A$ and $q_B D_B$ in place of D_A and D_B, respectively:

$$T_1 = \frac{\left| (q_A D_A / |s_A|^2)^{-1} u_A / s_A + (q_B D_B / |s_B|^2)^{-1} u_B / s_B \right|^2}{(q_A D_A / |s_A|^2)^{-1} + (q_B D_B / |s_B|^2)^{-1}}.$$

Then from Lemma 1 we have

$$T_1 = \frac{z_{A1}}{1 + z_{A1} + z_{A2}} + \frac{z_{B1}}{1 + z_{B1} + z_{B2}} - z_{AB''} \tag{4.17}$$

where the different coupling term $z_{AB''}$ is used instead of $z_{AB'}$. This MI test will be shown to outperform (4.15) for some situations.

4.3.2 Case 2: $\mathbf{R}_A > 0, \mathbf{R}_B = \sigma^2 \mathbf{I}$

Now suppose $\mathbf{R}_B = \sigma^2 \mathbf{I}$ with unknown σ^2, then the invariant group of transformations in this case is

$$g(\mathbf{X}) = \begin{bmatrix} \begin{bmatrix} \beta & \underline{\beta}_A^H \\ \underline{0} & \mathbf{M}_A \end{bmatrix} & \mathbf{X}_A & \begin{bmatrix} 1 & \underline{0}^T \\ \underline{0} & \mathbf{U}_A \end{bmatrix} \\ \beta & \mathbf{X}_B & \begin{bmatrix} 1 & \underline{0}^T \\ \underline{0} & \mathbf{U}_B \end{bmatrix} \end{bmatrix} \tag{4.18}$$

since $\mathbf{X}_B$ still remains Gaussian under this group except that a and σ^2 are replaced by $\tilde{a} = \beta a$ and $\tilde{\sigma}^2 = (\beta \sigma)^2$. Similarly to (4.12), the same scaling factor β captures the common amplitude in both regions.

Proposition 3 *With the partition in (4.11), the maximal invariant under the group of transformations in (4.18) is composed of*

$$z_{A1} = \frac{|u_A|^2}{D_A},$$
$$z_{A2} = \underline{x}_{A21}^H(\mathbf{X}_{A22}\mathbf{X}_{A22}^H)^{-1}\underline{x}_{A21},$$
$$z_B = \frac{|x_{B11}|^2}{\sum_{i=1}^n |\underline{x}_{Bi}|^2},$$
$$z_{AB} = \frac{u_A}{x_{B11}}$$

where u_A and D_A are same as defined in Proposition 2. But, since the maximal invariant is not unique, we can also define alternative forms for z_B and z_{AB}: z_B can be replaced by

$$z_{B'} = \frac{|x_{B11}|^2}{|\underline{x}_{B12}|^2 + |\underline{x}_{B21}|^2 + |\mathbf{X}_{B22}|_F^2},$$

and z_{AB} can be replaced by either of

$$z_{AB'} = \frac{|u_A/s_A - x_{B11}/s_B|^2}{\rho D_A/|s_A|^2 + v_1/|s_B|^2}$$

where

$$\rho = \frac{1}{(n - m_A)(1 + z_{A2})},$$
$$v_1 = \frac{|\underline{x}_{B12}|^2 + |\underline{x}_{B21}|^2 + |\mathbf{X}_{B22}|_F^2}{m_B n - 1},$$

or

$$z_{AB''} = \frac{|u_A/s_A - x_{B11}/s_B|^2}{q_A D_A/|s_A|^2 + v_2/|s_B|^2}$$

where $q_A = 1 + z_{A1} + z_{A2}$ and

$$v_2 = \frac{1}{m_B}\sum_{i=1}^n |\underline{x}_{Bi}|^2.$$

Proof: Bose and Steinhardt [6]. See the appendix for an independent derivation. ∎
z_{A1} and z_{A2} are same as those in Proposition 2, and the coupling terms are associated with the common scaling β for a. Finally, z_B or $z_{B'}$ are the maximal invariant for the case that only region B is considered. z_B or $z_{B'}$ can be interpreted as indexing the single orbit in $\mathbf{X}_B$ illustrated in Figure 4.1.

Bose and Steinhardt derived identical maximal invariants in the context of array detection problems and the above results can all be found in [6]. In [5], a representation for the joint pdf of the maximal invariants is derived which gives insight into the marginal
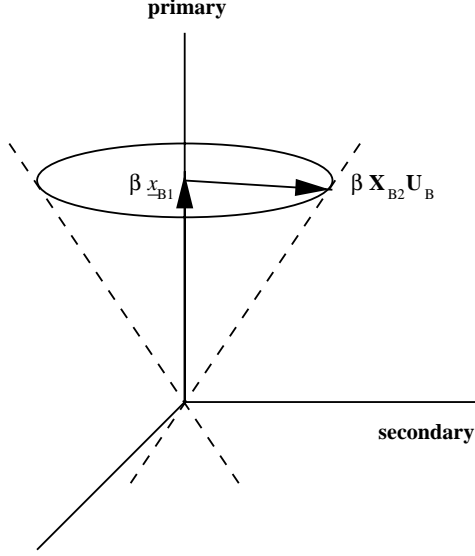
Figure 4.1: Invariance orbit of $\mathbf{X}_B$

distributions: z_{A1}, z_{A2} and z_B as F-statistics, and z_{AB} as complex Cauchy. Based on these statistics an invariant test was proposed in [6] which was shown to be approximately CFAR:

$$
T_{BS} = \frac{\left| \begin{bmatrix} \underline{s}_A^H & \underline{s}_B^H \end{bmatrix} \begin{bmatrix} \rho \mathbf{X}_{A2}\mathbf{X}_{A2}^H & \mathbf{O} \\ \mathbf{O} & v_1\mathbf{I} \end{bmatrix}^{-1} \begin{bmatrix} \underline{x}_{A1} \\ \underline{x}_{B1} \end{bmatrix} \right|^2}{\begin{bmatrix} \underline{s}_A^H & \underline{s}_B^H \end{bmatrix} \begin{bmatrix} \rho \mathbf{X}_{A2}\mathbf{X}_{A2}^H & \mathbf{O} \\ \mathbf{O} & v_1\mathbf{I} \end{bmatrix}^{-1} \begin{bmatrix} \underline{s}_A \\ \underline{s}_B \end{bmatrix}} \tag{4.19}
$$

where ρ and v_1 are as in Proposition 3. To see the maximal invariant representation, we write this test as

$$
T_{BS} = \frac{\left| (\rho D_A/|s_A|^2)^{-1} u_A/s_A + (v_1/|s_B|^2)^{-1} x_{B11}/s_B \right|^2}{(\rho D_A/|s_A|^2)^{-1} + (v_1/|s_B|^2)^{-1}}
$$

then from Lemma 1 we have

$$
\begin{aligned}
T_{BS} &= \frac{z_{A1}}{\rho} + \frac{|x_{B11}|^2}{v_1} - z_{AB'} \\
&= (n - m_A)z_{A1}(1 + z_{A2}) + (m_B n - 1)z_{B'} - z_{AB'}. \tag{4.20}
\end{aligned}
$$

However, we can construct another invariant test statistic by considering the structures of both the GLR test (4.8) and the MI test 1 (4.16):

$$T_2 = \frac{\left| \begin{bmatrix} \underline{s}_A^H & \underline{s}_B^H \end{bmatrix} \begin{bmatrix} q_A \mathbf{X}_{A2} \mathbf{X}_{A2}^H & \mathbf{O} \\ \mathbf{O} & v_2 \mathbf{I} \end{bmatrix}^{-1} \begin{bmatrix} \underline{x}_{A1} \\ \underline{x}_{B1} \end{bmatrix} \right|^2}{\begin{bmatrix} \underline{s}_A^H & \underline{s}_B^H \end{bmatrix} \begin{bmatrix} q_A \mathbf{X}_{A2} \mathbf{X}_{A2}^H & \mathbf{O} \\ \mathbf{O} & v_2 \mathbf{I} \end{bmatrix}^{-1} \begin{bmatrix} \underline{s}_A \\ \underline{s}_B \end{bmatrix}} \tag{4.21}$$

where ρ and v_1 in (4.19) are replaced by q_A and v_2 defined in Proposition 3. Then this MI test 2 has a maximal invariant form of

$$T_2 = \frac{z_{A1}}{1 + z_{A1} + z_{A2}} + m_B \cdot z_B - z_{AB''}. \tag{4.22}$$

Thus the weighting between the terms from region A and region B is maintained as in (4.8), and this test reduces exactly to the unstructured tests: (3.10) for $\mathbf{X}_A$ alone or (4.7) for $\mathbf{X}_B$ alone. This reduction does not hold for the Bose and Steinhardt's test (4.20).

4.3.3 Case 3: $\mathbf{R}_A > 0, \mathbf{R}_B = \mathbf{I}$

For this case, the invariant group of transformations is defined as

$$g(\mathbf{X}) = \begin{bmatrix} \begin{bmatrix} \beta & \underline{\beta}_A^H \\ \underline{0} & \mathbf{M}_A \end{bmatrix} & \mathbf{X}_A & \begin{bmatrix} 1 & \underline{0}^T \\ \underline{0} & \mathbf{U}_A \end{bmatrix} \\ & \mathbf{X}_B & \begin{bmatrix} 1 & \underline{0}^T \\ \underline{0} & \mathbf{U}_B \end{bmatrix} \end{bmatrix}$$

where, unlike the previous two cases, there is no scaling term on the left of $\mathbf{X}_B$ since the variance is exactly known in $\mathbf{X}_B$ and must not be altered by group actions. Thus $g(\mathbf{X})$ cannot have the common scaling term for the unknown amplitude in both regions, and the set of maximal invariants doesn't include any coupling term from regions A and B.

However, MI test 3 can be induced from MI test 2 (4.21) by replacing v_2 with $v_3 = n$, and we propose the following MI test 3

$$T_3 = \frac{z_{A1}}{q_A} + \frac{1}{n}|x_{B11}|^2 - \frac{|u_A/s_A - x_{B11}/s_B|^2}{q_A D_A/|s_A|^2 + n/|s_B|^2}. \tag{4.23}$$

Note that $|x_{B11}|^2$ can be interpreted as the maximal invariant when only region B is considered. This MI test 3 also reduces to either of the unstructured cases: (3.10) for $\mathbf{X}_A$ alone or (4.9) for $\mathbf{X}_B$ alone.

4.4 Conclusion

In this chapter, we have presented adaptive detection algorithms developed for a target in structured clutter. For this, we considered both the GLR and invariance procedures. For the GLR tests derived under 3 different cases, the test statistics are summarized in Table 4.1. Those GLR tests are represented as logs of the likelihood ratios where $p(a, \underline{s}_A, \mathbf{X}_A)$ and $q(a, \underline{s}_B, \mathbf{X}_B)$ are defined in (4.3) and (4.5), respectively. MI tests based on the MLE of the structured covariance matrix are reproduced in Table 4.2 where q_A and q_B are defined in Proposition 2. We have also shown that the MI tests are functions of the maximal invariants under each case, which are listed in Table 4.3.

The next chapter extends the detection problem to the multiple signal model. Finally, in Chapter 6 we compare and analyze the performance of the detectors.

Case	$\mathbf{R}_A$	$\mathbf{R}_B$	Log GLR : $\dfrac{1}{n}\ln\Lambda = \max_a\{\cdot\}$
1	?	?	$\ln\dfrac{1+p(0,\underline{s}_A,\mathbf{X}_A)}{1+p(a,\underline{s}_A,\mathbf{X}_A)} + \ln\dfrac{1+p(0,\underline{s}_B,\mathbf{X}_B)}{1+p(a,\underline{s}_B,\mathbf{X}_B)}$
2	?	$\sigma^2\mathbf{I}$	$\ln\dfrac{1+p(0,\underline{s}_A,\mathbf{X}_A)}{1+p(a,\underline{s}_A,\mathbf{X}_A)} + m_B\cdot\ln\dfrac{q(0,\underline{s}_B,\mathbf{X}_B)}{q(a,\underline{s}_B,\mathbf{X}_B)}$
3	?	$\mathbf{I}$	$\ln\dfrac{1+p(0,\underline{s}_A,\mathbf{X}_A)}{1+p(a,\underline{s}_A,\mathbf{X}_A)} + \dfrac{1}{n}\left[q(0,\underline{s}_B,\mathbf{X}_B) - q(a,\underline{s}_B,\mathbf{X}_B)\right]$

Table 4.1: GLR tests for Cases 1, 2 and 3 (The notation '?' denotes 'unknown' quantity in the model)

Case	$\mathbf{R}_A$	$\mathbf{R}_B$	MI test : $\dfrac{\left\| \begin{bmatrix} \underline{s}_A^H & \underline{s}_B^H \end{bmatrix} \begin{bmatrix} \mathbf{K}_A & \mathbf{O} \\ \mathbf{O} & \mathbf{K}_B \end{bmatrix}^{-1} \begin{bmatrix} \underline{x}_{A1} \\ \underline{x}_{B1} \end{bmatrix} \right\|^2}{\begin{bmatrix} \underline{s}_A^H & \underline{s}_B^H \end{bmatrix} \begin{bmatrix} \mathbf{K}_A & \mathbf{O} \\ \mathbf{O} & \mathbf{K}_B \end{bmatrix}^{-1} \begin{bmatrix} \underline{s}_A \\ \underline{s}_B \end{bmatrix}}$
1	?	?	$\mathbf{K}_A = q_A\mathbf{X}_{A2}\mathbf{X}_{A2}^H, \quad \mathbf{K}_B = q_B\mathbf{X}_{B2}\mathbf{X}_{B2}^H$
2	?	$\sigma^2\mathbf{I}$	$\mathbf{K}_A = q_A\mathbf{X}_{A2}\mathbf{X}_{A2}^H, \quad \mathbf{K}_B = v_2\mathbf{I} \quad (v_2 = \frac{1}{m_B}\sum_{i=1}^{n}|\underline{x}_{Bi}|^2)$
3	?	$\mathbf{I}$	$\mathbf{K}_A = q_A\mathbf{X}_{A2}\mathbf{X}_{A2}^H, \quad \mathbf{K}_B = v_3\mathbf{I} \quad (v_3 = n)$

Table 4.2: MI tests for Cases 1, 2 and 3

Case	$\mathbf{R}_A$	$\mathbf{R}_B$	MI test
1	?	?	$T_1 = \dfrac{z_{A1}}{q_A} + \dfrac{z_{B1}}{q_B} - \dfrac{\left|u_A/s_A - u_B/s_B\right|^2}{q_A D_A/|s_A|^2 + q_B D_B/|s_B|^2}$
2	?	$\sigma^2 \mathbf{I}$	$T_2 = \dfrac{z_{A1}}{q_A} + \dfrac{\left|x_{B11}\right|^2}{v_2} - \dfrac{\left|u_A/s_A - x_{B11}/s_B\right|^2}{q_A D_A/|s_A|^2 + v_2/|s_B|^2}$
3	?	$\mathbf{I}$	$T_3 = \dfrac{z_{A1}}{q_A} + \dfrac{\left|x_{B11}\right|^2}{v_3} - \dfrac{\left|u_A/s_A - x_{B11}/s_B\right|^2}{q_A D_A/|s_A|^2 + v_3/|s_B|^2}$

Table 4.3: MI tests in the maximal invariant forms

CHAPTER 5

Extension to One of Multiple Known Targets

5.1 Introduction

In this chapter, the previous results are extended to the problem of detecting the presence of one target from a known set of p possible targets. Previously, the target signature in the primary vector was assumed to be exactly known and the problem was to decide whether the one and only signal vector $\underline{s}$ is present or not. In real radar applications, however, a more realistic model can be considered. Suppose that we know the form of the target of interest, but don't know its position in the subimage. Then, as illustrated in Figure 5.1, different target signature vectors can be constructed according to different positions in that subimage. Also, a target can be viewed at different orientations and can have as many signatures. Figure 5.3 shows the SLICY canonical target in Figure 5.2 imaged at different degrees of target aspect pose.

To accommodate this scenario, let the image model have an $m \times p$ matrix $\mathbf{S} = \begin{bmatrix} \underline{s}_1, \dots, \underline{s}_p \end{bmatrix}$ for p target signatures:

$$a\,\mathbf{S}\,\underline{\epsilon}_k\,\underline{e}_1^T + \mathbf{N} \tag{5.1}$$

where $\underline{\epsilon}_k$ is a $p \times 1$ unit vector $[0, \dots, 0, 1, 0, \dots, 0]^T$ and '1' is in position k. Here $k \in \{1, \dots, p\}$, and $p \le m$ for unstructured clutter or $p \le \min\{m_A, m_B\}$ for structured clutter. The model (5.1) implies that only one of the signatures, $\underline{s}_k$, may be present at a time in the primary vector, and in the structured case this signature vector is written as

$$\underline{s}_k = \begin{bmatrix} \underline{s}_{Ak} \\ \underline{s}_{Bk} \end{bmatrix}. \tag{5.2}$$

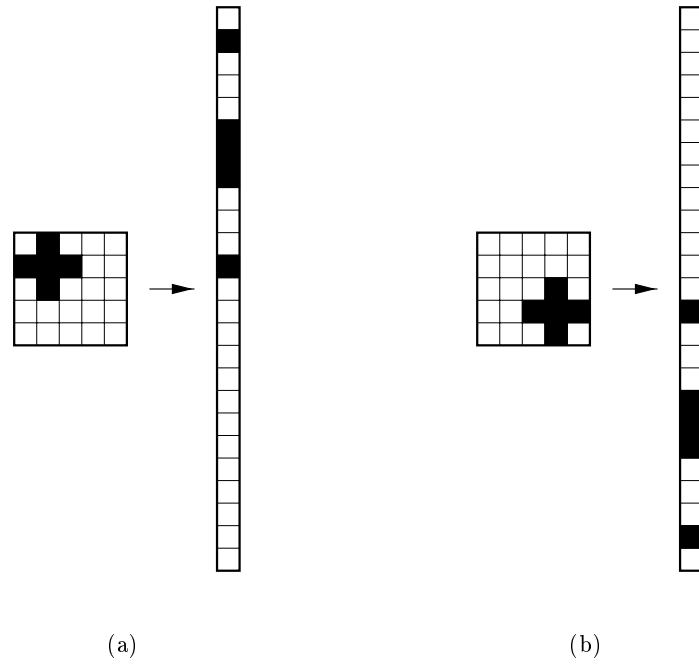(a)   (b)

Figure 5.1: A target of known form (3 × 3 '+' target) can seem differently according to its position in a subimage (5 × 5): (a) or (b).
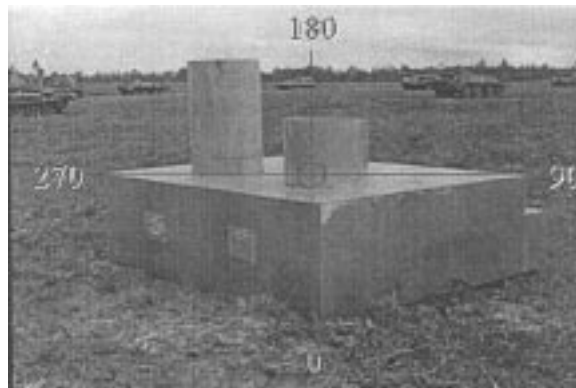

Figure 5.2: SLICY canonical target.

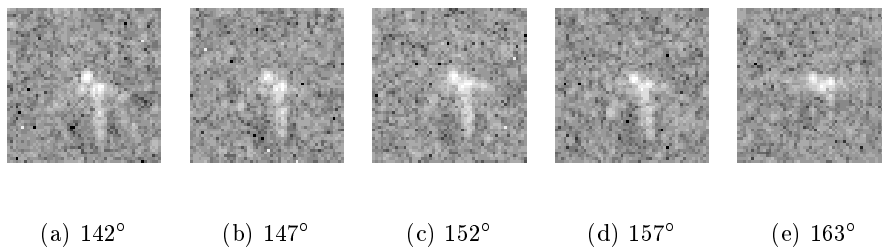(a) 142°   (b) 147°   (c) 152°   (d) 157°   (e) 163°

Figure 5.3: SLICY canonical target images at different degrees of aspect pose.

For the GLR tests (4.2), (4.8), and (4.10), it is easy to extend the results of the single target case to this multiple target case. We only need to replace $\underline{s}_A$ and $\underline{s}_B$ in the GLR tests with p possible target signatures $\underline{s}_{Ak}$ and $\underline{s}_{Bk}$, and maximize over $k = 1, \ldots, p$, i.e. for $i = 1, 2, 3$ indexing each of the block covariance cases discussed above:

$$\max_{k=1,\ldots,p} \frac{1}{n} \ln \Lambda_i(\underline{s}_{Ak}, \underline{s}_{Bk}).$$

Similarly, for the MI tests one can also propose to maximize over the p target signatures. In the following, the invariance procedure is applied to the model in (5.1) for both the unstructured and structured cases. For the structured cases, only Case 1 is investigated.

5.2   Unstructured Covariance Case

First, we consider the case of totally unknown covariance. Since $\mathbf{S}$ is known, we can define the canonical model from (5.1) as

$$\begin{aligned}
\mathbf{X} &= \left[\begin{array}{c} (\mathbf{S}^H \mathbf{S})^{-1} \mathbf{S}^H \\ \mathbf{P}_S \end{array} \right] \{ a\, \mathbf{S}\, \underline{\epsilon}_k\, \underline{e}_1^T + \mathbf{N} \} \qquad (5.3) \\
&= a \left[\begin{array}{c} \underline{\epsilon}_k \\ \underline{0} \end{array} \right] \underline{e}_1^T + \tilde{\mathbf{N}}
\end{aligned}$$

where an $(m - p) \times m$ matrix $\mathbf{P}_S$ is an orthogonal matrix to $(\mathbf{S}^H \mathbf{S})^{-1} \mathbf{S}^H$ and $\tilde{\mathbf{N}}$ is still zero-mean Gaussian with i.i.d. columns. We partition $\mathbf{X}$ as before

$$\mathbf{X} = [\underline{x}_1\ \mathbf{X}_2] = \left[\begin{array}{cc} \underline{x}_{11} & \mathbf{X}_{12} \\ \underline{x}_{21} & \mathbf{X}_{22} \end{array} \right] \qquad (5.4)$$

where the $p \times 1$ vector $\underline{x}_{11}$ may contain any of the target signatures which have been transformed to unit vectors $\{\underline{\epsilon}_k\}_{k=1}^p$. With this model, the group of transformations which preserves the problem is defined as

$$g(\mathbf{X}) = \left[\begin{array}{cc} \Delta & \mathbf{B} \\ \mathbf{O} & \mathbf{M} \end{array} \right] \mathbf{X} \left[\begin{array}{cc} 1 & \underline{0}^T \\ \underline{0} & \mathbf{U} \end{array} \right] \qquad (5.5)$$

where Δ is a $p \times p$ diagonal matrix, $\mathbf{B}$ $(p \times (m - p))$ and $\mathbf{M}$ $((m - p) \times (m - p))$ are arbitrary, and $\mathbf{U}$ is an $(n - 1) \times (n - 1)$ unitary matrix. Note that by putting the model (5.1) into the canonical form, we must restrict a diagonal matrix Δ in (5.5) instead of an arbitrary matrix in order to preserve the known canonical form of the signal $\underline{\epsilon}_k$. This group of transformations with larger degrees of freedom will lead to a larger set of maximal invariants in the following proposition compared to the single target case.

42

Proposition 4 *The maximal invariant of the model (5.4) under the group of transformations in (5.5) consists of $p + 2$ functions of the measurement:*

$$
\begin{aligned}
z_1 &= \underline{u}^H \mathbf{D}^{-1} \underline{u}, \\
z_2 &= \underline{x}_{21}^H (\mathbf{X}_{22} \mathbf{X}_{22}^H)^{-1} \underline{x}_{21}, \\
z_{3k} &= \underline{u}^H \mathbf{D}^{-1} \underline{\epsilon}_k (\underline{\epsilon}_k^T \mathbf{D}^{-1} \underline{\epsilon}_k)^{-1} \underline{\epsilon}_k^T \mathbf{D}^{-1} \underline{u}
\end{aligned}
$$

where $k = 1, \dots, p$ and

$$
\begin{aligned}
\underline{u} &= \underline{x}_{11} - \mathbf{X}_{12} \mathbf{X}_{22}^H (\mathbf{X}_{22} \mathbf{X}_{22}^H)^{-1} \underline{x}_{21}, \\
\mathbf{D} &= \mathbf{X}_{12} \left[\mathbf{I} - \mathbf{X}_{22}^H (\mathbf{X}_{22} \mathbf{X}_{22}^H)^{-1} \mathbf{X}_{22} \right] \mathbf{X}_{12}^H.
\end{aligned}
$$

Proof: See the appendix. ∎

Now the unstructured Kelly's test (3.8) can be modified by maximizing over the p target signatures $\{\underline{\epsilon}_k\}_{k=1}^p$:

$$
T_{Ku} = \max_{k=1,\dots,p} \frac{\left| \left[\underline{\epsilon}_k^T \ \underline{0}^T \right] (\mathbf{X}_2 \mathbf{X}_2^H)^{-1} \underline{x}_1 \right|^2}{\left[\underline{\epsilon}_k^T \ \underline{0}^T \right] (\mathbf{X}_2 \mathbf{X}_2^H)^{-1} \begin{bmatrix} \underline{\epsilon}_k \\ \underline{0} \end{bmatrix} \cdot \left\{ 1 + \underline{x}_1^H (\mathbf{X}_2 \mathbf{X}_2^H)^{-1} \underline{x}_1 \right\}}.
$$

We will next express this test as a function of the new maximal invariants. Since z_1 and z_2 are equivalent to those in Proposition 1 except for the dimension, it easily follows that

$$
1 + \underline{x}_1^H (\mathbf{X}_2 \mathbf{X}_2^H)^{-1} \underline{x}_1 = 1 + z_1 + z_2.
$$

Also using the inverse of the partitioned matrix [20] on $(\mathbf{X}_2 \mathbf{X}_2^H)^{-1}$, we can write

$$
(\mathbf{X}_2 \mathbf{X}_2^H)^{-1} = \begin{bmatrix} V_{11} & V_{12} \\ V_{21} & V_{22} \end{bmatrix}
$$

where

$$
\begin{aligned}
V_{11} &= \mathbf{D}^{-1}, \\
V_{21} &= -\mathbf{D}^{-1} \mathbf{X}_{12} \mathbf{X}_{22}^H (\mathbf{X}_{22} \mathbf{X}_{22}^H)^{-1}.
\end{aligned}
$$

Then we have

$$
\begin{aligned}
\left[\underline{\epsilon}_k^T \ \underline{0}^T \right] (\mathbf{X}_2 \mathbf{X}_2^H)^{-1} \begin{bmatrix} \underline{\epsilon}_k \\ \underline{0} \end{bmatrix} &= \underline{\epsilon}_k^T \mathbf{D}^{-1} \underline{\epsilon}_k, \\
\left[\underline{\epsilon}_k^T \ \underline{0}^T \right] (\mathbf{X}_2 \mathbf{X}_2^H)^{-1} \underline{x}_1 &= \underline{\epsilon}_k^T \mathbf{D}^{-1} \underline{u}
\end{aligned}
$$

and hence the Kelly's test is an invariant test of form

$$
T_{Ku} = \max_{k=1,\dots,p} \frac{z_{3k}}{1 + z_1 + z_2}.
$$

43

5.3 Structured Covariance Case

Next consider Case 1 for the structured model. In this case, the signal model is same as (5.1), but with the structured target signatures as in (5.2). Then, similarly to the above unstructured case, the canonical image model is defined as

$$\mathbf{X} = a \begin{bmatrix} \underline{\epsilon}_k \\ \underline{0}_A \\ \underline{\epsilon}_k \\ \underline{0}_B \end{bmatrix} \underline{e}_1^T + \mathbf{N} \tag{5.6}$$

where $\underline{0}_A$ and $\underline{0}_B$ are $(m_A - p) \times 1$ and $(m_B - p) \times 1$ zero vectors, respectively. Thus, this canonical form can be partitioned as

$$\mathbf{X} = \begin{bmatrix} \mathbf{X}_A \\ \mathbf{X}_B \end{bmatrix} = \begin{bmatrix} \underline{x}_{A11} & \mathbf{X}_{A12} \\ \underline{x}_{A21} & \mathbf{X}_{A22} \\ \underline{x}_{B11} & \mathbf{X}_{B12} \\ \underline{x}_{B21} & \mathbf{X}_{B22} \end{bmatrix}$$

and the invariant group of transformations on $\mathbf{X}$ is

$$g(\mathbf{X}) = \begin{bmatrix} \begin{bmatrix} \Delta & \mathbf{B}_A \\ \mathbf{O} & \mathbf{M}_A \end{bmatrix} & \mathbf{X}_A & \begin{bmatrix} 1 & \underline{0}^T \\ \underline{0} & \mathbf{U}_A \end{bmatrix} \\ \begin{bmatrix} \Delta & \mathbf{B}_B \\ \mathbf{O} & \mathbf{M}_B \end{bmatrix} & \mathbf{X}_B & \begin{bmatrix} 1 & \underline{0}^T \\ \underline{0} & \mathbf{U}_B \end{bmatrix} \end{bmatrix} \tag{5.7}$$

where we have the same $p \times p$ diagonal matrix Δ for $\mathbf{X}_A$ and $\mathbf{X}_B$ to preserve the signal vector $\underline{\epsilon}_k$ and the same amplitude in region A and B.

Proposition 5 *With the model (5.6) and the group of transformations in (5.7), the maximal invariant is obtained as*

$$
\begin{aligned}
z_{A1} &= \underline{u}_A^H \mathbf{D}_A^{-1} \underline{u}_A, \\
z_{A2} &= \underline{x}_{A21}^H (\mathbf{X}_{A22} \mathbf{X}_{A22}^H)^{-1} \underline{x}_{A21}, \\
z_{A3k} &= \underline{u}_A^H \mathbf{D}_A^{-1} \underline{\epsilon}_k (\underline{\epsilon}_k^T \mathbf{D}_A^{-1} \underline{\epsilon}_k)^{-1} \underline{\epsilon}_k^T \mathbf{D}_A^{-1} \underline{u}_A, \\
z_{B1} &= \underline{u}_B^H \mathbf{D}_B^{-1} \underline{u}_B, \\
z_{B2} &= \underline{x}_{B21}^H (\mathbf{X}_{B22} \mathbf{X}_{B22}^H)^{-1} \underline{x}_{B21}, \\
z_{B3k} &= \underline{u}_B^H \mathbf{D}_B^{-1} \underline{\epsilon}_k (\underline{\epsilon}_k^T \mathbf{D}_B^{-1} \underline{\epsilon}_k)^{-1} \underline{\epsilon}_k^T \mathbf{D}_B^{-1} \underline{u}_B, \\
z_{ABk} &= \frac{(\underline{\epsilon}_k^T \mathbf{D}_A^{-1} \underline{\epsilon}_k)^{-1} \underline{\epsilon}_k^T \mathbf{D}_A^{-1} \underline{u}_A}{(\underline{\epsilon}_k^T \mathbf{D}_B^{-1} \underline{\epsilon}_k)^{-1} \underline{\epsilon}_k^T \mathbf{D}_B^{-1} \underline{u}_B}
\end{aligned}
$$

where

$$\underline{u}_A = \underline{x}_{A11} - \mathbf{X}_{A12}\mathbf{X}_{A22}^H(\mathbf{X}_{A22}\mathbf{X}_{A22}^H)^{-1}\underline{x}_{A21},$$

$$\underline{u}_B = \underline{x}_{B11} - \mathbf{X}_{B12}\mathbf{X}_{B22}^H(\mathbf{X}_{B22}\mathbf{X}_{B22}^H)^{-1}\underline{x}_{B21},$$

$$\mathbf{D}_A = \mathbf{X}_{A12}\left[\mathbf{I} - \mathbf{X}_{A22}^H(\mathbf{X}_{A22}\mathbf{X}_{A22}^H)^{-1}\mathbf{X}_{A22}\right]\mathbf{X}_{A12}^H,$$

$$\mathbf{D}_B = \mathbf{X}_{B12}\left[\mathbf{I} - \mathbf{X}_{B22}^H(\mathbf{X}_{B22}\mathbf{X}_{B22}^H)^{-1}\mathbf{X}_{B22}\right]\mathbf{X}_{B12}^H$$

for $k = 1, \dots, p$. And the coupling term z_{ABk} can be replaced by

$$z_{ABk'} = \frac{\left|(\underline{\epsilon}_k^T\mathbf{D}_A^{-1}\underline{\epsilon}_k)^{-1}\underline{\epsilon}_k^T\mathbf{D}_A^{-1}\underline{u}_A - (\underline{\epsilon}_k^T\mathbf{D}_B^{-1}\underline{\epsilon}_k)^{-1}\underline{\epsilon}_k^T\mathbf{D}_B^{-1}\underline{u}_B\right|^2}{(\underline{\epsilon}_k^T\mathbf{D}_A^{-1}\underline{\epsilon}_k)^{-1} + (\underline{\epsilon}_k^T\mathbf{D}_B^{-1}\underline{\epsilon}_k)^{-1}}$$

or $z_{ABk''}$ which is equivalent to $z_{ABk'}$ except that $q_A\mathbf{D}_A$ and $q_B\mathbf{D}_B$ are substituted for $\mathbf{D}_A$ and $\mathbf{D}_B$, respectively, where $q_A = 1 + z_{A1} + z_{A2}$ and $q_B = 1 + z_{B1} + z_{B2}$.

    Proof: See the appendix.   ■

Note that z_{A1}, z_{A2}, z_{B1} and z_{B2} are again equivalent to those in Proposition 2 except for the dimension (p vs. 1).

    For Case 1, we had before the structured Kelly's test, T_{Ks} (4.13), and the MI test, T_1 (4.16). First, consider T_{Ks} modified to fit the multiple signature model:

$$T_{Ks} = \max_{k=1,\dots,p} \frac{\left|\underline{s}_k^H\mathbf{K}^{-1}\underline{x}_1\right|^2}{\underline{s}_k^H\mathbf{K}^{-1}\underline{s}_k \cdot \left\{1 + \underline{x}_1^H\mathbf{K}^{-1}\underline{x}_1\right\}}$$

where $\underline{x}_1$ and $\mathbf{K}$ are same as defined in (4.13), but for the target signature, we have structured one as in (5.6). Then, as before we have

$$1 + \underline{x}_1^H\mathbf{K}^{-1}\underline{x}_1 = 1 + z_{A1} + z_{A2} + z_{B1} + z_{B2}$$

and from the results of the previous section and Lemma 1, the remaining term can be written as

$$\frac{\left|\underline{s}_k^H\mathbf{K}^{-1}\underline{x}_1\right|^2}{\underline{s}_k^H\mathbf{K}^{-1}\underline{s}_k} = \frac{\left|\underline{\epsilon}_k^T\mathbf{D}_A^{-1}\underline{u}_A + \underline{\epsilon}_k^T\mathbf{D}_B^{-1}\underline{u}_B\right|^2}{\underline{\epsilon}_k^T\mathbf{D}_A^{-1}\underline{\epsilon}_k + \underline{\epsilon}_k^T\mathbf{D}_B^{-1}\underline{\epsilon}_k}. \tag{5.8}$$

Using the matrix identity [29], it can be verified that (5.8) is identical to $z_{A3k} + z_{B3k} - z_{ABk'}$. Thus T_{Ks} is a function of maximal invariant of form

$$T_{Ks} = \max_{k=1,\dots,p} \frac{z_{A3k} + z_{B3k} - z_{ABk'}}{1 + z_{A1} + z_{A2} + z_{B1} + z_{B2}}.$$

    MI test can also be modified by replacing the signal vector with $\underline{s}_k$ and maximizing over k. Therefore, the modified T_1 is equivalent to (5.8) except for $q_A\mathbf{D}_A$ and $q_B\mathbf{D}_B$ replacing

$\mathbf{D}_A$ and $\mathbf{D}_B$:

$$T_1 = \max_{k=1,\dots,p} \frac{\left| \underline{\epsilon}_k^T (q_A \mathbf{D}_A)^{-1} \underline{u}_A + \underline{\epsilon}_k^T (q_B \mathbf{D}_B)^{-1} \underline{u}_B \right|^2}{\underline{\epsilon}_k^T (q_A \mathbf{D}_A)^{-1} \underline{\epsilon}_k + \underline{\epsilon}_k^T (q_B \mathbf{D}_B)^{-1} \underline{\epsilon}_k}.$$

This can also be written as

$$T_1 = \max_{k=1,\dots,p} \left\{ \frac{z_{A3k}}{1 + z_{A1} + z_{A2}} + \frac{z_{B3k}}{1 + z_{B1} + z_{B2}} - z_{ABk''} \right\}.$$

5.4   Conclusion

In this chapter, the more realistic problem of detecting one from a set of known targets is considered. For both unstructured and structured cases, the invariance procedure is investigated as well as the simple GLR extension.

To obtain the canonical image model, the different transformation of the measurement as in (5.3) is used instead of QR decompositions described in Chapter 2. This transformation (5.3) leads to the invariant group (5.5) for the unstructured case or (5.7) for the structured case consisting of diagonal matrices. If we used unitary matrices obtained from QR decompositions as in Chapter 2, we might have had in (5.5) and (5.7) arbitrary matrices instead. Thus, using (5.5) and (5.7) with larger degrees of freedom, we can define larger sets of maximal invariants which are needed to modify invariant tests to fit this multiple target case. However, since this canonical transformation (5.3) is not an orthogonal transformation of the measurement, only Case 1 can be considered where the test statistics are not affected by this transformation. The extension problem for Cases 2 and 3 is not addressed in the present thesis, and applying invariance procedure to this problem is a topic for future research.

CHAPTER 6

Numerical Comparison and Analysis

6.1 Introduction

To analyze the performance of the GLR and MI tests derived under the three structured covariance assumptions, Case 1, 2, and 3, receiver operating characteristic (ROC) curves are generated and compared in this chapter. Even though the exact distributions of the test statistics are difficult to determine, it is well known that under H_0 the log GLR test statistic of the form $2 \ln \Lambda$ has asymptotically a chi-square distribution with number of degrees of freedom determined by the number of fixed parameters under H_0 and H_1 [3]. This asymptotic approximation can be used to determine the threshold on the GLR which ensures a given P_{FA}. In each simulation, we generated n 10×10 subimages containing 2 independent clutter regions of area m_A and m_B pixels, respectively, and a 5×5 synthetic canonical target is inserted into the first subimage in such a manner to straddle the boundary of the two different regions. Each of the subimages is then concatenated into a column vector of size 100 to obtain a $100 \times n$ measurement matrix. This procedure is illustrated in Figure 6.1. Each of the ROC curves (P_D vs. P_{FA}) shown below was obtained after 500 simulations.

In the following, the ROC curves are evaluated based on factors such as the target-to-clutter power ratio; the dimensional parameters, m_A, m_B and n; and the prior uncertainty on the spatial covariance $\mathbf{R}$. Case 1, 2 and 3 are considered separately under different assumptions on clutter covariance. In each case, the three GLR tests (4.2), (4.8), (4.10), and the three MI tests (4.17), (4.22), (4.23) matched to one of the three cases are compared. Also shown are ROC curves for the following tests proposed by other authors: Kelly's structured test (4.15) matched to Case 1, and Bose and Steinhardt's invariant test (4.20) matched to Case 2. We also experimented with a real image where both of our GLR and

47
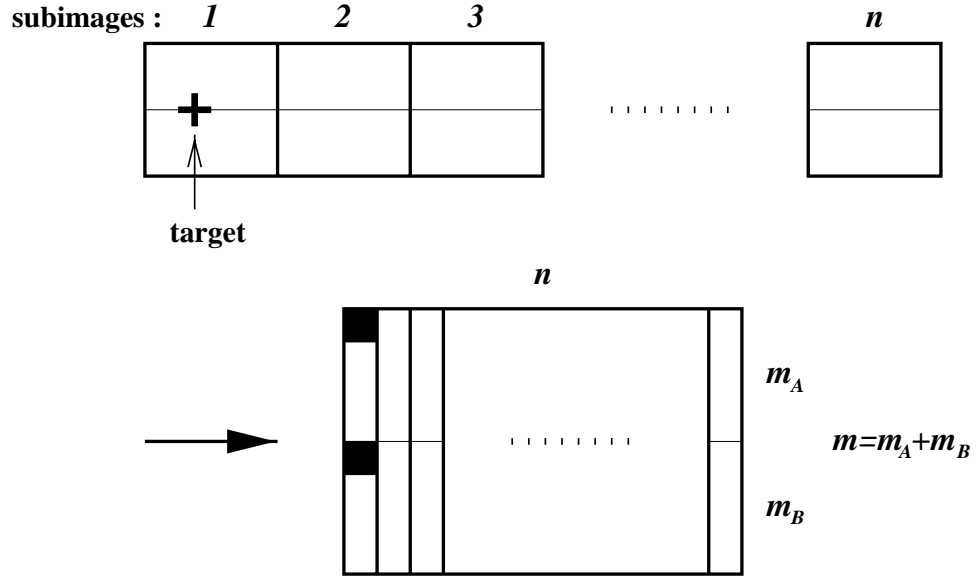
Figure 6.1: Image matrix formation for ROC simulation.

MI tests were applied to a SAR clutter image with an inserted real target at various pose angles.

6.2 ROC Simulation

6.2.1 Comparison with Different SNRs

First, we compared the detectors by varying SNR in region B (SNR_B) for Cases 1, 2 and 3. In Figures 6.2 - 6.4, the ROC curves of 8 different tests are compared for several SNRs: Structured Kelly's test (4.15), Bose and Steinhardt's test (4.20), MI test 1 (4.17), MI test 2 (4.22), MI test 3 (4.23), GLR 1 (4.2), GLR 2 (4.8), and GLR 3 (4.10). For each case, two tests stand out as significantly better than the other six: the GLR and MI tests which are matched to the underlying scenario, e.g. GLR 1 and MI test 1 for Case 1; and GLR 2 and MI test 2 for Case 2. This confirms the results from the previous section. For Case 1, we were able to achieve performance improvement by separating the same coupled denominator for both regions found in the matched Kelly's test (4.15). For Case 2, the ROC improvement over the matched Bose and Steinhardt's test is explained by the weighting between two different regions which is carefully managed in GLR 2 and MI test 2.

Note that, however, neither the GLR nor the MI test uniformly outperforms the other. Of particular interest are the curve crossings in the low P_{FA} regions between the GLR and

the MI tests. In Figure 6.2 (b), we can observe the gains in P_D of MI test 1 over GLR 1 for $P_{FA} < 0.1$. Moreover, it should be noted that the ROC of the structured Kelly's test is dominated by that of the MI test 1 in the low P_{FA} region and by that of the GLR 1 in the high P_{FA} region. In Case 2 (Figure 6.3 (b)), both the MI test 2 and GLR 2 outperform Bose and Steinhardt's matched invariant test and it appears that MI test 2 slightly outperforms GLR 2 for low P_{FA}. These crossings are also observed for mismatched cases: between MI test 1 and GLR 1 in Case 2 (Figure 6.3), and between MI test 2 and GLR 2 in Case 1 (Figure 6.2 (b)).

For Case 3 (Figure 6.4), the ROC curves for GLR 2 approach those of the matched GLR 3 in both (a) and (b) since a large number of pixels ($m_B n = 60 \times 61$) are available to generate good MLEs of the unknown variance in region B. In Figure 6.5, those tests derived under Cases 2 and 3 are compared with different σ^2 in region B. As illustrated, the performance of GLR 2 and MI test 2 is not affected by the underlying variance. But GLR 3 and MI test 3 which assume $\sigma^2 = 1$ approximate GLR 2 and MI teat 2 better when the underlying variance is large ((b)) than when small ((a)). And again, we cannot separate the tests for Case 2 and the tests for Case 3 with large number of data even when $\sigma^2 = 1$ ((c)).

To compare GLR 2 and GLR 3, consider the second terms associated with region B. For GLR 2 (4.8), this second term can be rewritten as

$$m_B \cdot \ln \left[1 + \frac{1}{m_B n \hat{\sigma}^2} \{ q(0, \underline{s}_B, \mathbf{X}_B) - q(\hat{a}, \underline{s}_B, \mathbf{X}_B) \} \right]$$

where

$$\hat{\sigma}^2 = \frac{1}{m_B n} q(\hat{a}, \underline{s}_B, \mathbf{X}_B).$$

Thus, as $m_B n$ gets large, $\hat{\sigma}^2$ goes to 1 under Case 3 and this term approaches that of the matched GLR 3 (4.10):

$$\frac{1}{n} [q(0, \underline{s}_B, \mathbf{X}_B) - q(\hat{a}, \underline{s}_B, \mathbf{X}_B)].$$

In fact, in a typical radar detection problem, m_B and n are quite large since they are the number of pixels in a subimage and the number of subimages, respectively, and GLR 2 is expected to perform as well as GLR 3 under Case 3. Thus, in the following, we will concentrate on the relative performance of GLR vs. MI tests for Cases 1 and 2.

6.2.2 Comparison with Different Windows

In this section, ROC curves are compared with different ratios of m_A/m_B by up and down shifting the 10×10 windows used to collect the subimages along the boundary. In Figure 6.6 for Case 1, GLR 1 performs better as m_B decreases since fewer parameters can be more accurately estimated with the same number of chips ($n = 61$): the GLR test has to estimate a covariance matrix ($\mathbf{R}_B$) of size 60×60 in (a), but only of size 40×40 in (c). For the smaller size covariance of (b), the structured Kelly's test is almost as accurate as the GLR and MI tests. Conversely, in Figure 6.7 of Case 2, GLR 2 performs better as m_B increases since in this case it only needs to estimate the scalar variance in region B and the number of pixels available increases as m_B increases ((a) $m_B n = 60 \times 61$ vs. (c) $m_B n = 40 \times 61$). Also Bose and Steinhardt's test is more sensitive to the number m_B than MI test 2 and GLR 2, and its ROC falls below even those of the mismatched tests shown in (b) and (c).

The relative advantages of MI vs. GLR tests are more closely investigated in the next two figures. In Figures 6.8 and 6.9, we consider Case 1 and Case 2, respectively. In (a) of both figures, we increased the number of chips n while fixing SNR. Note that the GLR and MI tests have ROCs which are virtually indistinguishable for large n. In (b), however, we fixed n and increased SNR. The P_{FA} positions of the crossings of the ROCs for the GLR and MI tests decreased with increasing SNR. In particular, if one fixes a level of false alarm, say $P_{FA} = 0.1$, then note from Figure 6.8 (b) that the GLR test dominates the MI test for SNR = 19 dB while the reverse is true for SNR = 7 dB. This behavior is best explained by the fact that at high SNR, the MLE is an accurate estimate of target amplitude, while at low SNR the MLE degrades significantly. Therefore, the GLR which depends on the accuracy of the MLE for accurate detection breaks down for low SNR.

6.3 Experiment with SAR Images

We consider an application to real SAR imagery in Figure 6.10. The image shown is a rural scene near Redstone Arsenal at Huntsville, Alabama, reproduced from the data collected using the Sandia National Laboratories Twin Otter SAR sensor payload operating at X band (center frequency = 9.6 GHz, band width = 590 MHz). This clutter image consists of a forest canopy on top and a field on bottom, separated by a coarse boundary. The boundary was hand extracted, and a sequence of 9×7 SLICY targets at different

poses were also hand extracted from the image data in Figure 6.11. The images in Figure 6.11 correspond to the same target but viewed at different pose angles of azimuth. The elevation of $39°$ was fixed for all poses. The data from which these images are reproduced was downloaded from the moving and stationary target recognition programs (MSTAR) SAR database at the Center for Imaging Science [9].

In a first experiment the target signature at pose of azimuth $163°$ from Figure 6.11 (e) was tested at different positions along the boundary. In Figure 6.10, the target is inserted additively with the center at column 305 so that it straddles the boundary. From the realigned image in Figure 6.12, we took subimages (chips) along the boundary by centering a 20×20 window at the boundary and sliding it over the image from left to right. Each of these subimages is then concatenated into a column vector of size $m = 400$ where $m_A = 200$ and $m_B = 200$. Since we need at least 200 secondary chips to implement the structured detectors, clutter-alone pixels above and below those 20×20 subimages taken along the boundary were used to generate enough secondary data for region A and B, respectively. Each of the subimages along the boundary was tested as a primary chip, and the test statistics derived under Case 1 were calculated and maximized over each possible location in the subimage. After normalizing the known target signature, we obtained the minimum magnitude of target amplitude required for each test to detect the target at the correct location. The resulting amplitude is the minimum detectable threshold for each of the detectors and these thresholds are shown in Table 6.1 for different number of secondary chips $(n - 1)$. As can be seen, with a large number of chips $(n - 1 = 250)$, both the GLR and MI tests perform as well as the structured Kelly's test. On the other hand, with a limited number of chips $(n - 1 = 200)$, MI test 1 successfully detects the target down to a significantly lower threshold than for GLR 1 and structured Kelly detectors.

Test	$|a|$	
	$(n - 1 = 250)$	$(n - 1 = 200)$
MI test 1	1.454×10^{-2}	0.609×10^{-1}
GLR 1	1.462×10^{-2}	1.042×10^{-1}
Structured Kelly	1.407×10^{-2}	1.049×10^{-1}

Table 6.1: Minimum detectable amplitudes for detection of the target at the correct location.

As a next experiment we maximized the test statistics over the different target poses in Figure 6.11 as well as over all possible locations along the boundary. Again the normalized

signature from Figure 6.11 (e) was inserted with $|a| = 0.015$, and 250 secondary chips were obtained from the surrounding clutter. Test values for the 3 detectors under Case 1 are obtained using 9 different target signatures. For each test the peak values for 9 target signatures are plotted in Figure 6.13. Note that all the tests successfully picked the signature at the true pose and location for this target amplitude.

6.4   Robustness of the Structured Detectors to Segmentation Errors

Both of our structured GLR and MI tests are derived under the known boundary assumption separating two different regions. Thus these tests could only be implemented and compared with the pre-segmented clutter regions so far. However, edge detection or image segmentation is not a simple task in SAR images in which a natural blur due to the finite aperture and speckle noise are well known problems [14, 47]. In this section, sensitivity of the structured detectors to segmentation errors is investigated.

First, the effect of the false boundary information is illustrated in Figure 6.14. Figure 6.14 (a) shows the true underlying boundary and the false boundary moved downward by one pixel in all subimages. Note that even one pixel difference in a subimage will lead to a much larger difference (number of columns in each subimage) after reshaping those subimages into column vectors of the measurement matrix. In (b), ROC curves obtained with the biased boundary are compared with those using the true boundary. The overall performance of each test is deteriorated with the false information, but we can still observe the crossing of the ROC curves between the GLR and MI tests. Next we compare the ROC performance with the estimated boundary utilizing Sobel's edge detection method [27, 41]. As illustrated in Figure 6.15 (a), we consider the effect of segmentation errors only in the secondary clutter-alone subimages to preserve the same target signature in the primary subimage for both simulations with the true boundary and the estimated boundary. The relative advantages of the GLR and MI tests can still be observed in this case (Figure 6.15 (b)).

Finally, we experiment with the SAR images in Figure 6.10 and 6.11, and compare with the results in Section 6.3. Figure 6.16 shows the clutter image in Figure 6.10 with the hand-extracted boundary superimposed on it. We obtain the estimated boundary using Sobel's method and its deviation from the hand-extracted boundary is plotted in Figure

6.17. As in Section 6.3, minimum detectable amplitudes for the GLR and MI tests are obtained using the estimated boundary. Note that we only apply the estimated boundary to the clutter-alone chips so that we can have the same target signature as used for the results in Table 6.1. Table 6.2 shows the results for 200 secondary chips using two different boundary information. As in the ROC simulation, both detectors need larger amplitudes for correct detection, but we can conclude that the MI test is more robust than the GLR test.

Test	$|a|$ $(n - 1 = 200)$	
	(with hand-extracted boundary)	(with estimated boundary)
MI test 1	0.609×10^{-1}	2.327×10^{-1}
GLR 1	1.042×10^{-1}	8.655×10^{-1}

Table 6.2: Minimum detectable amplitudes with the hand-extracted boundary and the estimated boundary.

6.5 Conclusion

These numerical results confirm the intuitions developed in Chapter 4. We could observe the effects of such factors on the detector performance as the prior uncertainty in the structured clutter covariance, the target-to-clutter power ratio, and several dimensional parameters. In particular, the existing Kelly's structured test and Bose and Steinhardt's test are more sensitive to m_A or m_B than the new GLR and MI tests, as expected from their maximal invariant forms. However, these results also indicate that neither GLR nor MI tests dominate the other in terms of ROC performance. Simply stated, the GLR test is good only when the high estimator accuracy is attainable, and there exists a threshold number of data points in each region for which the sufficient high accuracy can be obtained favoring the GLR test. Otherwise, the MI test is better, especially in low P_{FA}, because it tries to smooth over unknown parameters rather than estimate them.

In our studies, both of the GLR and MI detectors are derived assuming that the boundary of two different regions is known a priori. These tests can only be implemented in the realigned image along the boundary. In the context of a real radar imaging application, however, we must estimate the boundaries at the same time as detecting the target. Boundary segmentation will be hampered when a strong target lies along the boundary,

even though target detection might normally be expected to improve for a strong target. A future goal is to combine optimal boundary estimation and target detection. This would ideally involve a fully automated procedure which is capable of detecting a target in any subimage located in clutter by applying the appropriate structure to the clutter covariance whenever a boundary exists. In any such procedure, it will be necessary to establish the tradeoffs between segmentation and detection, and the sensitivity of the detector to the unknown boundary. The tools and approach developed in previous chapters will be useful for attaining this goal.
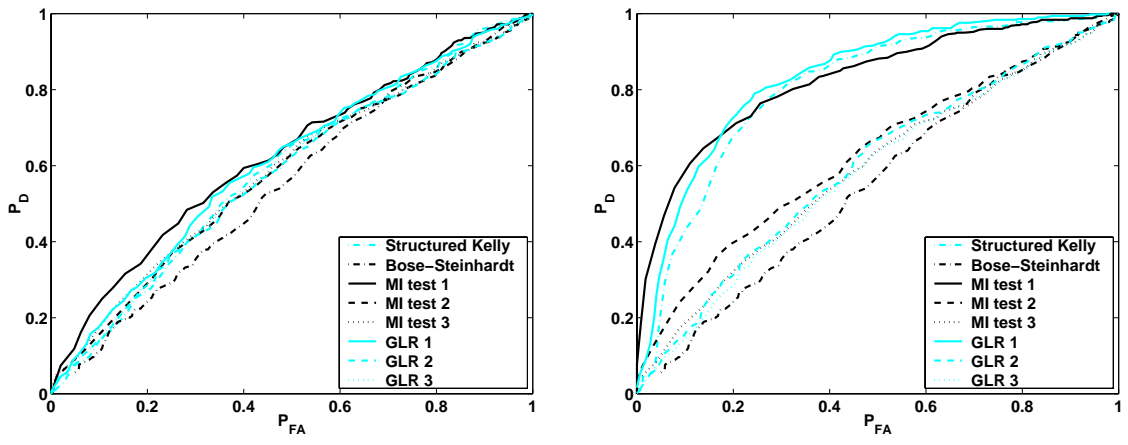
(a) $\mathrm{SNR}_A = 11$ dB, $\mathrm{SNR}_B = 10$ dB   (b) $\mathrm{SNR}_A = 11$ dB, $\mathrm{SNR}_B = 22$ dB

Figure 6.2: ROC curves for Case 1 with (a) SNR $= 14$ dB, (b) SNR $= 22$ dB ($m_A = 50, m_B = 50, n = 51$).
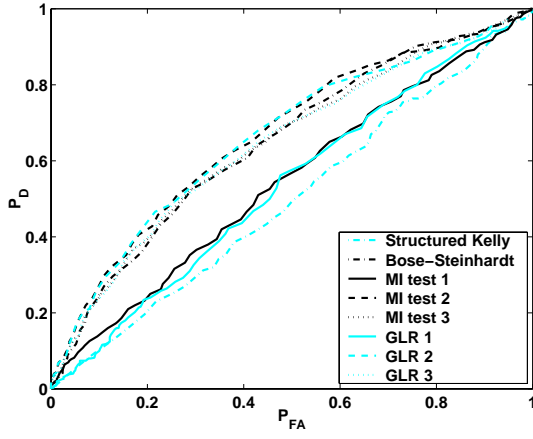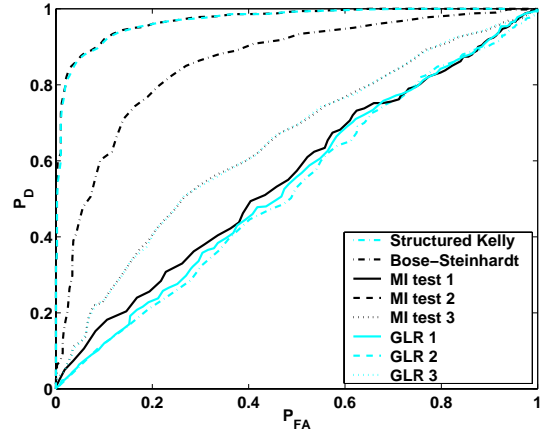
(a) SNR$_A$ = 3 dB, SNR$_B$ = -6 dB   (b) SNR$_A$ = 3 dB, SNR$_B$ = 8 dB

Figure 6.3: ROC curves for Case 2 with (a) SNR = 4 dB, (b) SNR = 10 dB ($m_A = 40, m_B = 60, n = 61$).
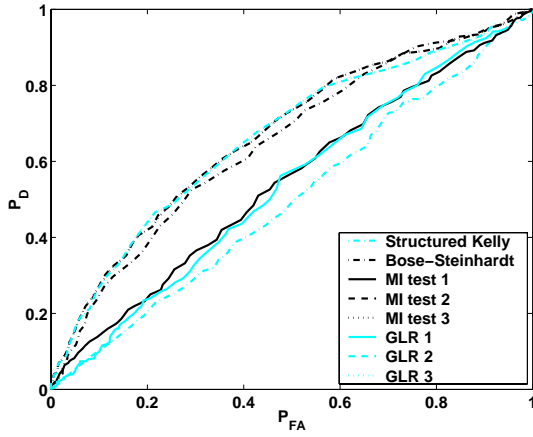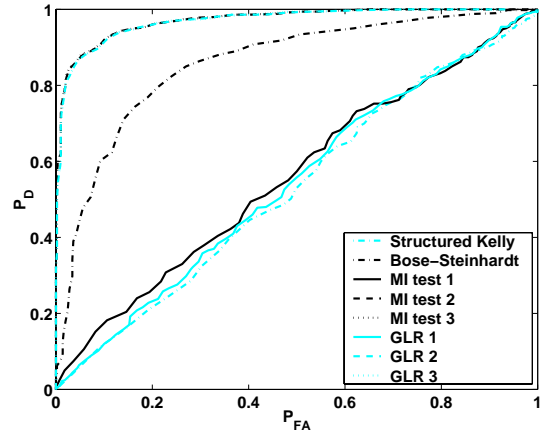
(a) SNR$_A$ = 3 dB, SNR$_B$ = -6 dB   (b) SNR$_A$ = 3 dB, SNR$_B$ = 8 dB

Figure 6.4: ROC curves for Case 3 with (a) SNR = 4 dB, (b) SNR = 10 dB ($m_A = 40, m_B = 60, n = 61$).
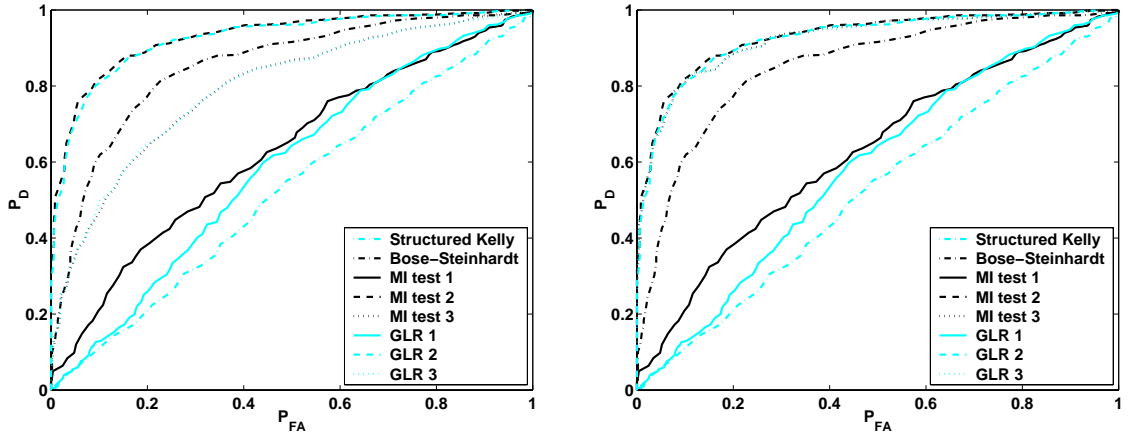
(a) $\sigma^2 = 0.1$

(b) $\sigma^2 = 10$
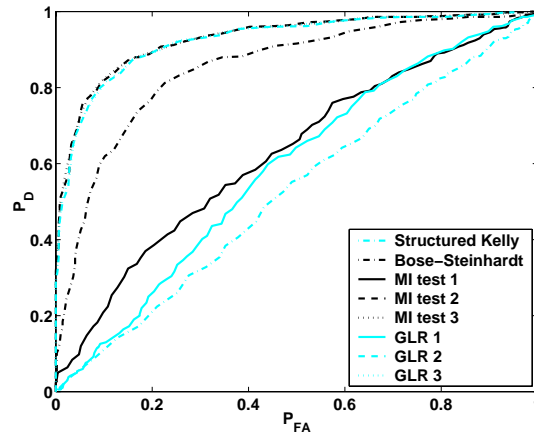
(c) $\sigma^2 = 1$

Figure 6.5: Comparison of tests derived under Case 2 and Case 3 with regard to σ^2 in region B with SNR = 10 dB ($m_A = 40, m_B = 60, n = 61$).
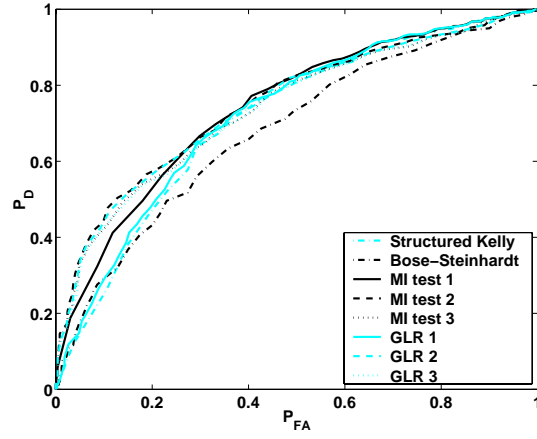
(a) $m_A = 40, m_B = 60$
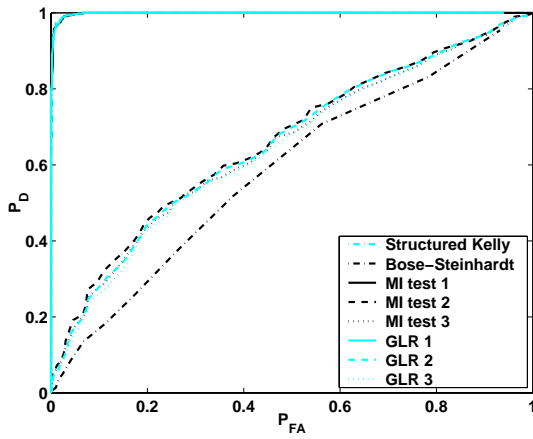
(b) $m_A = 50, m_B = 50$
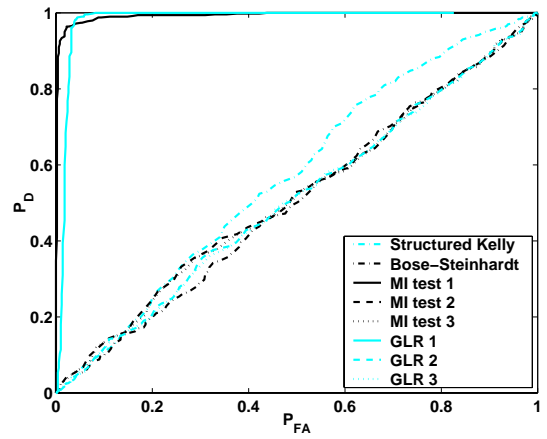
(c) $m_A = 60, m_B = 40$

Figure 6.6: ROC curves for Case 1 with different ratios of m_A/m_B, and SNR = 19 dB ($n = 61$).
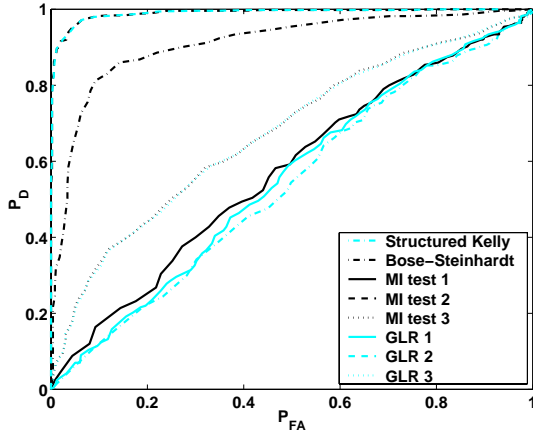
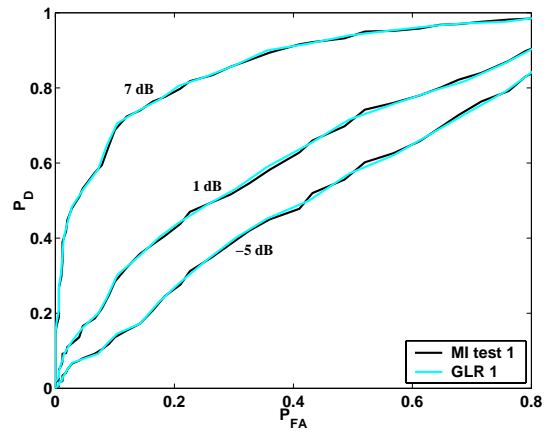(a) $m_A = 40, m_B = 60$
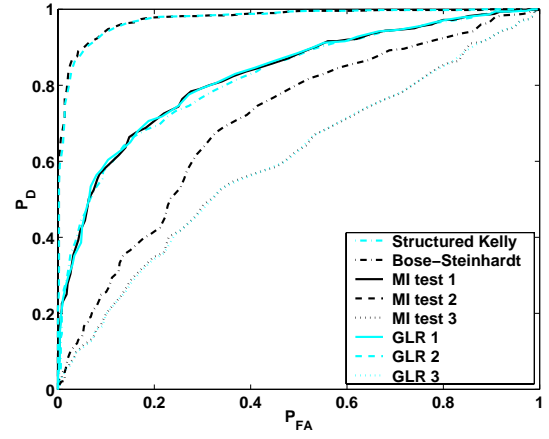
(b) $m_A = 50, m_B = 50$
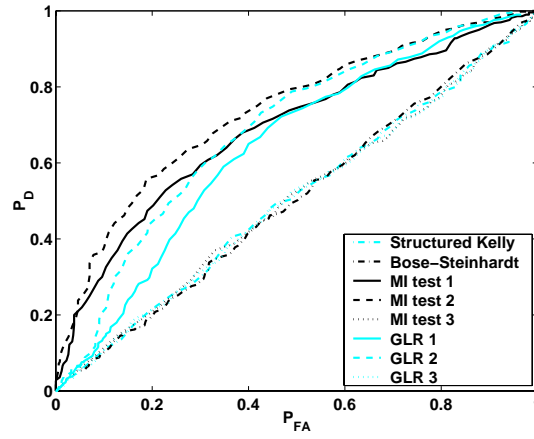
(c) $m_A = 60, m_B = 40$

Figure 6.7: ROC curves for Case 2 with different ratios of m_A/m_B, and SNR = 10 dB ($n = 61$).
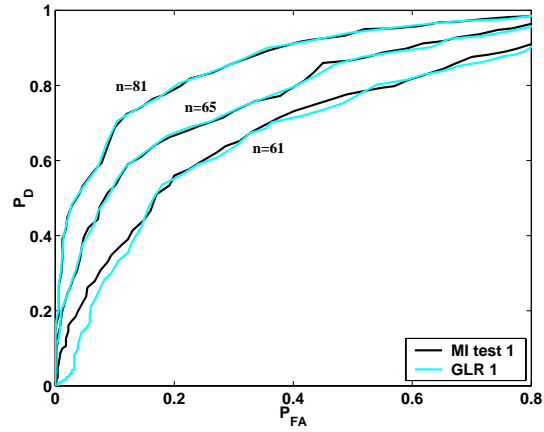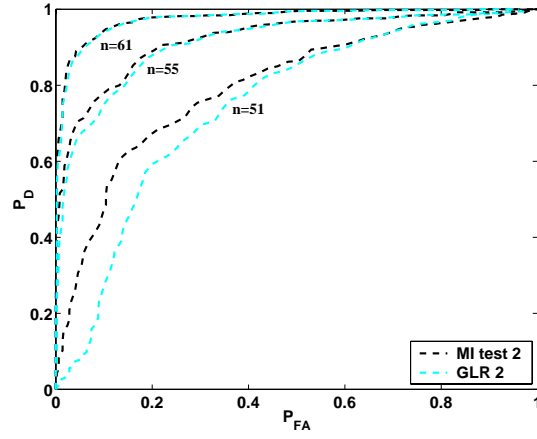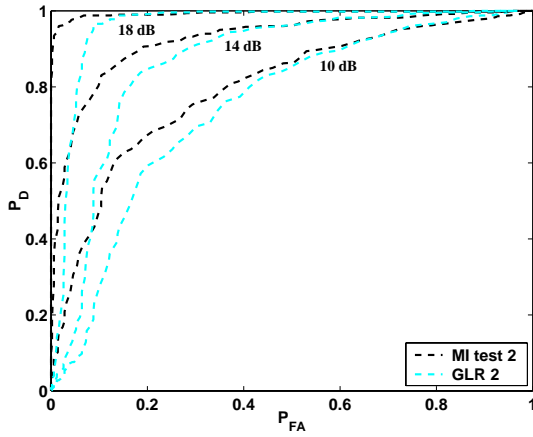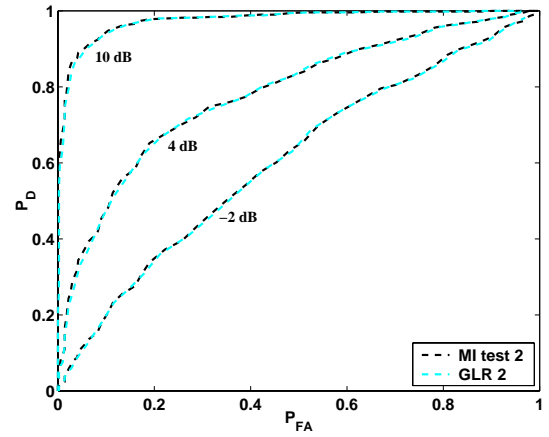
(a) SNR = 7 dB
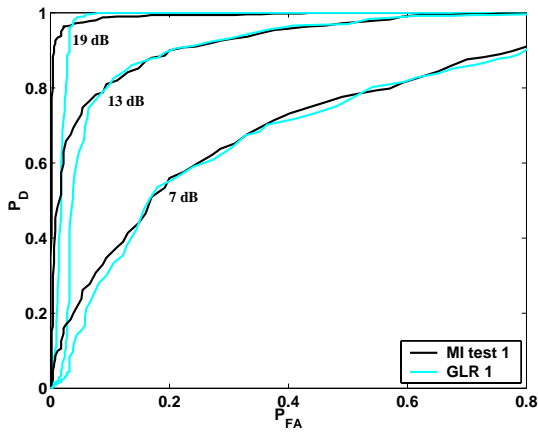
(b) $n = 61$

(c) $n = 81$

Figure 6.8: Comparison of GLR and MI tests for Case 1 by (a) varying n with fixed SNR, (b) increasing SNR with small n, and (c) decreasing SNR with large n ($m_A = 60, m_B = 40$).

(a) SNR = 10 dB

(b) $n = 51$

(c) $n = 61$

Figure 6.9: Comparison of GLR and MI tests for Case 2 by (a) varying n with fixed SNR, (b) increasing SNR with small n, and (c) decreasing SNR with large n ($m_A = 50, m_B = 50$).
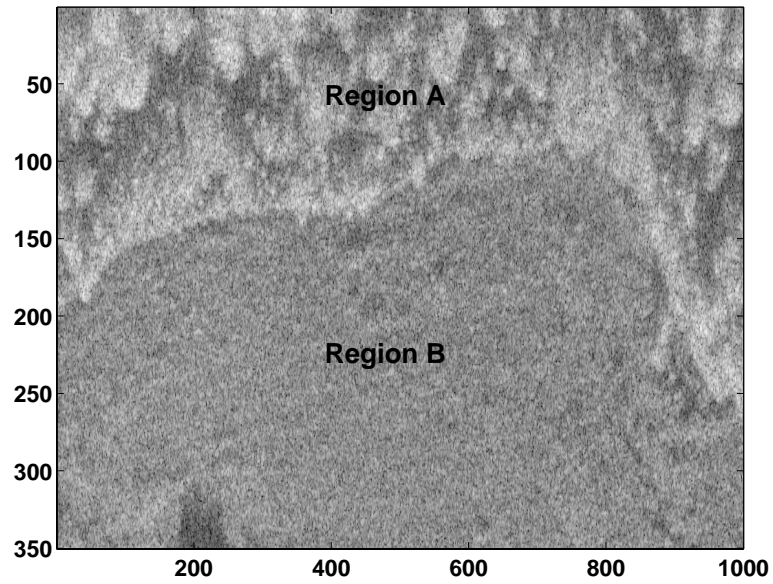
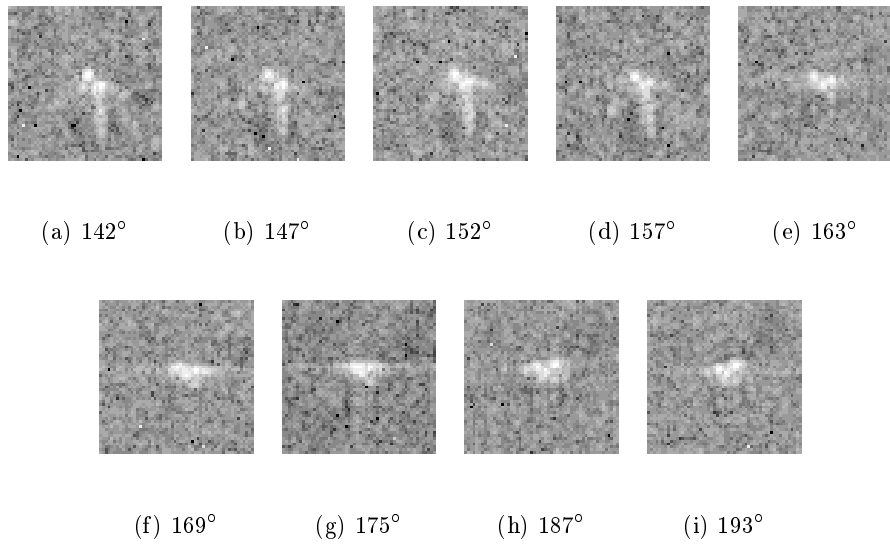Figure 6.10: SAR clutter image with a target in Figure 6.11 (e) straddling the boundary at column 305.

(a) 142°   (b) 147°   (c) 152°   (d) 157°   (e) 163°

(f) 169°   (g) 175°   (h) 187°   (i) 193°

Figure 6.11: SLICY canonical target images (54×54) at elevation 39° and different azimuth angles. Image in (e) is inserted in Figure 6.10.
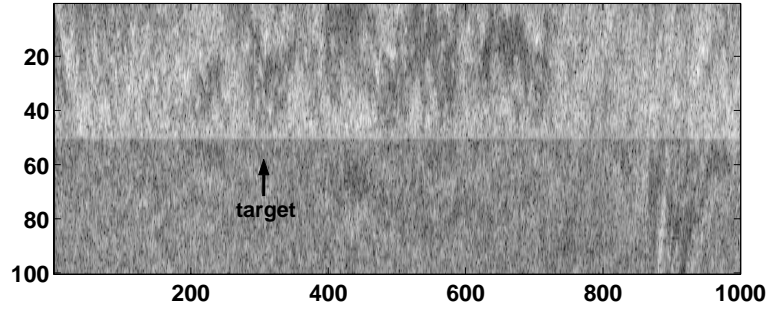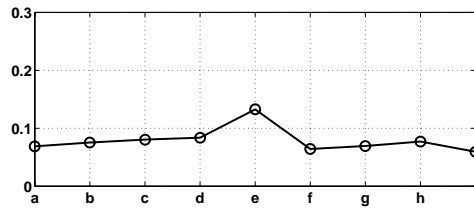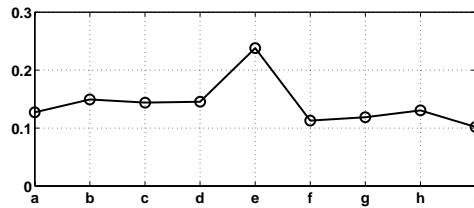
Figure 6.12: Image realigned along the extracted boundary. SLICY target is located at column 305 with $|a| = 0.015$. This target is just above the minimal detectable threshold for the three tests investigated in Figure 6.13.

(a) Structured Kelly's test values

(b) MI test values
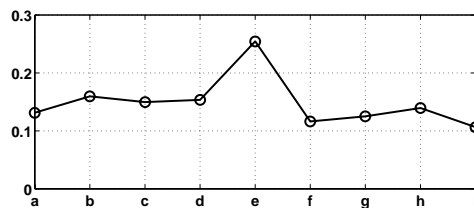
(c) GLR test values

Figure 6.13: Peak values obtained by (a) structured Kelly's test, (b) MI test 1 and (c) GLR 1 for 9 different target images in Figure 6.11 ($|a| = 0.015, n - 1 = 250$).

TRUE boundary
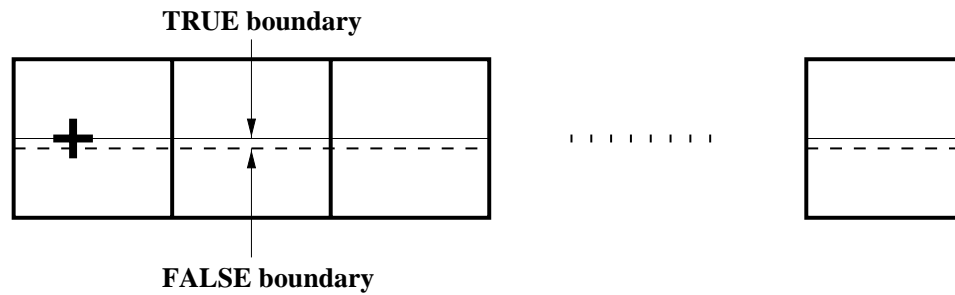
FALSE boundary

(a) True and false information on the boundary
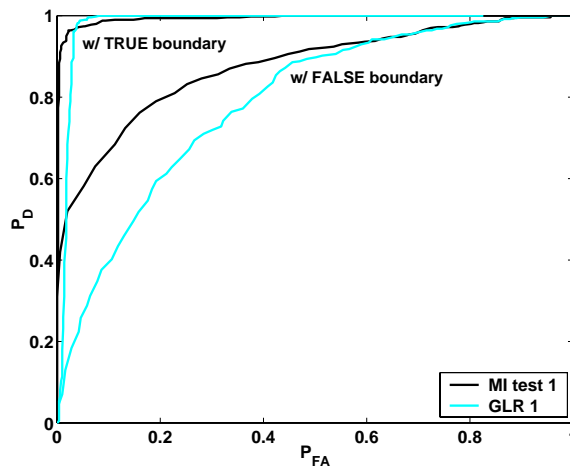
(b) ROC comparison

Figure 6.14: Comparison of ROC curves for Case 1 using true boundary and false boundary moved downward by one pixel in each snapshot (True values: $m_A = 60, m_B = 40, n = 61$).
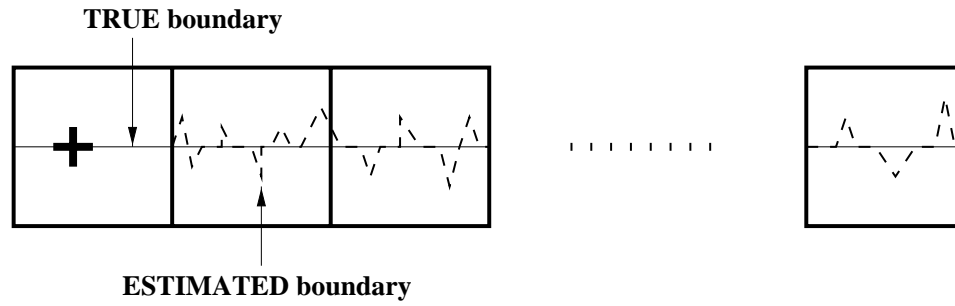
(a) Estimated boundary in secondary chips
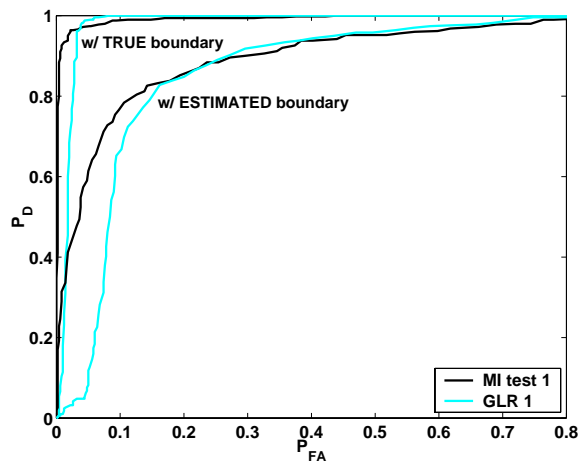
(b) ROC comparison

Figure 6.15: Comparison of ROC curves for Case 1 using true boundary and estimated boundary in secondary snapshots (True values: $m_A = 60, m_B = 40, n = 61$).

Figure 6.16: Hand-extracted boundary superimposed on the initial image in Figure 6.10.

Figure 6.17: Difference between the estimated boundary and the hand-extracted boundary.

CHAPTER 7

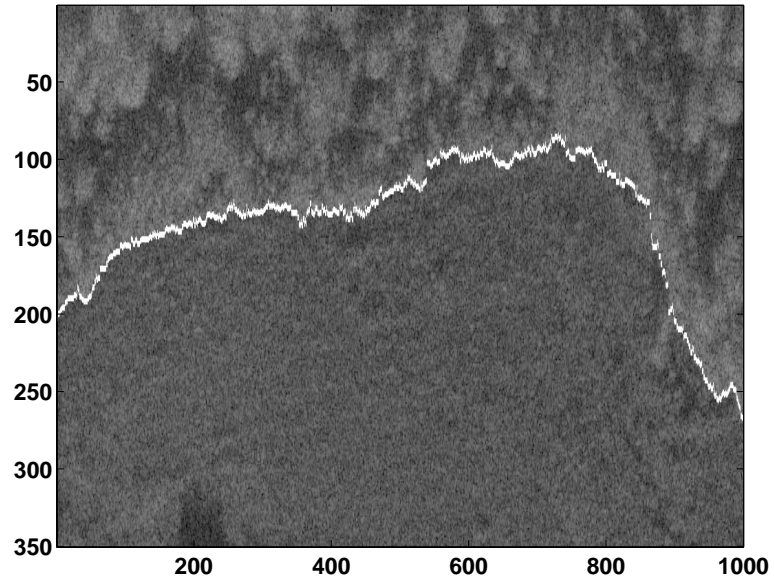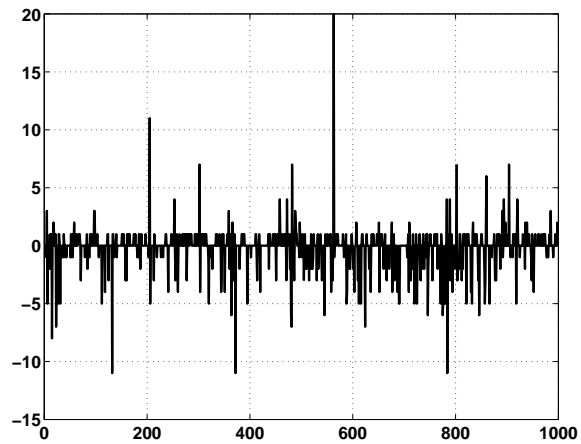# Conclusion

7.1 Summary

In this thesis, we have presented the adaptive target detection algorithms developed under structured clutter covariance. From the assumption that a target of interest may lie along a boundary of two statistically independent clutter regions, three instances of the structured covariance model were considered for different clutter scenarios. In all three cases, for which no uniform optimality is possible, two detection strategies were investigated: generalized likelihood ratio (GLR) and maximal invariant (MI) test procedures. Even though the maximization over a complex quartic equation in each GLR could only be implemented numerically, its architecture provided us with an insight to forming MI test statistics with the sets of maximal invariants. Since the maximal invariant provides data compression through a group of transformations leaving the decision problem unchanged, this is of great help in image detection problems characterized by large dimensional data and parameter spaces.

Both the GLR and MI detectors have comparable receiver operating characteristic (ROC) performance when a large number of independent clutter samples are available. However, when a sufficient number of clutter samples are not available, we have shown that the GLR test is outperformed by the MI test particularly in low probability of false alarm (P_{FA}) regime. In addition, this relative advantage was shown to be robust to boundary segmentation errors. Therefore, the MI test not only plays an important role as an alternative to the GLR test, but also features the desirable property of reliable performance in low P_{FA} which is of particular interest in radar detection applications.

7.2   Future Research

In this section, we address several issues for further research including both theoretical and experimental extensions of results presented in this thesis.

7.2.1   Probabilistic Analysis

The characteristics of the structured GLR and MI tests such as the ROC performance and the CFAR property should be explained analytically with their probability distributions. While Kelly and Forsythe [35] obtained statistical properties of the unstructured GLR test which is also a function of maximal invariants, for the structured model used here this is a very challenging problem. Fortunately, the analysis of the GLR test using well known asymptotic (non-central) chi-square properties [3] will be helpful for this analysis. With this asymptotic property, we may define an upper bound for detection power of the tests at least in the large sample regime. The problem is that the marginal distributions [5] of the maximal invariants are not sufficient to describe their interactions in a test statistic unless the maximal invariants can be transformed into a set of independent statistics. This is frequently possible in simpler version of our problem; in the example of an i.i.d. Gaussian vector, illustrated in Section 3.4.1, the scalar maximal invariant in (3.3) is a function of the sample mean and the sample variance which are independent statistics. However, a number of issues regarding the maximal invariant under the structured covariance model remain unanswered.

7.2.2   Generalization of the Problem

We studied the target detection problem in clutter composed of two different regions with a known boundary. We also assumed that the two clutter regions are statistically independent and multivariate Gaussian with unknown covariance. Several useful generalizations which immediately arise from this model are as follows:

- The linearity assumption between a target and clutter should be relaxed to accommodate canopy interactions with the target. This is a very challenging problem, but is relevant to SAR imaging modalities.

- For applications where the Gaussian clutter assumption may not be appropriate, non-Gaussian models should be investigated. A promising model might be the class of

elliptically symmetric distributions or spherically invariant random vector (SIRV) distributions. Some results exist for GLR and invariant tests for these models when no covariance structure is present [30].

- For spatial acquisition mode SAR, the case should be considered where a target may lie across two different chips.

- We may also come across a case in which a target lies across several boundaries separating more than two regions. The covariance model should be adjusted correspondingly.

- Since the known boundary assumption may not be realistic, as we remarked in Section 6.4, edge/boundary estimation and its interaction with detection should be further investigated. There are two conceivable ways in which a structured detector can be implemented with the unknown boundary. One is to make an estimate of this boundary and plug it into the test. The other is to execute boundary segmentation and detection simultaneously using the GLR principle or the theory of simultaneous detection and estimation developed in [2]. Once this problem is resolved, we may be able to extend our analysis to include: sensitivity of detector performance to boundary estimation, and tradeoffs between optimal segmentation and optimal detection.

7.2.3 Other Applications

The methods described herein can be applied to other detection problems involving boundary and target interactions. Examples include: detection of cancer nodules embedded on lung tissues, and detection of astronomical objects through a partially turbulent atmosphere. As we mentioned in Section 2.2, another application is the multi-path array environment with a low-rank interference component superimposed on ambient and internal sensor noise. These results are also applicable to a wide range of problems in communications and signal processing where there exists covariance structure.

APPENDICES

APPENDIX A

Proof of Proposition 1

Maximal invariant should satisfy both the invariant and the maximal properties under the defined group of transformations. Before showing those properties, note that the group action can be partitioned as

$$g(\mathbf{X}) = \begin{bmatrix} \underline{\beta}^H \underline{x}_1 & \underline{\beta}^H \mathbf{X}_2 \mathbf{U} \\ \mathbf{M}\underline{x}_{21} & \mathbf{M}\mathbf{X}_{22}\mathbf{U} \end{bmatrix}$$

where $\underline{\beta}^H = \begin{bmatrix} \beta_1 & \underline{\beta}_2^H \end{bmatrix}$. Then the invariant property follows directly;

$$
\begin{aligned}
z_{1'}(g(\mathbf{X})) &= \underline{x}_1^H \underline{\beta}(\underline{\beta}^H \mathbf{X}_2 \mathbf{U}\mathbf{U}^H \mathbf{X}_2^H \underline{\beta})^{-1}\underline{\beta}^H \underline{x}_1 \\
&= \underline{x}_1^H (\mathbf{X}_2\mathbf{X}_2^H)^{-1}\underline{x}_1 \\
&= z_{1'}(\mathbf{X}), \\
z_2(g(\mathbf{X})) &= \underline{x}_{21}^H \mathbf{M}^H (\mathbf{M}\mathbf{X}_{22}\mathbf{U}\mathbf{U}^H \mathbf{X}_{22}^H \mathbf{M}^H)^{-1}\mathbf{M}\underline{x}_{21} \\
&= \underline{x}_{21}^H (\mathbf{X}_{22}\mathbf{X}_{22}^H)^{-1}\underline{x}_{21} \\
&= z_2(\mathbf{X}).
\end{aligned}
$$

Now to show the maximal property, let $z_{1'}(\mathbf{X}) = z_{1'}(\mathbf{Y})$ or

$$\underline{x}_1^H (\mathbf{X}_2\mathbf{X}_2^H)^{-1}\underline{x}_1 = \underline{y}_1^H (\mathbf{Y}_2\mathbf{Y}_2^H)^{-1}\underline{y}_1.$$

Then by the Vinograd's theorem [66] (Theorem A9.5 in [44]),

$$(\mathbf{Y}_2\mathbf{Y}_2^H)^{-\frac{1}{2}}\underline{y}_1 = \mathbf{H}(\mathbf{X}_2\mathbf{X}_2^H)^{-\frac{1}{2}}\underline{x}_1$$

for some $m \times m$ orthogonal matrix $\mathbf{H}$, and we have

$$\underline{y}_1 = \mathbf{F}\underline{x}_1 \qquad (\text{A.1})$$

70

where $\mathbf{F} = (\mathbf{Y}_2\mathbf{Y}_2^H)^{\frac{1}{2}}\mathbf{H}(\mathbf{X}_2\mathbf{X}_2^H)^{-\frac{1}{2}}$. Also from this result,

$$\underline{y}_1^H(\mathbf{Y}_2\mathbf{Y}_2^H)^{-1}\underline{y}_1 = \underline{x}_1^H\mathbf{F}^H(\mathbf{Y}_2\mathbf{Y}_2^H)^{-1}\mathbf{F}\underline{x}_1,$$

thus $(\mathbf{Y}_2\mathbf{Y}_2^H)^{-1} = (\mathbf{F}\mathbf{X}_2\mathbf{X}_2^H\mathbf{F}^H)^{-1}$ or

$$\mathbf{Y}_2 = \mathbf{F}\mathbf{X}_2\mathbf{U} \tag{A.2}$$

for some $(n-1) \times (n-1)$ orthogonal matrix $\mathbf{U}$. Therefore, from (A.1) and (A.2), we have

$$\mathbf{Y} = \mathbf{F}\mathbf{X}\begin{bmatrix} 1 & \underline{0}^T \\ \underline{0} & \mathbf{U} \end{bmatrix}. \tag{A.3}$$

Next by using z_2, i.e. $\underline{x}_{21}^H(\mathbf{X}_{22}\mathbf{X}_{22}^H)^{-1}\underline{x}_{21} = \underline{y}_{21}^H(\mathbf{Y}_{22}\mathbf{Y}_{22}^H)^{-1}\underline{y}_{21}$, and the Vinograd's theorem again, we have

$$\begin{bmatrix} \underline{y}_{21} & \mathbf{Y}_{22} \end{bmatrix} = \begin{bmatrix} \underline{0} & \mathbf{M} \end{bmatrix}\begin{bmatrix} \underline{x}_1 & \mathbf{X}_2 \end{bmatrix}\begin{bmatrix} 1 & \underline{0}^T \\ \underline{0} & \mathbf{U} \end{bmatrix} \tag{A.4}$$

where $\mathbf{M} = (\mathbf{Y}_{22}\mathbf{Y}_{22}^H)^{\frac{1}{2}}\mathbf{J}(\mathbf{X}_{22}\mathbf{X}_{22}^H)^{-\frac{1}{2}}$ for some $(m-1) \times (m-1)$ orthogonal matrix $\mathbf{J}$. Then from (A.3) and (A.4), it is verified that $\mathbf{Y} = g(\mathbf{X})$. Therefore, $\{z_{1'}, z_2\}$ satisfies both the invariant and the maximal properties, and hence uniquely indexes the orbits of $\mathbf{X}$ under the group action.

Now we can easily verify that $z_{1'} = z_1 + z_2$ by using the relations for the inverse of a partitioned matrix [20]. Define

$$(\mathbf{X}_2\mathbf{X}_2^H)^{-1} = \begin{bmatrix} \underline{x}_{12}\underline{x}_{12}^H & \underline{x}_{12}\mathbf{X}_{22}^H \\ \mathbf{X}_{22}\underline{x}_{12}^H & \mathbf{X}_{22}\mathbf{X}_{22}^H \end{bmatrix}^{-1} = \begin{bmatrix} V_{11} & V_{12} \\ V_{21} & V_{22} \end{bmatrix},$$

then from the relations;

$$\begin{aligned} V_{11} &= \{\underline{x}_{12}\left[\mathbf{I} - \mathbf{X}_{22}^H(\mathbf{X}_{22}\mathbf{X}_{22}^H)^{-1}\mathbf{X}_{22}\right]\underline{x}_{12}^H\}^{-1}, \\ V_{12} &= -V_{11}\underline{x}_{12}\mathbf{X}_{22}^H(\mathbf{X}_{22}\mathbf{X}_{22}^H)^{-1}, \\ V_{21} &= -V_{11}(\mathbf{X}_{22}\mathbf{X}_{22}^H)^{-1}\mathbf{X}_{22}\underline{x}_{12}^H, \\ V_{22} &= (\mathbf{X}_{22}\mathbf{X}_{22}^H)^{-1} + V_{11}(\mathbf{X}_{22}\mathbf{X}_{22}^H)^{-1}\mathbf{X}_{22}\underline{x}_{12}^H\underline{x}_{12}\mathbf{X}_{22}^H(\mathbf{X}_{22}\mathbf{X}_{22}^H)^{-1}. \end{aligned}$$

Therefore, plugging these values into the equation

$$z_{1'} = x_{11}^H V_{11} x_{11} + \underline{x}_{21}^H V_{21} x_{11} + x_{11}^H V_{12}\underline{x}_{21} + \underline{x}_{21}^H V_{22}\underline{x}_{21},$$

we have

$$z_{1'} = V_{11} \left| x_{11} - \underline{x}_{12} \mathbf{X}_{22}^H (\mathbf{X}_{22} \mathbf{X}_{22}^H)^{-1} \underline{x}_{21} \right|^2 + \underline{x}_{21}^H (\mathbf{X}_{22} \mathbf{X}_{22}^H)^{-1} \underline{x}_{21}$$

$$= z_1 + z_2$$

and hence $\{z_1, z_2\}$ can also serve as the maximal invariant.

APPENDIX B

Proof of Proposition 2

From Proposition 1, we can see clearly that $\{z_{A1}, z_{A2}\}$ is the maximal invariant corresponding to the group of transformations

$$g_A(\mathbf{X}_A) = \begin{bmatrix} \beta_1 & \underline{\beta}_A^H \\ \underline{0} & \mathbf{M}_A \end{bmatrix} \mathbf{X}_A \begin{bmatrix} 1 & \underline{0}^T \\ \underline{0} & \mathbf{U}_A \end{bmatrix} \tag{B.1}$$

and $\{z_{B1}, z_{B2}\}$ to the group of transformations

$$g_B(\mathbf{X}_B) = \begin{bmatrix} \beta_2 & \underline{\beta}_B^H \\ \underline{0} & \mathbf{M}_B \end{bmatrix} \mathbf{X}_B \begin{bmatrix} 1 & \underline{0}^T \\ \underline{0} & \mathbf{U}_B \end{bmatrix} \tag{B.2}$$

where we can only use arbitrary β_1 and β_2 separately for each group. So it suffices to show that z_{AB} is in the maximal invariant set which gives $\beta_1 = \beta_2 = \beta$.

Since the group action (4.12) can be partitioned as

$$g(\mathbf{X}) = \begin{bmatrix} \beta x_{A11} + \underline{\beta}_A^H \underline{x}_{A21} & (\beta \underline{x}_{A12} + \underline{\beta}_A^H \mathbf{X}_{A22})\mathbf{U}_A \\ \mathbf{M}_A \underline{x}_{A21} & \mathbf{M}_A \mathbf{X}_{A22} \mathbf{U}_A \\ \beta x_{B11} + \underline{\beta}_B^H \underline{x}_{B21} & (\beta \underline{x}_{B12} + \underline{\beta}_B^H \mathbf{X}_{B22})\mathbf{U}_B \\ \mathbf{M}_B \underline{x}_{B21} & \mathbf{M}_B \mathbf{X}_{B22} \mathbf{U}_B \end{bmatrix}$$

with the partition in (4.1), the following results are first calculated for convenience;

$$\begin{aligned} u_A(g(\mathbf{X})) &= \beta u_A(\mathbf{X}) \\ D_A(g(\mathbf{X})) &= |\beta|^2 D_A(\mathbf{X}), \end{aligned}$$

and

$$\begin{aligned} u_B(g(\mathbf{X})) &= \beta u_B(\mathbf{X}) \\ D_B(g(\mathbf{X})) &= |\beta|^2 D_B(\mathbf{X}). \end{aligned}$$

Then, it is easily verified that z_{AB} is invariant under $g(\mathbf{X})$ since

$$z_{AB}(g(\mathbf{X})) = \frac{\beta u_A}{\beta u_B} = z_{AB}(\mathbf{X}).$$

Now for the maximal property we need to show that

$$z_{AB}(\mathbf{X}) = z_{AB}(\mathbf{Y}) \implies \beta_1 = \beta_2$$

where

$$\mathbf{Y} = \begin{bmatrix} \mathbf{Y}_A \\ \mathbf{Y}_B \end{bmatrix} = \begin{bmatrix} g_A(\mathbf{X}_A) \\ g_B(\mathbf{X}_B) \end{bmatrix} \tag{B.3}$$

with g_A in (B.1) and g_B in (B.2). Then it is also straightforward since, from $z_{AB}(\mathbf{X}) = z_{AB}(\mathbf{Y})$, we have

$$\frac{u_A}{u_B} = \frac{\beta_1 u_A}{\beta_2 u_B}.$$

Thus $\beta_1 = \beta_2$ and we have proved that

$$\mathbf{Y} = g(\mathbf{X}).$$

Next, $z_{AB'}$ and $z_{AB''}$ can be shown to be the alternative terms for z_{AB} by expressing them as functions of the maximal invariant previously verified. First, we can write

$$z_{AB'} = \frac{|u_B/s_B|^2 \cdot \left| \dfrac{u_A/s_A}{u_B/s_B} - 1 \right|^2}{D_B/|s_B|^2 \cdot \left(\dfrac{D_A/|s_A|^2}{D_B/|s_B|^2} + 1 \right)}.$$

Thus, $z_{AB'}$ is a function of the maximal invariant of form

$$z_{AB'} = z_{B1} \cdot \frac{\left| z_{AB} \cdot \dfrac{s_B}{s_A} - 1 \right|^2}{\dfrac{D_A}{D_B} \cdot \dfrac{|s_B|^2}{|s_A|^2} + 1}$$

where s_A and s_B is known, and D_A/D_B is just a supplementary term to z_{AB}. Also $z_{AB''}$ can be represented similarly with the additional terms q_A and q_B which are already functions of the maximal invariant, and this completes the proof.

74

APPENDIX C

Proof of Proposition 3

We know from Proposition 2 that $\{z_{A1}, z_{A2}\}$ is the maximal invariant to the group of transformations on $\mathbf{X}_A$

$$g_A(\mathbf{X}_A) = \begin{bmatrix} \beta_1 & \underline{\beta}_A^H \\ \underline{0} & \mathbf{M}_A \end{bmatrix} \mathbf{X}_A \begin{bmatrix} 1 & \underline{0}^T \\ \underline{0} & \mathbf{U}_A \end{bmatrix} \tag{C.1}$$

where $\beta_1 \neq 0$ is an arbitrary scalar. Therefore, we need to show that z_B is the maximal invariant to the group action on $\mathbf{X}_B$

$$g_B(\mathbf{X}_B) = \beta_2 \mathbf{X}_B \begin{bmatrix} 1 & \underline{0}^T \\ \underline{0} & \mathbf{U}_B \end{bmatrix} \tag{C.2}$$

where $\beta_2 \neq 0$ is also an arbitrary scalar, and finally $\beta_1 = \beta_2$ with z_{AB}.

First, write z_B as

$$z_B = \frac{|x_{B11}|^2}{tr\{\mathbf{X}_B^H \mathbf{X}_B\}}.$$

Then the invariant property is easily followed;

$$z_B(g(\mathbf{X})) = \frac{|\beta x_{B11}|^2}{tr\{(\beta \mathbf{X}_B)^H (\beta \mathbf{X}_B)\}} = z_B(\mathbf{X})$$

since

$$tr\{\mathbf{A}\} = tr\{\mathbf{P}^H \mathbf{A} \mathbf{P}\}$$

for any $n \times n$ matrix $\mathbf{A}$ and orthogonal matrix $\mathbf{P}$, [20]. Next, for the maximal property, let $z_B(\mathbf{X}_B) = z_B(\mathbf{Y}_B)$, then

$$\frac{|x_{B11}|^2}{tr\{\mathbf{X}_B^H \mathbf{X}_B\}} = \frac{|y_{B11}|^2}{tr\{\mathbf{Y}_B^H \mathbf{Y}_B\}}$$

or

$$x_{B11}^H \left[tr\{\mathbf{X}_B^H \mathbf{X}_B\} \right]^{-1} x_{B11} = y_{B11}^H \left[tr\{\mathbf{Y}_B^H \mathbf{Y}_B\} \right]^{-1} y_{B11}.$$

Thus, from the Vinograd's theorem, we have

$$y_{B11} = \beta_2 x_{B11} \tag{C.3}$$

where $\beta_2 = \left[tr\{\mathbf{Y}_B^H \mathbf{Y}_B\} \right]^{1/2} \mathbf{H} \left[tr\{\mathbf{X}_B^H \mathbf{X}_B\} \right]^{-1/2}$ for some orthogonal matrix $\mathbf{H}$. Then, we can also write

$$\frac{|\beta_2 x_{B11}|^2}{tr\{\mathbf{Y}_B^H \mathbf{Y}_B\}} = \frac{|x_{B11}|^2}{tr\{\mathbf{X}_B^H \mathbf{X}_B\}}$$

and from this, we have

$$tr\{\mathbf{Y}_B^H \mathbf{Y}_B\} = tr\{(\beta_2 \mathbf{X}_B)^H (\beta_2 \mathbf{X}_B)\}$$

or

$$\mathbf{Y}_B = \beta_2 \mathbf{X}_B \mathbf{U} \tag{C.4}$$

for some unitary matrix $\mathbf{U}$. From (C.3) and (C.4), we can say $\mathbf{Y}_B = g_B(\mathbf{X}_B)$ as in (C.2) and z_B is the maximal invariant under g_B on $\mathbf{X}_B$. In addition, since z_B can be written as

$$z_B = \frac{|x_{B11}|^2}{|x_{B11}|^2 + |\underline{x}_{B12}|^2 + |\underline{x}_{B21}|^2 + |\mathbf{X}_{B22}|_F^2} = \frac{1}{1 + 1/z_{B'}},$$

$z_{B'}$ is also a maximal invariant which can be substituted for z_B.

Now it is quite simple to prove z_{AB} as in the proof of Proposition 2. As before, the invariant property is easily verified since

$$z_{AB}(g(\mathbf{X})) = \frac{\beta u_A}{\beta x_{B11}} = z_{AB}(\mathbf{X}),$$

and for the maximal property, we have

$$\frac{u_A(\mathbf{X}_A)}{x_{B11}} = \frac{u_A(\mathbf{Y}_A)}{y_{B11}} \tag{C.5}$$

from $z_{AB}(\mathbf{X}) = z_{AB}(\mathbf{Y})$. Since we have already proved that $\mathbf{Y}_A = g_A(\mathbf{X}_A)$ with g_A in (C.1) and $\mathbf{Y}_B = g_B(\mathbf{X}_B)$ with g_B in (C.2), we can write

$$u_A(\mathbf{Y}_A) = \beta_1 u_A(\mathbf{X}_A),$$

$$y_{B11} = \beta_2 x_{B11}.$$

Thus, from (C.5), $\beta_1 = \beta_2$ and z_{AB} implies the common scaling term β in (4.18).

Finally, the proof for the alternative terms, $z_{AB'}$ and $z_{AB''}$, are easily followed from the proof of Proposition 2 since both terms are equivalent to $z_{AB''}$ in Proposition 2 except for x_{B11} instead of u_B, and the invariant terms ρ, v_1 and v_2.

76

APPENDIX D

Proof of Proposition 4

Since the group action $g(\mathbf{X})$ in (5.5) can be partitioned as

$$
g(\mathbf{X}) = \left[
\begin{array}{cc}
\Delta\underline{x}_{11} + \mathbf{B}\underline{x}_{21} & (\Delta\mathbf{X}_{12} + \mathbf{B}\mathbf{X}_{22})\mathbf{U} \\
\mathbf{M}\underline{x}_{21} & \mathbf{M}\mathbf{X}_{22}\mathbf{U}
\end{array}
\right],
$$

the following results are first calculated for convenience;

$$
\begin{aligned}
\underline{u}(g(\mathbf{X})) &= (\Delta\underline{x}_{11} + \mathbf{B}\underline{x}_{21}) - (\Delta\mathbf{X}_{12} + \mathbf{B}\mathbf{X}_{22})\mathbf{X}_{22}(\mathbf{X}_{22}\mathbf{X}_{22}^H)^{-1}\underline{x}_{21} \\
&= \Delta\{\underline{x}_{11} - \mathbf{X}_{12}\mathbf{X}_{22}(\mathbf{X}_{22}\mathbf{X}_{22}^H)^{-1}\underline{x}_{21}\} \\
&= \Delta\underline{u}(\mathbf{X}), \\
\mathbf{D}(g(\mathbf{X})) &= (\Delta\mathbf{X}_{12} + \mathbf{B}\mathbf{X}_{22})\left[\mathbf{I} - \mathbf{X}_{22}^H(\mathbf{X}_{22}\mathbf{X}_{22}^H)^{-1}\mathbf{X}_{22}\right](\mathbf{X}_{12}^H\Delta^H + \mathbf{X}_{22}^H\mathbf{B}^H) \\
&= \Delta\{\mathbf{X}_{12}\left[\mathbf{I} - \mathbf{X}_{22}^H(\mathbf{X}_{22}\mathbf{X}_{22}^H)^{-1}\mathbf{X}_{22}\right]\mathbf{X}_{12}^H\}\Delta^H \\
&= \Delta\mathbf{D}(\mathbf{X})\Delta^H.
\end{aligned}
$$

Then with the partitioned structure of $\mathbf{X}$ and the above results, we can easily verify the invariant property as follows;

$$
\begin{aligned}
z_1(g(\mathbf{X})) &= \underline{u}^H\Delta^H(\Delta\mathbf{D}\Delta^H)^{-1}\Delta\underline{u} \\
&= \underline{u}^H\mathbf{D}^{-1}\underline{u} \\
&= z_1(\mathbf{X}), \\
z_2(g(\mathbf{X})) &= \underline{x}_{21}^H\mathbf{M}^H(\mathbf{M}\mathbf{X}_{22}\mathbf{U}\mathbf{U}^H\mathbf{X}_{22}^H\mathbf{M}^H)^{-1}\mathbf{M}\underline{x}_{21} \\
&= \underline{x}_{21}^H(\mathbf{X}_{22}\mathbf{X}_{22}^H)^{-1}\underline{x}_{21} \\
&= z_2(\mathbf{X}),
\end{aligned}
$$

and

$$
\begin{aligned}
z_{3k}(g(\mathbf{X})) &= \underline{u}^H \Delta^H (\Delta \mathbf{D} \Delta^H)^{-1} \underline{\epsilon}_k \left[\underline{\epsilon}_k^T (\Delta \mathbf{D} \Delta^H)^{-1} \underline{\epsilon}_k \right]^{-1} \underline{\epsilon}_k^T (\Delta \mathbf{D} \Delta^H)^{-1} \Delta \underline{u} \\
&= \underline{u}^H \mathbf{D}^{-1} (\Delta^{-1} \underline{\epsilon}_k) \left[(\Delta^{-1} \underline{\epsilon}_k)^H \mathbf{D}^{-1} (\Delta^{-1} \underline{\epsilon}_k) \right]^{-1} (\Delta^{-1} \underline{\epsilon}_k)^H \mathbf{D}^{-1} \underline{u} \\
&= \underline{u}^H \mathbf{D}^{-1} \underline{\epsilon}_k (\underline{\epsilon}_k^T \mathbf{D}^{-1} \underline{\epsilon}_k)^{-1} \underline{\epsilon}_k^T \mathbf{D}^{-1} \underline{u} \\
&= z_{3k}(\mathbf{X}).
\end{aligned}
$$

Next, for the maximal property, it is easily followed from Proposition 1 that $z_1(\mathbf{X}) = z_1(\mathbf{Y})$ and $z_2(\mathbf{X}) = z_2(\mathbf{Y})$ gives

$$
\mathbf{Y} = \begin{bmatrix} \mathbf{A} & \mathbf{B} \\ \mathbf{O} & \mathbf{M} \end{bmatrix} \mathbf{X} \begin{bmatrix} 1 & \underline{0}^T \\ \underline{0} & \mathbf{U} \end{bmatrix}
$$

where we have a $p \times p$ non-zero matrix $\mathbf{A}$ instead of β_1 in (3.9) and others are defined in (5.5). Note that this is a general case of Proposition 1 ($p = 1$) and the proof directly follows that of Proposition 1 except for the dimension.

Now we only need to show that $\mathbf{A}$ is a $p \times p$ diagonal matrix with z_{3k}. Let $\mathbf{A}^{-1} = \left[\underline{\gamma}_1, \dots, \underline{\gamma}_p \right]$, then

$$
\begin{aligned}
z_{3k}(\mathbf{Y}) &= \underline{u}^H \mathbf{A}^H (\mathbf{A} \mathbf{D} \mathbf{A}^H)^{-1} \underline{\epsilon}_k \left[\underline{\epsilon}_k^T (\mathbf{A} \mathbf{D} \mathbf{A}^H)^{-1} \underline{\epsilon}_k \right]^{-1} \underline{\epsilon}_k^T (\mathbf{A} \mathbf{D} \mathbf{A}^H)^{-1} \mathbf{A} \underline{u} \\
&= \underline{u}^H \mathbf{D}^{-1} (\mathbf{A}^{-1} \underline{\epsilon}_k) \left[(\mathbf{A}^{-1} \underline{\epsilon}_k)^H \mathbf{D}^{-1} (\mathbf{A}^{-1} \underline{\epsilon}_k) \right]^{-1} (\mathbf{A}^{-1} \underline{\epsilon}_k)^H \mathbf{D}^{-1} \underline{u} \\
&= \underline{u}^H \mathbf{D}^{-1} \underline{\gamma}_k (\underline{\gamma}_k^H \mathbf{D}^{-1} \underline{\gamma}_k)^{-1} \underline{\gamma}_k^H \mathbf{D}^{-1} \underline{u}.
\end{aligned}
$$

Then from $z_{3k}(\mathbf{X}) = z_{3k}(\mathbf{Y})$,

$$
\underline{u}^H \mathbf{D}^{-1} \frac{\underline{\epsilon}_k \underline{\epsilon}_k^T}{\underline{\epsilon}_k^T \mathbf{D}^{-1} \underline{\epsilon}_k} \mathbf{D}^{-1} \underline{u} = \underline{u}^H \mathbf{D}^{-1} \frac{\underline{\gamma}_k \underline{\gamma}_k^H}{\underline{\gamma}_k^H \mathbf{D}^{-1} \underline{\gamma}_k} \mathbf{D}^{-1} \underline{u}.
$$

Thus we have

$$
\frac{\underline{\epsilon}_k \underline{\epsilon}_k^T}{\underline{\epsilon}_k^T \mathbf{D}^{-1} \underline{\epsilon}_k} = \frac{\underline{\gamma}_k \underline{\gamma}_k^H}{\underline{\gamma}_k^H \mathbf{D}^{-1} \underline{\gamma}_k}
$$

, which gives $\underline{\gamma}_k = \delta_k^{-1} \underline{\epsilon}_k$ for some scalar $\delta_k \neq 0$ and $k = 1, \dots, p$. This means that

$$
\mathbf{A} = diag(\underline{\delta})
$$

where $\underline{\delta} = [\delta_1, \dots, \delta_p]$.

APPENDIX E

Proof of Proposition 5

From the proof of Proposition 4, we know that $\{z_{A1}, z_{A2}, z_{A3k}\}$ and $\{z_{B1}, z_{B2}, z_{B3k}\}$ are associated with the groups

$$g_A(\mathbf{X}_A) = \begin{bmatrix} \Delta_A & \mathbf{B}_A \\ \mathbf{O} & \mathbf{M}_A \end{bmatrix} \mathbf{X}_A \begin{bmatrix} 1 & \underline{0}^H \\ \underline{0} & \mathbf{U} \end{bmatrix}$$

$$\text{and} \quad g_B(\mathbf{X}_B) = \begin{bmatrix} \Delta_B & \mathbf{B}_B \\ \mathbf{O} & \mathbf{M}_B \end{bmatrix} \mathbf{X}_B \begin{bmatrix} 1 & \underline{0}^H \\ \underline{0} & \mathbf{U} \end{bmatrix},$$

respectively. So it suffices to show that $\Delta_A = \Delta_B = \Delta$ with z_{ABk}.

First, the invariant property of z_{ABk} directly follows from the properties of $\underline{u}$ and $\mathbf{D}$ on $g(\mathbf{X})$ in the proof of Proposition 4. Next, for the maximal property of z_{ABk}, let $z_{ABk}(\mathbf{X}) = z_{ABk}(\mathbf{Y})$ with

$$\mathbf{Y} = \begin{bmatrix} g_A(\mathbf{X}_A) \\ g_B(\mathbf{X}_B) \end{bmatrix}$$

where $\Delta_A = diag([\delta_{A1}, \dots, \delta_{Ap}])$ and $\Delta_B = diag([\delta_{B1}, \dots, \delta_{Bp}])$, then

$$\frac{(\underline{\epsilon}_k^T \mathbf{D}_A^{-1} \underline{\epsilon}_k)^{-1} \underline{\epsilon}_k^T \mathbf{D}_A^{-1} \underline{u}_A}{(\underline{\epsilon}_k^T \mathbf{D}_B^{-1} \underline{\epsilon}_k)^{-1} \underline{\epsilon}_k^T \mathbf{D}_B^{-1} \underline{u}_B} = \frac{\delta_{Ak} (\underline{\epsilon}_k^T \mathbf{D}_A^{-1} \underline{\epsilon}_k)^{-1} \underline{\epsilon}_k^T \mathbf{D}_A^{-1} \underline{u}_A}{\delta_{Bk} (\underline{\epsilon}_k^T \mathbf{D}_B^{-1} \underline{\epsilon}_k)^{-1} \underline{\epsilon}_k^T \mathbf{D}_B^{-1} \underline{u}_B}.$$

Therefore, $\delta_{Ak} = \delta_{Bk}$ for $k = 1, \dots, p$ and we have proved that $\Delta_A = \Delta_B$.

Finally, we can substitute $z_{ABk'}$ for z_{ABk} since $z_{ABk'}$ is a function of the previously obtained maximal invariant of form

$$z_{ABk'} = z_{B3k} \cdot \frac{|z_{ABk} - 1|^2}{\dfrac{(\underline{\epsilon}_k^T \mathbf{D}_A^{-1} \underline{\epsilon}_k)^{-1}}{(\underline{\epsilon}_k^T \mathbf{D}_B^{-1} \underline{\epsilon}_k)^{-1}} + 1}$$

79

where $(\underline{\epsilon}_k^T \mathbf{D}_A^{-1} \underline{\epsilon}_k)^{-1}/(\underline{\epsilon}_k^T \mathbf{D}_B^{-1} \underline{\epsilon}_k)^{-1}$ is just a supplementary term for z_{ABk}. Similarly, $z_{ABk''}$ can also be shown to be a substitute for the coupling term with the additional functions of the maximal invariant q_A and q_B.

APPENDIX F

Proof of Lemma 1

We can write the equation as

$$(\underline{u}_A^H \mathbf{D}_A^{-1} + \underline{u}_B^H \mathbf{D}_B^{-1})(\mathbf{D}_A^{-1} + \mathbf{D}_B^{-1})^{-1}(\mathbf{D}_A^{-1} \underline{u}_A + \mathbf{D}_B^{-1} \underline{u}_B)$$

$$= \quad \underline{u}_A^H \mathbf{D}_A^{-1}(\mathbf{D}_A^{-1} + \mathbf{D}_B^{-1})^{-1}\mathbf{D}_A^{-1} \underline{u}_A + \underline{u}_A^H \mathbf{D}_A^{-1}(\mathbf{D}_A^{-1} + \mathbf{D}_B^{-1})^{-1}\mathbf{D}_B^{-1} \underline{u}_B$$

$$+ \quad \underline{u}_B^H \mathbf{D}_B^{-1}(\mathbf{D}_B^{-1} + \mathbf{D}_A^{-1})^{-1}\mathbf{D}_A^{-1} \underline{u}_A + \underline{u}_B^H \mathbf{D}_B^{-1}(\mathbf{D}_B^{-1} + \mathbf{D}_A^{-1})^{-1}\mathbf{D}_B^{-1} \underline{u}_B$$

and from the Woodbury identity, we have

$$(\mathbf{D}_A^{-1} + \mathbf{D}_B^{-1})^{-1} \quad = \quad \mathbf{D}_A - \mathbf{D}_A(\mathbf{D}_B + \mathbf{D}_A)^{-1}\mathbf{D}_A,$$

$$\text{or} \quad (\mathbf{D}_B^{-1} + \mathbf{D}_A^{-1})^{-1} \quad = \quad \mathbf{D}_B - \mathbf{D}_B(\mathbf{D}_A + \mathbf{D}_B)^{-1}\mathbf{D}_B.$$

Thus, applying this identity, the equation becomes

$$(\underline{u}_A^H \mathbf{D}_A^{-1} + \underline{u}_B^H \mathbf{D}_B^{-1})(\mathbf{D}_A^{-1} + \mathbf{D}_B^{-1})^{-1}(\mathbf{D}_A^{-1} \underline{u}_A + \mathbf{D}_B^{-1} \underline{u}_B)$$

$$= \quad \underline{u}_A^H \mathbf{D}_A^{-1} \underline{u}_A + \underline{u}_B^H \mathbf{D}_B^{-1} \underline{u}_B - (\underline{u}_A - \underline{u}_B)^H (\mathbf{D}_A + \mathbf{D}_B)^{-1}(\underline{u}_A - \underline{u}_B) + L_1 + L_2$$

where

$$L_1 \quad = \quad \underline{u}_A^H \left[\mathbf{D}_B^{-1} - (\mathbf{D}_A + \mathbf{D}_B)^{-1} - (\mathbf{D}_A + \mathbf{D}_B)^{-1}\mathbf{D}_A\mathbf{D}_B^{-1} \right] \underline{u}_B,$$

$$L_2 \quad = \quad \underline{u}_B^H \left[\mathbf{D}_A^{-1} - (\mathbf{D}_A + \mathbf{D}_B)^{-1} - (\mathbf{D}_A + \mathbf{D}_B)^{-1}\mathbf{D}_B\mathbf{D}_A^{-1} \right] \underline{u}_A.$$

Now we can remove the extra terms L_1 and L_2 since

$$L_1 \quad = \quad \underline{u}_A^H (\mathbf{D}_A + \mathbf{D}_B)^{-1} \left[(\mathbf{D}_A + \mathbf{D}_B) - \mathbf{D}_B - \mathbf{D}_A \right] \mathbf{D}_B^{-1} \underline{u}_B = 0,$$

$$L_2 \quad = \quad \underline{u}_B^H (\mathbf{D}_A + \mathbf{D}_B)^{-1} \left[(\mathbf{D}_A + \mathbf{D}_B) - \mathbf{D}_A - \mathbf{D}_B \right] \mathbf{D}_A^{-1} \underline{u}_A = 0$$

and this completes the proof.

BIBLIOGRAPHY

BIBLIOGRAPHY

[1] T. W. Anderson, *An Introduction to Multivariate Statistical Analysis*, New York: Wiley, 1958.

[2] B. Baygün and A. O. Hero, "Optimal simultaneous detection and estimation under a false alarm constraint," *IEEE Transactions on Information Theory*, vol. 41, no. 3, pp. 688-703, May 1995.

[3] P. J. Bickel and K. A. Doksom, *Mathematical Statistics: Basic Ideas and Selected Topics*, San Francisco: Holden-Day, 1977.

[4] P. Billingsley, *Probability and Measure*, 3rd ed., New York: Wiley, 1995.

[5] S. Bose, "Invariant hypothesis testing with sensor arrays," Ph. D. thesis, Cornell University, Ithaca, NY, January 1995.

[6] S. Bose and A. O. Steinhardt, "A maximal invariant framework for adaptive detection with structured and unstructured covariance matrices," *IEEE Transactions on Signal Processing*, vol. 43, no. 9, pp. 2164-2175, September 1995.

[7] S. Bose and A. O. Steinhardt, "Adaptive array detection of uncertain rank one waveforms," *IEEE Transactions on Signal Processing*, vol. 44, no. 11, pp. 2801-2809, November 1996.

[8] K. A. Burgess and B. D. Van Veen, "Subspace-based adaptive generalized likelihood ratio detection," *IEEE Transactions on Signal Processing*, vol. 44, no. 4, pp. 912-927, April 1996.

[9] Center for Imaging Science, *Sensor Database*, http://cis.jhu.edu/sensor_data

[10] C. T. Chen, *Linear System Theory and Design*, New York: Oxford, 1984.

[11] J. Y. Chen and I. S. Reed, "A detection algorithm for optical targets in clutter," *IEEE Transactions on Aerospace and Electronic Systems*, vol. AES-23, no. 1, pp. 46-59, January 1987.

[12] W. B. Davenport and W. L. Root, *An Introduction to the Theory of Random Signals and Noise*, New York: McGraw-Hill, 1958.

[13] R. D. De Roo, F. T. Ulaby, A. E. El-Rouby, and A. Y. Nashashibi, "MMW radar scattering statistics of terrain at near grazing incidence," *IEEE Transactions on Aerospace and Electronic Systems*, vol. 35, no. 3, pp. 1010-1018, July 1999.

[14] J. M. B. Dias, T. A. M. Silva, and J. M. N. Leitao, "Adaptive restoration of speckled SAR images using a compound random Markov field," *Proceedings of IEEE International Conference on Image Processing*, vol. 2, pp. 79-83, October 1998.

[15] M. L. Eaton, *Multivariate Statistics: A Vector Space Approach*, New York: Wiley, 1983.

[16] M. L. Eaton, *Group Invariance Applications in Statistics, Regional Conference Series in Probability and Statistics*, vol. 1, Institute of Mathematical Statistics, 1989.

[17] W. Feller, *An Introduction to Probability Theory and its Applications*, New York: Wiley, 1966.

[18] T. S. Ferguson, *Mathematical Statistics: A Decision Theoretic Approach*, New York: Academic Press, 1967.

[19] D. Fuhrmann, "Application of Toeplitz covariance estimation to adaptive beamforming and detection," *IEEE Transactions on Acoustics, Speech, and Signal Processing*, vol. 39, no. 10, pp. 2194-2198, October 1991.

[20] F. A. Graybill, *Matrices with Applications in Statistics*, 2nd ed., Belmont, CA: Wadsworth, 1983.

[21] S. Haykin, *Array Signal Processing*, Englewood Cliffs, NJ: Prentice Hall, 1985.

[22] S. Haykin, *Blind Deconvolution*, Englewood Cliffs, NJ: Prentice Hall, 1994.

[23] S. Haykin and A. Steinhardt, *Adaptive Radar Detection and Estimation*, New York: Wiley, 1992.

[24] A. O. Hero and C. Guillouet, "Robust detection of SAR/IR targets via invariance," *Proceedings of IEEE International Conference on Image Processing*, vol. 3, pp. 472-475, October 1997.

[25] R. A. Horn, *Matrix Analysis*, New York: Cambridge University Press, 1985.

[26] I. A. Ibragimov and R. Z. Hasminskii, *Statistical Estimation: Asymptotic Theory*, New York: Springer-Verlag, 1981.

[27] A. K. Jain, *Fundamentals of Digital Image Processing*, Englewood Cliffs, NJ: Prentice Hall, 1989.

[28] C. V. Jakowatz, D. E. Wahl, P. H. Eichel, D. C. Ghiglia, and P. A. Thompson, *Spotlight-Mode Synthetic Aperture Radar: A Signal Processing Approach*, Norwell, MA: Kluwer, 1996.

[29] T. Kailath, *Linear Systems*, Englewood Cliffs, NJ: Prentice Hall, 1980.

[30] T. Kariya and B. K. Sinha, *Robustness of Statistical Tests*, San Diego: Academic Press, 1989.

[31] S. M. Kay, "Asymptotically optimal detection in unknown colored noise via autoregressive modeling," *IEEE Transactions on Acoustics, Speech, and Signal Processing*, vol. ASSP-31, no. 4, pp. 927-940, August 1983.

[32] S. M. Kay, "Asymptotically optimal detection in incompletely characterized non-Gaussian noise," *IEEE Transactions on Acoustics, Speech, and Signal Processing*, vol. 37, no. 5, pp. 627-633, May 1989.

[33] S. M. Kay, *Fundamentals of Statistical Signal Processing: Estimation Theory*, Englewood Cliffs, NJ: Prentice Hall, 1993.

[34] E. J. Kelly, "An adaptive detection algorithm," *IEEE Transactions on Aerospace and Electronic Systems*, vol. AES-22, pp. 115-127, March 1986.

[35] E. J. Kelly and K. M. Forsythe, "Adaptive detection and parameter estimation for multidimensional signal models," Technical Report no. 848, Lincoln Laboratory, Massachusetts Institute of Technology, April 1989.

[36] C. G. Khatri and C. R. Rao, "Effects of estimated noise covariance matrix in optimal signal detection," *IEEE Transactions on Acoustics, Speech, and Signal Processing*, vol. ASSP-35, no. 5, pp. 671-679, May 1987.

[37] H. S. Kim and A. O. Hero, "Adaptive target detection across a clutter boundary: GLR and maximally invariant detectors," *Proceedings of IEEE International Conference on Image Processing*, vol. 1, pp. 681-684, September 2000.

[38] H. S. Kim and A. O. Hero, "When is a maximal invariant hypothesis test better than the GLRT?," *Proceedings of IEEE Asilomar Conference on Signals, Systems, and Computers*, October 2000.

[39] H. S. Kim and A. O. Hero, "Comparison of GLR and invariance methods applied to adaptive target detection in structured clutter," Technical Report no. 323, Communications and Signal Processing Laboratory, University of Michigan, Ann Arbor, MI, November 2000.

[40] E. L. Lehmann, *Testing Statistical Hypotheses*, New York: Wiley, 1959.

[41] J. S. Lim, *Two-Dimensional Signal and Image Processing*, Englewood Cliffs, NJ: Prentice Hall, 1990.

[42] E. B. Manoukian, *Modern Concepts and Theorems of Mathematical Statistics*, New York: Springer-Verlag, 1986.

[43] D. Middleton, *An Introduction to Statistical Communication Theory*, New York: McGraw-Hill, 1960.

[44] R. J. Muirhead, *Aspects of Multivariate Statistical Theory*, New York: Wiley, 1982.

[45] C. Oliver and S. Quegan, *Understanding Synthetic Aperture Radar Images*, Boston: Artech House, 1998.

[46] A. Papoulis, *Probability, Random Variables, and Stochastic Processes*, New York: McGraw-Hill, 1991.

[47] I. Pollak, A. S. Willsky and H. Krim, "Image segmentation and edge enhancement with stabilized inverse diffusion equations," *IEEE Transactions on Image Processing*, vol. 9, no. 2, pp. 256-266, February 2000.

[48] H. V. Poor, *An Introduction to Signal Detection and Estimation*, New York: Springer-Verlag, 1988.

[49] J. G. Proakis and D. G. Manolakis, *Digital Signal Processing: Principles, Algorithms, and Applications*, Upper Saddle River, NJ: Prentice Hall, 1996.

[50] I. S. Reed, J. D. Mallet, and L. E. Brennan, "Rapid convergence rate in adaptive arrays," *IEEE Transactions on Aerospace and Electronic Systems*, vol. AES-10, no. 6, pp. 853-863, November 1974.

[51] I. S. Reed and X. Yu, "Adaptive multiple-band CFAR detection of an optical pattern with unknown spectral distribution," *IEEE Transactions on Acoustics, Speech, and Signal Processing*, vol. 38, no. 10, pp. 1760-1770, October 1990.

[52] C. D. Richmond, "Derived PDF of maximum likelihood signal estimator which employs an estimated noise covariance," *IEEE Transactions on Signal Processing*, vol. 44, no. 2, pp. 305-315, February 1996.

[53] F. C. Robey, D. R. Fuhrmann, E. J. Kelly, and R. Nitzberg, "A CFAR adaptive matched filter detector," *IEEE Transactions on Aerospace and Electronic Systems*, vol. AES-28, no. 1, pp. 208-216, January 1992.

[54] S. M. Ross, *Stochastic Processes*, New York: Wiley, 1983.

[55] L. L. Scharf, "Invariant Gauss-Gauss detection," *IEEE Transactions on Information Theory*, vol. IT-19, no. 4, pp. 422-427, July 1973.

[56] L. L. Scharf, *Statistical Signal Processing: Detection, Estimation, and Time Series Analysis*, Reading, MA: Addison-Wesley, 1991.

[57] L. L. Scharf and D. W. Lytle, "Signal detection in Gaussian noise of unknown level: an invariance application," *IEEE Transactions on Information Theory*, vol. IT-17, no. 4, pp. 404-411, July 1971.

[58] L. L. Scharf and B. Friedlander, "Matched subspace detectors," *IEEE Transactions on Signal Processing*, vol. 42, no. 8, pp. 2146-2157, August 1994.

[59] R. A. Schowengerdt, *Techniques for Image Processing and Classification in Remote Sensing*, New York: Academic Press, 1983.

[60] R. A. Schowengerdt, *Remote Sensing: Models and Methods for Image Processing*, San Diego: Academic Press, 1997.

[61] R. E. Schwartz, "Minimax CFAR detection in additive Gaussian noise of unknown covariance," *IEEE Transactions on Information Theory*, vol. IT-15, no. 6, pp. 722-725, November 1969.

[62] M. D. Srinath, P. K. Rajasekaran and R. Viswanathan, *Introduction to Statistical Signal Processing with Applications*, Englewood Cliffs, NJ: Prentice Hall, 1996.

[63] H. Stark and J. W. Woods, *Probability, Random Processes and Estimation Theory for Engineers*, Upper Saddle River, NJ: Prentice Hall, 1994.

[64] F. T. Ulaby, R. K. Moore, and A. K. Fung, *Microwave Remote Sensing: Active and Passive*, Reading, MA: Addison-Wesley, 1981.

[65] H. L. Van Trees, *Detection, Estimation, and Modulation Theory: Part I*, New York: Wiley, 1968.

[66] B. Vinograd, "Canonical positive definite matrices under internal linear transformation," *Proceedings of the American Mathematical Society*, 1, 159-161, 1950.

[67] X. Yu, I. S. Reed, and A. D. Stocker, "Comparative performance analysis of adaptive multispectral detectors," *IEEE Transactions on Signal Processing*, vol. 41, no. 8, pp. 2639-2656, February 1996.